Convention on Long-Range Transboundary Air Pollution

emep
emep
emep

Co-operative programme for monitoring and evaluation of the long-range transmission of air pollutants in Europe

TECHNICAL REPORT
1/2016 August 2016

Heavy metals and persistent organic pollutants: model assessment of pollution and research activities

EMEP/MSC-E Technical Report 1/2016

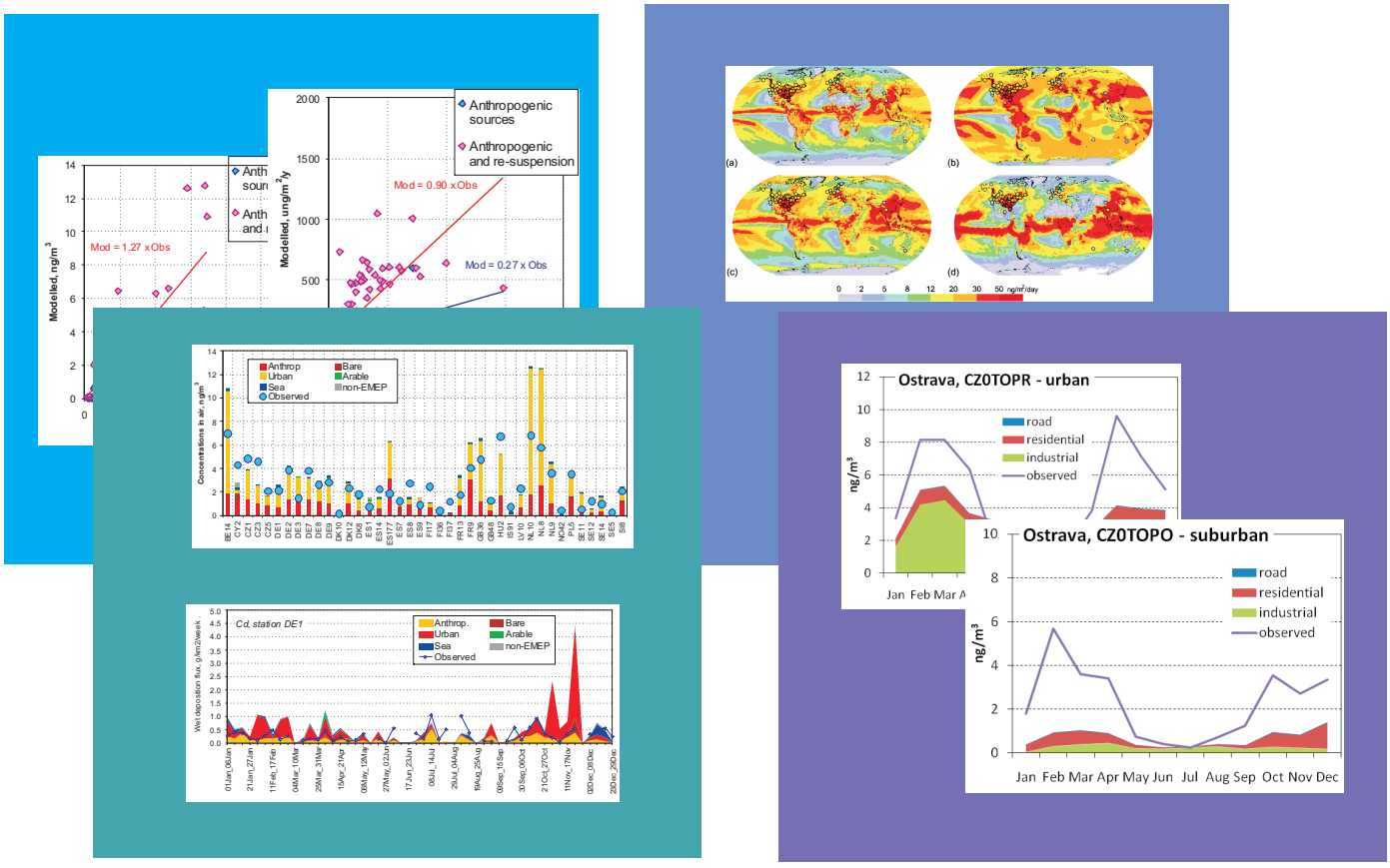

Meteorological Synthesizing Centre - East

EMEP/MSC-E Technical Report 1/2016
August 2016

Heavy metals and persistent organic pollutants: model assessment of pollution and research activities

Shatalov V., Ilyin I., Gusev A., Travnikov O.

MCS-E

Meteorological Synthesizing Centre - East

2nd Roshchinsky proezd, 8/5, 115419 Moscow, Russia
Tel: +7 926 906 91 78; Fax: +7 495 956 19 44; E-mail: msce@msceast.org; www.msceast.org

CONTENTS

Introduction 5

9

1. HEAVY METALS 9
   1.1. Update of re-suspension scheme of heavy metals 9
   1.2. Evaluation of modelling results vs. observations 20
   1.3. Multi-model study of mercury atmospheric processes 29
      1.3.1. Measurements data and model setup 31
      1.3.2. Gaseous elemental mercury 34
      1.3.3. Reactive mercury 36
      1.3.4. Wet deposition 39
      1.3.5. Concluding remarks 40

2. PERSISTENT ORGANIC POLLUTANTS 40
   2.1. Country-specific trend analysis for PCB-153 40
      2.1.1. Modification of the methodology of trend analysis 40
      2.1.2. Results and discussion 46
      2.1.3. Concluding remarks 48
   2.2. Preparation of PCDD/F congener-specific emission data for modelling 49
      2.2.1. Description of the literature data used in the analysis 51
      2.2.2. Proposed methodology (preliminary analysis) 51
      2.2.3. Concluding remarks 55
   2.3. Evaluation of B[a]P contamination in urban/suburban areas of the Czech Republic 56
      2.3.1. Input data (measurements and model results) 57
      2.3.2. Investigation of contamination in 2007 58
      2.3.3. Evaluation of contamination of urban regions 65
      2.3.4. Concluding remarks 72

References 73

Annex A. Literature sources on PCDD/Fs congener composition 77

INTRODUCTION

Heavy metals (HMs) and persistent organic pollutants (POPs) are persistent toxic substances characterized by high ability to dispersion in the atmosphere over long distances (up to hundreds or thousands of kilometres). They (particularly POPs and mercury) are characterized by significant potential to accumulation in the environmental media (soil, seawater, sediments, vegetation). These substances cause a risk of adverse health effects in humans and wildlife.

These substances are within the scope of the UNECE Convention on Long-range Transboundary Air Pollution (CLRTAP). Protocols on HMs and POPs are aimed at reduction of HM and POP emissions and decrease of the environmental pollution by these contaminants. HMs and POPs being in focus of the EMEP activities are lead (Pb), cadmium (Cd) and mercury (Hg), targeted by the Protocol on HMs, and polyaromatic hydrocarbons (PAHs), dibenzo-para-dioxins and dibenzofurans (PCDD/Fs), polychlorinates biphenils (PCBs) and hexachlorobenzene (HCB), targeted by the Protocol on POPs.

Along with routine work on evaluation of environmental levels and transboundary transport of HMs and POPs in the EMEP domain for 2014, MSC-E undertakes activities for both model development (refinement of model design and generation of input data, in particular, on congener composition of PCDD/F mixture) and for generating additional information on evaluation of pollution levels in urban areas within the EMEP region.

In this context, the following activities have been carried out in the current year (2014).

Update of re-suspension scheme of heavy metals

There are three main groups of sources responsible for heavy metal pollution levels in the EMEP region. First, these are primary (direct anthropogenic) emission sources such as industry, transport, energy production etc within and outside the EMEP region. Second re-suspension of wind-blown dust containing previously deposited metals, and, third natural emission and re-emission of gaseous form of mercury. Second and third source group together are called secondary emissions.

It was found that re-suspension may essentially contribute to the HM contamination. Parameterization of re-suspension of particulate metals (e.g., Pb and Cd) was already included in the MSCE-HM model as described in [*Gusev et al,* 2006]. However, although the inclusion of re-suspension in modelling resulted to the improvement of the model performance in 'general', at some stations and in some periods it led to overestimation of the observed levels.

Further improvement of re-suspension scheme for HMs used for the model calculations was undertaken in the current year with the help of optimization using source-receptor calculations. The results of this work are presented in Section 1.1.

Comparison of modelled and observed pollution levels for 2014

There are numerous reasons leading to discrepancy between modelled and observed levels, namely uncertainties of emission data, quality of measurements and uncertainties of the model parameterizations and input data. In section 1.2 these uncertainties were overviewed. Besides, attention was paid to evaluation of modelling results against monitoring data. Modelled concentrations in air and wet deposition were compared with the levels observed at the EMEP monitoring network.

Examination of mercury atmospheric processes

Oxidation chemistry and speciation of mercury in the atmosphere determine its ability to long-term atmospheric transport and deposition to various terrestrial and aquatic regions. Current knowledge on mercury behaviour in the atmosphere and its potential to cycling between different environmental media is still incomplete. There are significant gaps in the understanding of chemical processes affecting mercury atmospheric transport and deposition, characteristics of the air-surface exchange and processes responsible for re-emission of mercury to the atmosphere.

To facilitate a better understanding of the principal mechanisms governing Hg dispersion and cycling in the environment the multi-model study of mercury atmospheric processes has been performed. This work was organized as a part of Mercury Modelling Task Force organized within the framework of the EU funded GMOS (Global Mercury Observation System) project [www.gmos.eu]. The study includes simulations by four models and uses a large observation dataset (50 sites measuring Hg air concentrations and 124 sites measuring wet deposition flux) from a number of measurement networks. The results of this work are presented in Section 1.3 of the report.

Country-specific trend analysis for PCB-153

Information on long-term trends of HMs and POPs is important for understanding effectiveness of environmental policy in the EMEP countries, in particular, implementation of the Protocols on Heavy Metals and POPs. Last year the work on investigation of long-term trends of POP and HM pollution in the EMEP region with the help of the approach worked out by MSC-E for pollutants with variable reduction rates for the period beginning from 1990 to 2010 was initiated. The results of this analysis (including evaluation of country-specific trends of PAHs represented by “indicator chemical” B[a]P) were contributed to the CLRTAP scientific assessment report [*Maas and Grennfelt*, 2016], to the TFMM assessment report [*Colette et al*., 2016], and to the WGE assessment report [*de Wit et al.,* 2015].

This year the work on the evaluation of trends of POP contamination has been continued. The work was focused at examination of country-specific trends of contamination by PCB-153 (used as indicator compound for PCBs) in the EMEP region on the basis of model results. To do this average

annual means of contamination of the EMEP countries by PCB-153 for the period from 1990 to 2014 were estimated with the help of MSCE-POP regional model. The model used official emission data complemented by expert estimates by *Breivik et al*. [2007].

It should be stressed that for evaluation of trends for PCB-153 (as well as for HCB) a modification of the approach to the trend analysis compared with that for B[a]P and heavy metals is needed. Detailed description of this modification is presented in the report (Section 2.1) including evaluation of number of exponential compounds.

Preparation of PCDD/F congener-specific emission data for modelling

Evaluation of PCDD/F environmental toxicity is under special attention of a lot of national and international organizations, such as CLRTAP, Stockholm Convention, US EPA, German Environmental protection agency (UBA), Swedish Environmental Protection agency (SEPA) and others. This section is devoted to the construction of emission scenarios for PCDD/Fs modelling aimed at closer agreement between model predictions and available measurements.

It is known that emission inventories for PCDD/Fs are subject to essential uncertainties. These uncertainties arise due to uncertainties in both total toxicity of the mixture of 17 toxic PCDD/F congeners and due to uncertainties of congener composition of this mixture. It should be noted also that due to differences in their physical-chemical properties, environmental fate of different PCDD/F congeners differ from one another so that uncertainties in congener composition of the considered pollutants can lead to the inaccuracy of evaluation of PCDD/F toxicity. This is especially important for the evaluation of PCDD/F levels in the environmental media, particularly in soil and seawater.

To construct congener-specific emission scenarios for model evaluation of PCDD/F contamination in the EMEP region, MSC-E has initiated the study on constructing typical congener pattern for various emission sectors. The study is based on the information available in literature. At the initial stage a preliminary analysis of the collected information was done and possible approaches for evaluation of typical congener patterns were proposed. The results of this work are presented in Section 2.2 of the report.

Evaluation of B[a]P contamination in urban/suburban areas

Each year, in accordance with the requirements of POP Protocol, MSC-E performs evaluation of pollution of the EMEP region and transboundary fluxes of persistent organic pollutants including B[a]P as an indicator compound of PAHs. It should be mentioned that the model underestimates air concentrations in urban and suburban areas. This underestimation is conditioned by averaging of air concentrations over the cells of modelling grid. The comparison of modelled concentrations with measurements from the EU database AirBase and measurement data from the UNEP Stockholm Convention Global Monitoring Plan (SC GMP) Data Warehouse shows that the model underestimates

B[a]P concentrations in urban/suburban regions from 3 to 5 times. However, evaluation of highly populated areas (including cities) is now in the focus of attention of the world community.

At the first stage contamination in cities with high population density in the Czech Republic (Prague and Ostrava regions) for 2013 was investigated. This year was selected for the analysis since a lot of measurement data for this year were available. In addition, to make the results of the present study consistence with the results of evaluation of Cd contamination obtained earlier for the Czech Republic (see [*Ilyin et al*., 2012]), calculations were provided for 2007 with resolution 5×5 km^2.

In the current year the work on the elaboration of regression model for evaluation B[a]P air concentrations in urban areas is initiated. For the evaluation of urban concentrations regression model using modelling results together with emission data and some meteorological parameters (wind speed) is applied. In future to refine estimates of B[a]P air concentrations for urban areas further improvement of regression model is required, namely, inclusion of additional meteorological and geophysical parameters influencing urban air concentrations (e.g. relief data, atmospheric stability, mixing layer height, etc.). The results of this work are presented in Section 2.2 of the report.

Short description of all above results is given in EMEP Status Reports 2016 [*Gusev et al*., 2016, *Ilyin et al,* 2016]. This report contains more detailed presentation of the above studies complemented by some additional results and technical details describing used approaches.

1. HEAVY METALS

This section is focused on description of approach aimed at correction of parameterization of heavy metal re-suspension from soils. The modelling results based on original and corrected versions of the parameterization are compared. Brief description of this approach is described in the EMEP Status Report 2/2016 [*Ilyin et al.*, 2016]. Besides, the changes in spatial distribution of lead pollution levels and total deposition to the EMEP countries in 2014 are discussed.

1.1. Update of re-suspension scheme of heavy metals

There are three main groups of sources responsible for heavy metal pollution levels in the EMEP region. First of all, these are primary (direct anthropogenic) emission sources such as industry, transport, energy production etc. Another type of sources is so-called secondary emissions. They include re-suspension of wind-blown dust containing previously deposited metals, and natural emission and re-emission of gaseous form of mercury. Finally, some contribution is made by sources (both anthropogenic and secondary) located outside the the EMEP region.

Parameterization of re-suspension of particulate metals (e.g., Pb and Cd) included in the MSCE-HM model is described in [*Gusev et al,* 2006]. It is assumed that re-suspension takes place from agricultural lands in autumn and spring, urban territories and bare lands (mainly, deserts of the northern part of Africa and Middle East). Vertical flux of wind blown dust F_d is calculated taking into account soil texture and meteorological conditions (friction velocity and soil moisture). Flux of heavy metals F_m is a product of dust flux and concentration of metals in topsoil C_{soil}:

$$F_m = F_d \cdot C_{soil} \qquad [1.1]$$

Concentrations of heavy metals in topsoil are derived data obtained in the framework of FOREGS project [http://weppi.gtk.fi/publ/foregsatlas/index.php], aimed at surveying chemical composition of environmental media such as soil, stream water and sediments. However, sampling was carried out presumably in regions without known sources of contamination. In order to take into account long-term accumulation previously deposited heavy metals, it was assumed that actual concentrations in soil were higher than those observed in background environment. Therefore, so-called enrichment factor was introduced:

$$F_m = F_d \cdot C_{soil0} \cdot (1 + EF) \qquad [1.2]$$

Here C_{soil0} –content of heavy metals in background soils, and *EF* – enrichment factor. When *EF* is zero, natural emission flux of the metals is calculated. Since enrichment is caused by pollution of anthropogenic origin, it has been assumed that EF is spatially distributed in proportion to total deposition from anthropogenic emission sources in the EMEP region:

$$F_m = F_d \cdot C_{soil0} \cdot (1 + D_a \cdot k) \qquad [1.3]$$

Where D_a is normalized deposition form anthropogenic sources averaged over two recent decades, and k – coefficient of proportionality. This coefficient is uniform over the space but differs for the considered land-cover categories. The value of the coefficient is selected so that satisfactory agreement between modelled and observed levels is gained.

The use of wind re-suspension in modelling of heavy metal atmospheric transport and deposition helps to improve modelling results compared to measurements. For example, model simulations for 2013, performed with the usage of anthropogenic emissions only resulted to significant (by 60-70% on average) underestimation of the observed levels both for annual mean concentrations in air and wet deposition fluxes (Fig. 1.1, Table 1.1). When re-suspension of heavy metals is included, the agreement between modelled and observed levels significantly improved (Fig. 1.1, Table 1.1).

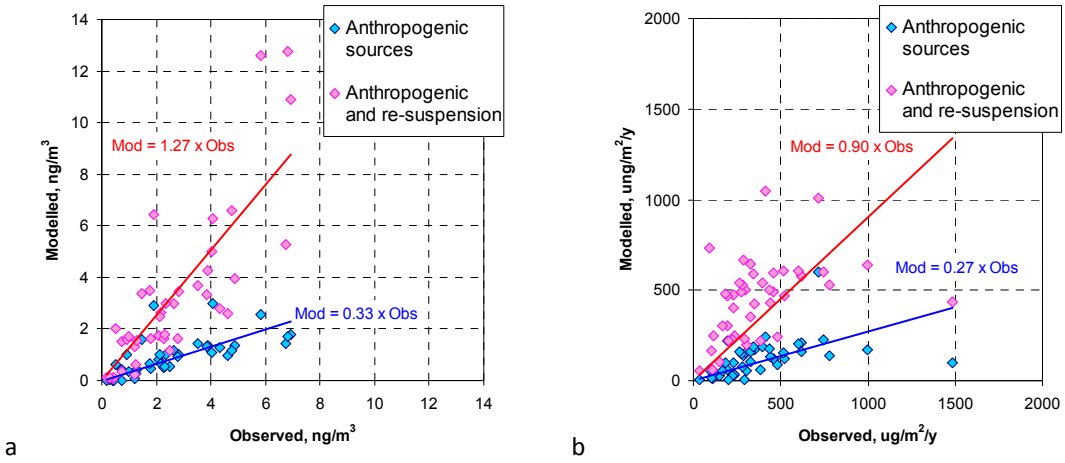

Fig. 1.1. *Modelled and observed annual mean lead concentrations in air (a) and annual wet deposition fluxes (b) in the EMEP region in 2013*

Table 1.1. *Main statistical indicators of agreement between annual modelled and measured levels of air concentrations and wet deposition fluxes of lead in 2013*

	Without re-suspension		With re-suspension	
	C_{air}	Wet Dep	C_{air}	Wet Dep
Relative bias, %	-64.0	-68.2	22.2	24.6
Correlation coefficient	0.66	0.45	0.82	0.45
NRMSE	0.85	0.93	0.74	0.58
F2, %	15	20	73	79
F3, %	45	38	88	100

C_{air} – concentration in air

Wet Dep – wet deposition flux

NRMSE – Normalized Root Mean Square Error

F2 – fraction of values fitting to factor of 2 difference

F3 – fraction of values fitting to factor of 3 difference

However, although the inclusion of re-suspension in modelling resulted to the improvement of the model performance in 'general', at some stations and in some periods it led to overestimation of the observed levels. For example, annual mean air concentrations of lead at the Dutch and Belgium stations were overestimated by 2-3 fold. Concentrations or deposition fluxes in individual periods of time also exhibit high peaks caused by re-suspension and not confirmed by observed levels, for example at stations in Germany and the United Kingdom (Fig. 1.2).

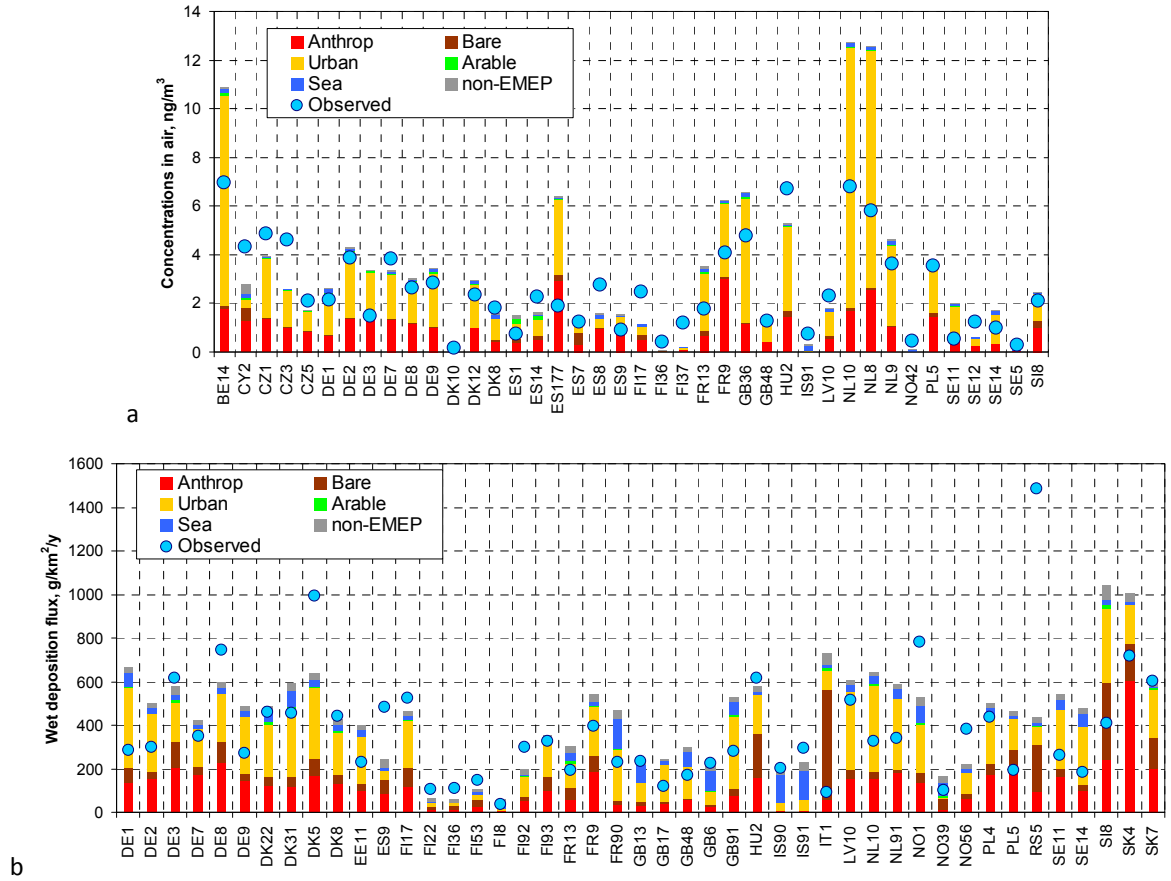

Fig. 1.2. *Modelled and observed concentrations of lead in air (a) and wet deposition fluxes (b). Modelled values are split into contributions from different types of sources: anthropogenic emission, re-suspension from urban, bare, arable lands and sea surface, and from non-EMEP sources*

Taking into account complexity of physical description of re-suspension process and limited input data, calculated re-suspension flux of heavy metals is subject to uncertainties. Possible reasons of the overestimation of re-suspension in particular period at some stations were overestimation of dust flux and overestimation of heavy metal concentrations in soil (enrichment factor).

Large re-suspension of dust particles taken place in the eastern part of Ukraine in 2007 was used as a basis for evaluation of wind re-suspension scheme for agricultural lands [*Shatalov et al*., 2012]. Atmospheric transport of fine particles from this country let to short-term rise of PM10 and PM2.5 concentrations measured at stations in Czech Republic, Slovakia, Germany, the Netherlands and the United Kingdom [*Birmili et al.,* 2008; *Bessagnet et al.,* 2007]. The advantage of these data is explained by the fact that both source area of dust particles and measurement stations which fixed

elevated levels of particulate matter from this area are located within the EMEP modelling domain. However, it is hard to apply the same approach for validation of dust suspension from deserts in Africa. Even if outbreaks of Sahara dust are often observed from satellites and by the dust particles are measured by stations in southern Europe, the source area is located partly or fully outside the EMEP modelling domain. Application of global-scale modelling would be helpful for evaluation of dust suspension and transport to Europe from the northern and eastern parts of Africa.

Another source of uncertainty is enrichment factor. Direct measurements of this parameter have not found been in literature, and thus this parameter is difficult to validate. This chapter is focused on adjustment of spatial distribution of this factor in order to remove the most significant overestimation at some stations caused by re-suspension.

Contribution of re-suspension from different types of land cover was determined (Fig. 1.2). As seen, the major contributor is made by type 'urban'. Besides, type 'bare lands' is also important contributor to simulated wet deposition fluxes. Therefore, most likely, that current contribution of re-suspension from urban territories should be diminished to achieve better agreement between modelled and observed levels.

In order to determine the regions, where enrichment factor should to be changed, source-receptor calculations were performed. Contributions of re-suspension from different regions of the EMEP domain were established. For example, at the station DE1 more than a half of contribution of re-suspension from urban areas came from German lands Schleswig-Holstein and Nordrhein-Westfalen, Denmark and the Netherlands (Fig. 1.3a). Wet deposition at the same station was formed partly from the same sources (Nordrhein-Westfalen, the Netherlands) and partly from more remote sources (Belgium, the United Kingdom, the Czech Republic) (Fig. 1.3b). Similar information was also obtained for other stations.

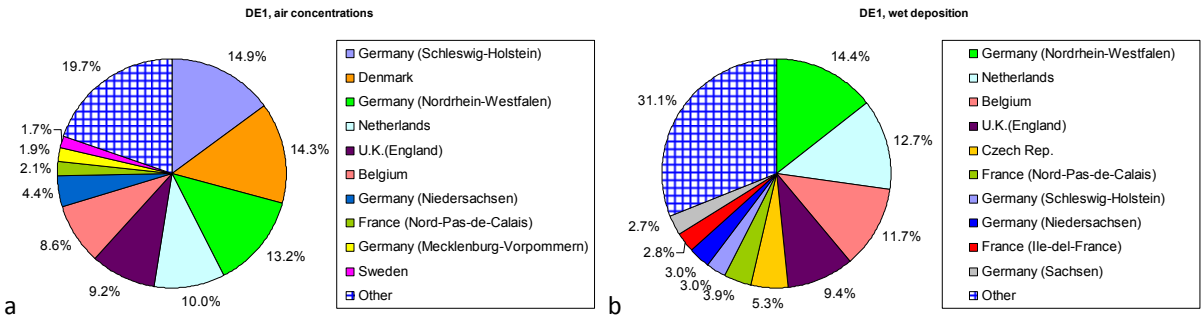

Fig. 1.3. *Contributions of different source regions to calculated component of re-suspension from urban territories for annual mean concentrations of lead in air (a) and wet deposition (b) at station DE1 (Westerland, Germany) in 2013*

On the base of calculated contributions of different regions increasing or decreasing coefficients for each region were established using a method of least squares. Minimum of the sum *S* of squared differences between modelled and measured values was found:

$$S = \sum_{i=1}^{N_{st}} \left(M_i - O_i\right)^2 \qquad [1.4]$$

Here O_i and M_i – normalized observed and modelled values of annual mean concentration in air or wet deposition flux at ith station, and N_{st} – number of stations involved in a process of adjustment.

Each modelled value can be presented as a sum of 'constant' contributors (C_i), i.e., those which are not intended to be adjusted (anthropogenic sources, re-suspension from sea surfaces, arable lands, etc.) and 'adjustable' contributors, i.e. re-suspension from urban or bare areas (U_i). Therefore, [1.4] is changed to the following expression:

$$S = \sum_{i=1}^{N_{st}} \left(C_i + x_1 \cdot U_{i,1} + x_2 \cdot U_{i,2} + \ldots + x_{Nsrc} \cdot U_{i,Nsrc} - O_i\right)^2 \qquad [1.5]$$

Here x_1, x_2, …x_{Nsrc} are multiplication factors by which re-suspension from each region has to be increased or declined, and *Nsrc* – number of considered regions. In order to find thee factors we minimize expression [1.5] by taking partial derivatives by x_1, x_2 … x_{Nsrc} and equating them to zero. Hence, the following the system of linear equations is obtained:

$$\begin{cases} \sum_{i=1}^{N_{st}} C_i \cdot U_{i,1} + \sum_{i=1}^{N_{st}} U_{i,1}^2 \cdot x_1 \quad + \quad \sum_{i=1}^{N_{st}} U_{i,1} \cdot U_{i,2} \cdot x_2 + \ldots + \sum_{i=1}^{N_{st}} U_{i,1} \cdot U_{i,Nsrc} \cdot x_{Nsrc} - \sum_{i=1}^{N_{st}} O_i \cdot U_{i,1} = 0 \\ \sum_{i=1}^{N_{st}} C_i \cdot U_{i,2} + \sum_{i=1}^{N_{st}} U_{i,1} \cdot U_{i,2} \cdot x_1 + \sum_{i=1}^{N_{st}} U_{i,2}^2 \cdot x_2 + \ldots \; + \quad \sum_{i=1}^{N_{st}} U_{i,2} \cdot U_{i,Nsrc} \cdot x_{Nsrc} - \sum_{i=1}^{N_{st}} O_i \cdot U_{i,2} = 0 \\ \ldots\ldots\ldots\ldots\ldots\ldots\ldots\ldots \\ \sum_{i=1}^{N_{st}} C_i \cdot U_{i,Nsrc} + \sum_{i=1}^{N_{st}} U_{i,1} \cdot U_{i,Nsrc} \cdot x_1 + \sum_{i=1}^{N_{st}} U_{i,2} \cdot U_{i,Nsrc} \cdot x_2 + \ldots + \sum_{i=1}^{N_{st}} U_{i,Nsrc}^2 \cdot x_{Nsrc} - \sum_{i=1}^{N_{st}} O_i \cdot U_{i,Nsrc} = 0 \end{cases} \qquad [1.6]$$

The system of linear equations was solved by Gauss method and x_1, x_2 … x_{Nsrc} values were found. However, this method does not prevent originating negative values of roots of this system. Values of x_i below zero are not feasible, since re-suspension flux must not be negative. In order to suppress negative values, penalty functions are introduced in [1.4]:

$$S = \sum_{i=1}^{N_{st}} \left(M_i - O_i\right)^2 + \sum_{j=1}^{Nsrc} w_j \cdot \left(1 - x_j\right)^2 \qquad [1.7]$$

In [1.7] w_i are penalty functions which are individual for each region. The higher value of w_i, the lower chance of appearing of negative values, but also the higher deviation of the minimum of the

sum of squares. Numerical experiments were carried out with various values of w_i, and it was found that their optimum values were 0.1 for most of regions.

Original and adjusted fields of enrichment factors for lead over urban areas are demonstrated in Fig. 1.4. As seen, the major changes took place in the Benelux region and the north-western lands of Germany. Some decrease is also noted for the United Kingdom, Spain, the southern part of France and southern Sweden. Some increase of EF takes place in southern part of Germany, the Czech Republic, Hungary and the Balkan region.

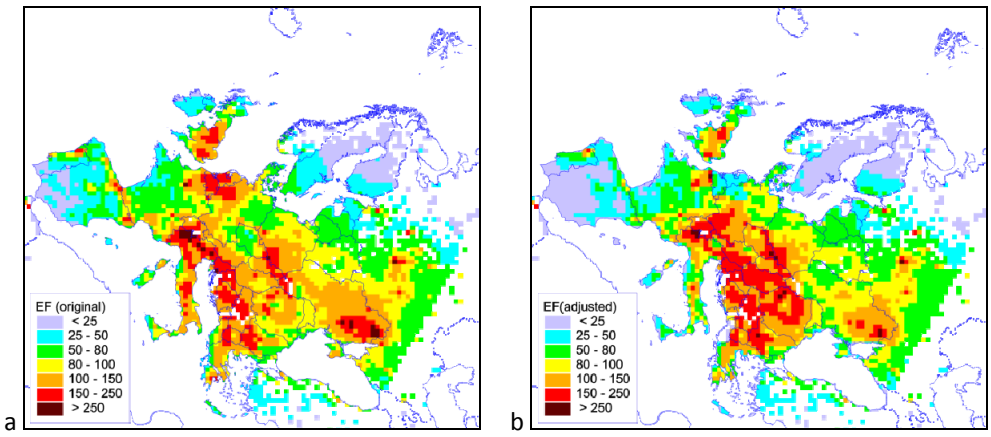

Fig. 1.4. *Spatial distribution of original (a) and adjusted (b) enrichment factor for lead concentrations in soils of urban land-cover type*

Adjustment of enrichment factors field led to decrease of discrepancies between modelled and observed concentrations in air and wet deposition fluxes of lead in 2013 (Table 1.2). Mean relative bias declined from 22 to –6% for concentrations in air and from 25% to -3% for wet deposition flux. Spatial correlation coefficients increased and NRMSE decreased which also meant the improvement of modelling results for the EMEP region as a whole.

Table 1.2. *Main statistical indicators of agreement between annual modelled and measured levels of air concentrations and wet deposition fluxes of lead in 2013*

	Original		Adjusted	
	C_{air}	Wet Dep	C_{air}	Wet Dep
Relative bias, %	22.2	24.6	-5.8	-3.1
Correlation coefficient	0.82	0.45	0.87	0.48
NRMSE	0.74	0.58	0.37	0.63
F2, %	73	79	75	87
F3, %	88	100	90	96

C_{air} – concentration in air

Wet Dep – wet deposition flux

NRMSE – Normalized Root Mean Square Error

F2 – fraction of values fitting to factor of 2 difference

F3 – fraction of values fitting to factor of 3 difference

Figure 1.5 (a, b) allows to identify stations where decline of discrepancies between modelled and observed values takes place. The most obvious positive effect for concentrations in air is noted for stations in the Netherlands and Belgium (Fig. 1.5, a). Positive changes are also seen for French, British, Czech, and Hungarian stations. Improvement of agreement between modelled and observed wet deposition fluxes is also noted for stations in France, the United Kingdom, the Netherlands, Sweden and Slovenia (Fig. 1.5, b).

For some stations the overestimation of observed levels remained significant. At some stations (ES178 for concentrations in air, PL5 for wet deposition) observed levels are even somewhat lower than the value of anthropogenic contribution. Overestimation of wet deposition fluxes at the station SI8 (Slovenia) is explained by large contribution of re-suspension from desert lands in the northern part of Africa, where coefficient of enrichment is not high and, therefore, its adjustment has small effect on the modelled levels. One of possible reason for this is that global mean values of lead concentrations in soils for this region are used in modelling. Therefore, data on heavy metals soils based on field measurements in this region could be helpful for improvement of model assessment for the southern part of Europe. Calculated wet deposition fluxes at some German stations remained overestimated compared to observations, although the adjustment favoured some improvement at DE1, DE2 and DE9.

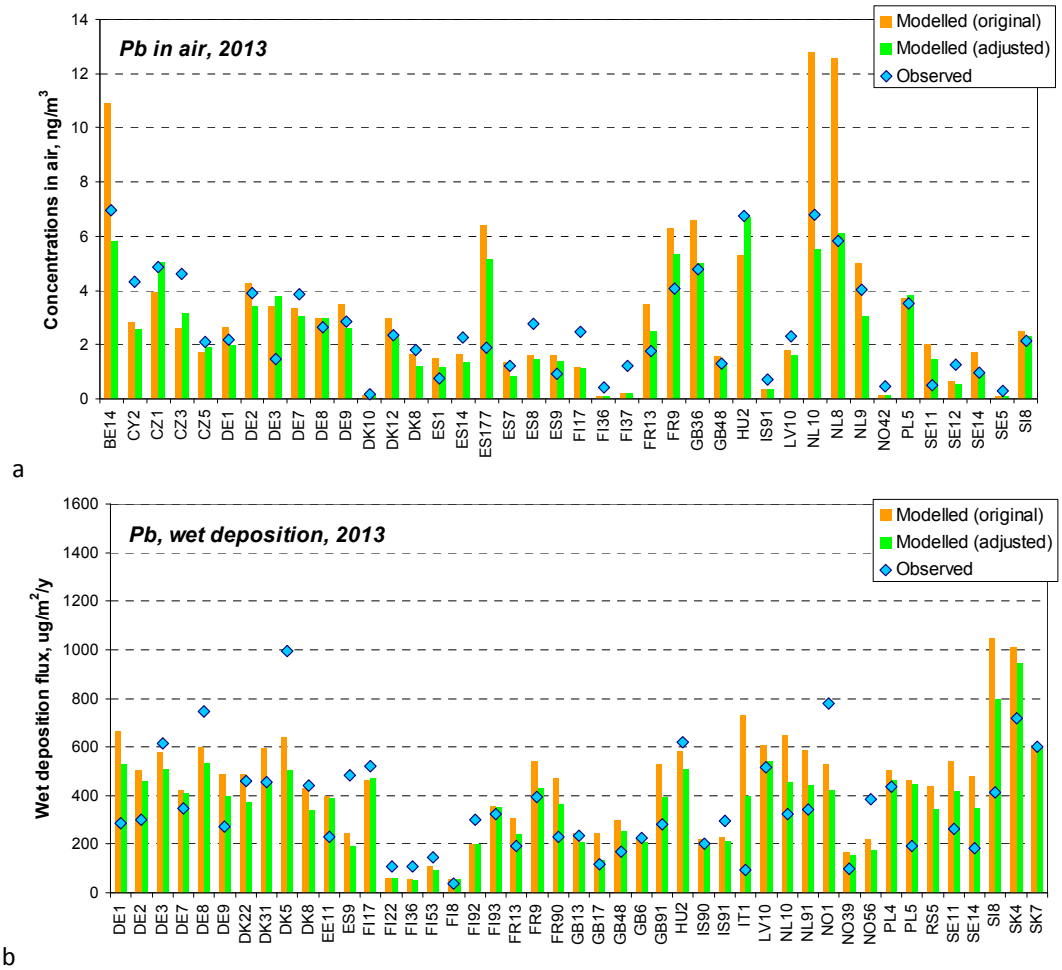

Fig. 1.5. *Modelled (original and adjusted) and observed concentrations in air (a) and wet deposition (b) of lead in 2013*

At some stations application of the adjustment led to significant improvement of short-term variability of calculated compared to observed values. For example, most of high peaks of calculated concentrations of lead in air at station NL9 were removed (Fig. 1.6). Due to the adjustment annual relative bias for this station reduced from 24% to 0.2%, and correlation coefficient increased from 0.45 to 0.53.

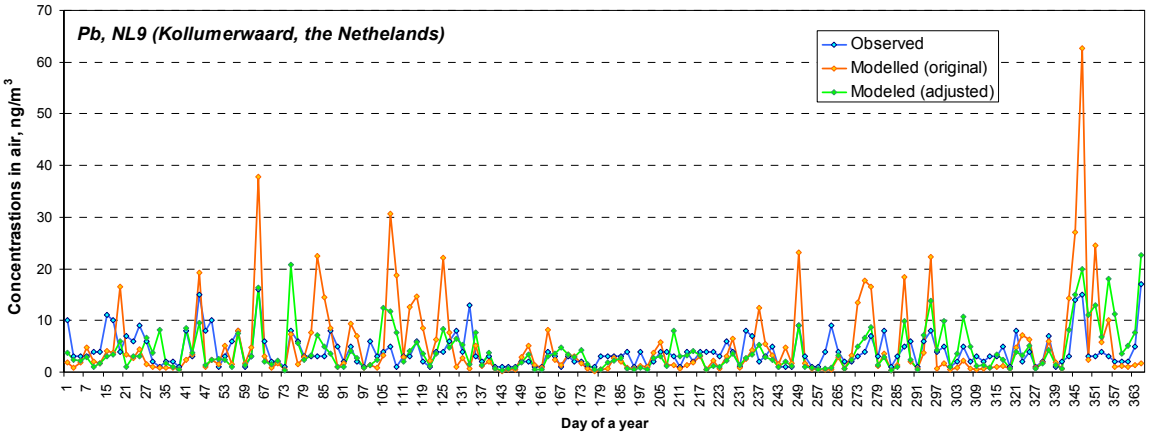

Fig. 1.6. *Daily mean modelled (original and adjusted) and observed concentrations of lead in air in 2013 at station NL9 (Kollumerwaard, the Netherlands)*

However, at some other stations the adjustment has no significant effect on short-term variability of modelled levels. For example, high modelled peaks of wet deposition fluxes in middle of May, beginning of September and in December at the station DE9, not confirmed by observations, have not changed much because of the adjustment (Fig. 1.7a). Another example is the British station GB48, where similar situation takes place in March and October (Fig. 1.7b). Possible reason for this could be explained by uncertainties of parameterization of wind-blown dust suspension. Wind-blown dust suspension (and, thus, re-suspension of heavy metals) is initiated when two major conditions are met: dry soil and strong wing. Probably, in the noted periods the parameterization predicts the existence of dust suspension whereas real meteorological conditions are not favourable for it. Therefore, adjustment of enrichment factors is likely not efficient for improving modelling results in these situations. This problem has to be further investigated.

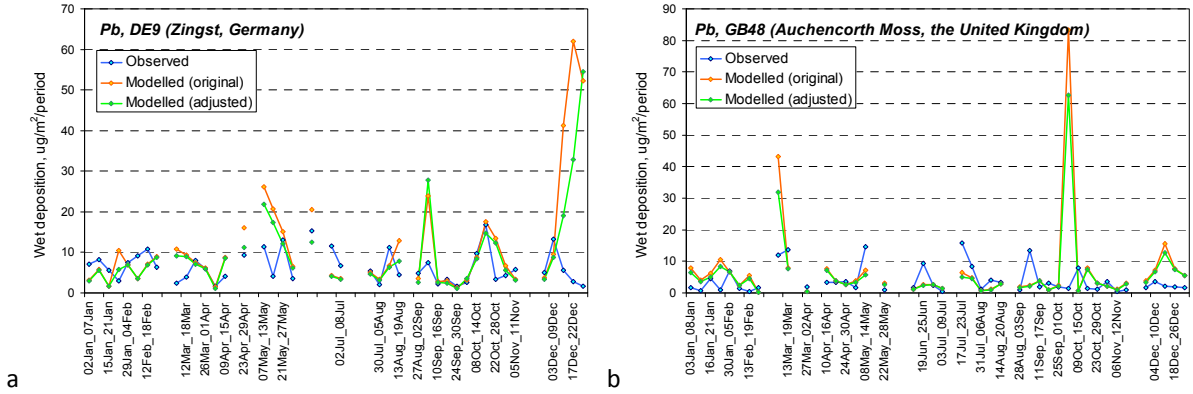

Fig. 1.7*. Weekly mean modelled (original and adjusted) and observed wet deposition fluxes of lead in 2013 at stations DE9 (Zingst, Germany) (a) and GB48 (Auchencorth Moss, the United Kingdom) (b)*

Data on concentrations in street dust measured in various cities over the globe are available in scientific literature. Table 1.3 provides short overview of concentrations of lead observed in Europe, Eastern Asia (China), Middle East and north of Africa.

Table 1.3. *Concentrations of lead in street dust measured in different cities over the globe*

Region	Concentration range, ug/g	Reference
Various cities of China	54 - 383	*Li et al.,* 2013 and references therein
Utrecht (Netherlands)	325*	*Amato et al.*, 2013
Barcelona (Spain)	125*	*Amato et al.*, 2013
Mieres (Spain)	318	*Loredo et al.*, 2004
Aviles (Spain)	514	*Ordonez et al.*, 2003
Madrid (Spain)	1927	*De Miguel et al.*, 1997
Kavala (Greece)	301	*Christoforidis and Stamatis*, 2009
Oslo (Norway)	180	*De Miguel et al.*, 1997
Gela (Italy)	30-124 (< 20 um)	*Manno et al.*, 2006
Sarajevo (Bosnia-Herzegovina)	44.82 – 620.0	*Razanica et al*, 2014
Hilla (Iraq)	430.8 - 738.4	*Al-Fatlawi and Al-Alwani,* 2012
Istanbul (Turkey)	240.50	*Sezgin et al.*, 2003
Jeddah (Saudi Arabia)	58.64- 97.36	*Khoder et al.*, 2012
Arak (Iran)	39.62	*Ghadimi et al.*, 2013
Cairo (Egypt)	92.38	*Journal of American Science,* 2012;8(6)
Aswan (Egypt)	308	*Rashed*, 2008.

* - estimated from equilibrium loadings of PM10 and lead

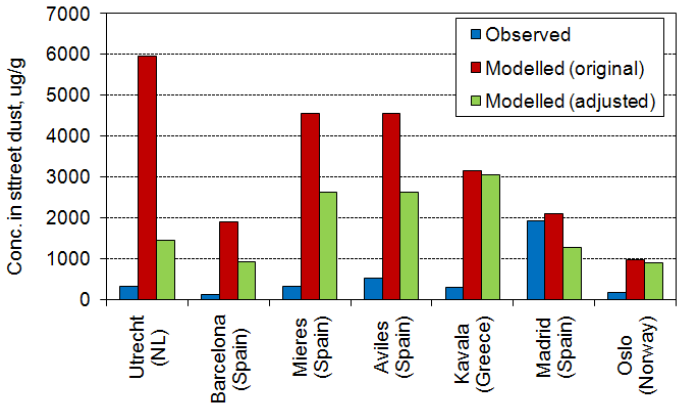

Fig. 1.8. *Modelled (original and adjusted) and observed concentrations of lead in urban street dust in European cities*

Concentrations in urban dust were calculated using data on soil concentrations and adjusted enrichment factors (Fig. 1.8). These concentrations were compared with data on concentrations in street dust measured in European cities (Table 1.3). As seen, original estimated concentrations of lead in street dust significantly (by an order of magnitude) exceed those derived from measurements. The adjustment led to some decrease of the modelled concentrations, but they

remained still much higher than the observed ones. Possible reason for this could be connected with underestimated flux of re-suspended dust from urban surfaces. If the dust flux should be several times higher, the adjustment procedure should lead to the lower enrichment factor (see formula [1.1]). However, to test this hypothesis the comparison of concentrations of modelled primary particles with observed particulate levels in cities is needed.

The presented approach to correction of enrichment factors was applied to analysis of lead pollution levels in 2014. Correction of enrichment factor resulted to changes of annual total deposition and mean air concentrations from -50% to +15% over the EMEP countries (Fig. 1.9). The most significant reduction of the pollution levels took place in the western and south-western parts of Europe, while in the eastern and central part the increase of pollution levels is noted. In particular, the highest decline of deposition and concentrations is noted for the Netherlands, Spain and Belgium (Fig. 1.10). The most significant increase is seen for the Czech Republic. It is interesting to note that magnitudes of concentration and deposition changes are different and for some countries even opposite. The main reason for this is fact that air concentrations are related to only lower (~70m) model layer, while deposition characterizes entire of the atmosphere from the surface to the top of clouds, i.e., all model layers where precipitation occur.

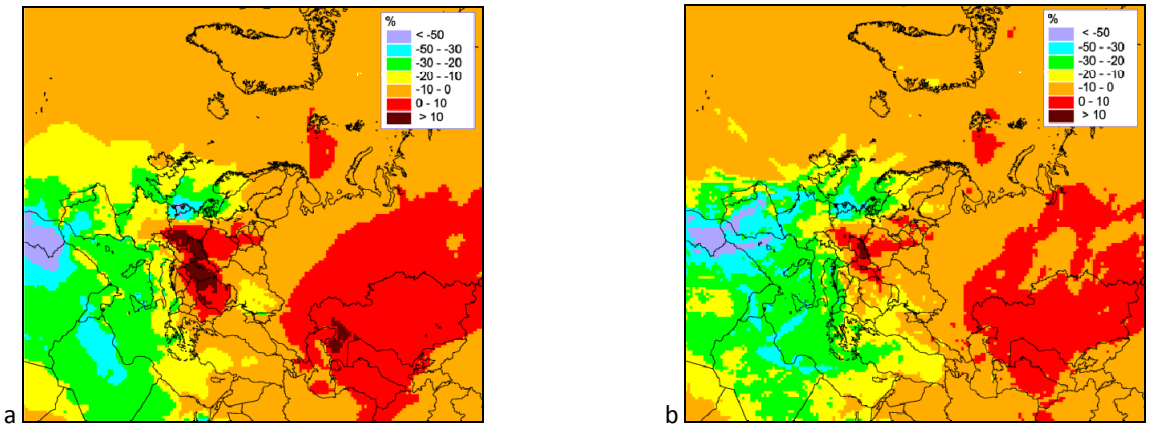

Fig. 1.9. *Relative change of lead annual total deposition (a) and annual mean concentration in air (b) in 2014 due to correction of enrichment factor. Positive change means increase, and negative – decrease of pollution levels*

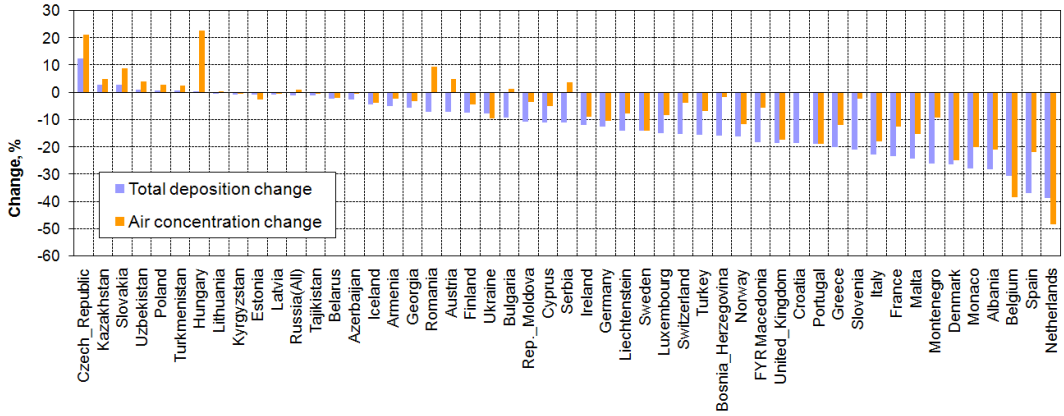

Fig. 1.10. *Change (%) of country-mean total deposition and surface air concentrations due to correction of enrichment factor. Positive change means increase, and negative – decrease of pollution levels*

Modelling results based on the corrected emission factors for 2014 were evaluated via comparison with monitoring data. Statistical indices characterizing model performance demonstrate that the correction led to improvement of modelling results. In particular, spatial correlation coefficients increased and NRMSE declined (Table 1.4). Besides, mean relative bias for air concentrations reduced from 11.7 to 4.3%. The bias for wet deposition declined from 8.6 to -10%, which mean that some overestimation of observed levels changed to some underestimation.

Table 1.4. *Main statistical indicators of agreement between annual modelled and measured levels of air concentrations and wet deposition fluxes in 2014*

	Concentration in air		Wet deposition flux	
	Original	Corrected	Original	Corrected
Mean relative bias, %	11.7	4.3	8.6	-10.0
Correlation coefficient	0.76	0.82	0.44	0.50
NRMSE	0.5	0.4	0.7	0.6
F2, %	82.9	88.9	65.7	77.1
F3, %	97.1	97.2	94.3	94.3

C_{air} – concentration in air
Wet Dep – wet deposition flux
NRMSE – Normalized Root Mean Square Error
F2 – fraction of values fitting to factor of 2 difference
F3 – fraction of values fitting to factor of 3 difference

Figures 1.11 demonstrate comparison of original and corrected modelled concentrations in air and wet deposition fluxes with observed levels. Considerable improvement of modelling of concentrations in air is noted for stations in the Netherlands, Belgium, Sweden and some stations in Germany. At other stations the improvement was not high, or even some insignificant increase took place. For wet deposition improvement is noted for stations in France.

On the base of the analysis it is possible to conclude that the adjustment of enrichment factor favoured decrease of discrepancies between the modelling results and observations for the EMEP region as a whole and for particular monitoring stations. Regions where the improvement of model assessment of lead pollution levels took place include the Netherlands, Belgium, France and the United Kingdom. However, there is importance of further investigation and improvement of issues related to wind re-suspension. First of all, effects of meteorological parameters (namely, soil wetness and friction velocity) on wind suspension have to be further studied. Besides, information on soil concentrations in the desert regions of Africa and Asia is needed. Finally, evaluation of magnitude of dust flux in cities would favour improvement of modelling results.

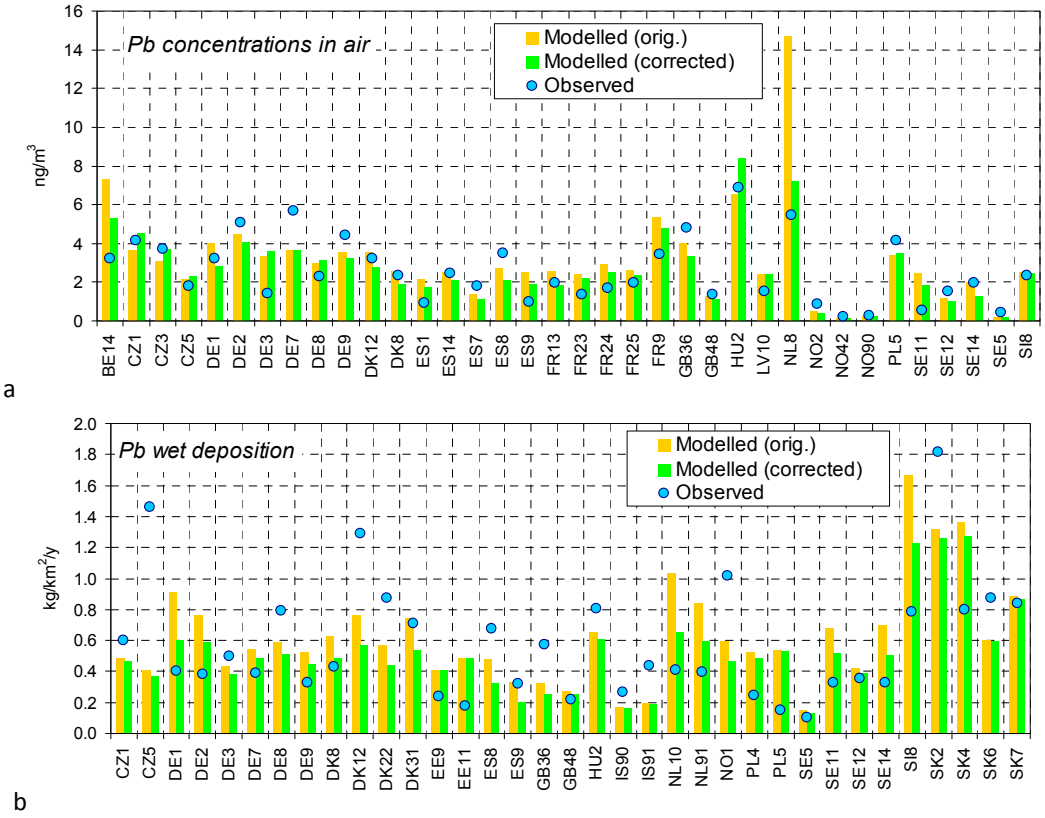

Fig. 1.11. *Concentrations in air (a) and wet deposition fluxes (b) of lead, modelled with original and corrected enrichment factor and observed at the EMEP monitoring stations in 2014*

1.2. Evaluation of modelling results vs. observations

This section gives overview the main sources of uncertainties of modelling results, such as emissions, measurement data and model parameterizations. Besides, special attention is paid to verification of modelling results against monitoring data. Briefly these issues are already reflected in the EMEP status report 2/20116 [*Ilyin et al.*, 2016]. In this section the presented comparison is more detailed.

Uncertainties of the modelling results are combined of three components: uncertainties of emission data, of monitoring information and of the model as such. Uncertainties of anthropogenic emission data are estimated and reported by some EMEP countries [*CEIP*, 2016]. As seen, the uncertainties of annual emission data of lead, cadmium and mercury reaches almost 500%, 430% and 145%, respectively (Table 1.5).

Monitoring uncertainties occur at different stages of obtaining measurements, such as sampling, transporting, storing, laboratory analysis. At present only uncertainty of laboratory analysis is regularly evaluated during annual laboratory intercomparison tests, undertaken under CCC supervision. Numerical characteristic of analytical uncertainty is relative deviation of concentration, analyzed in a laboratory, from theoretical value. In order to characterize quality of laboratory analysis, so-called Data quality objectives (DQO) was introduced by CCC. For heavy metals DQO are equal to ±15% of high concentrations (typical for background levels in the central and eastern parts

of Europe) and ±25% for low concentrations (typical for Scandinavia). The most recent results of laboratory intercomparison tests for lead and cadmium demonstrated that for most of laboratories quality of the analysis fits DQO criteria [*CCC*, 2015].

Table 1.5. *Uncertainties (%) of the reported emission data in 2014*

2014	Pb	Cd	Hg
Belarus	182	175	107
Belgium	271	231	145
Croatia	136	278	76
Cyprus	95	81	13
Denmark	488	427	91
Estonia	139	130	138
Finland	±28	-30 +31	±21
France	148	28	20
Latvia	78	80	66
Poland	70	70	53
Sweden	18	35	56
United Kingdom	53	-30 to >50	-30 to 50

Model uncertainties have been evaluated in [*Travnikov and Ilyin*, 2005]. It was demonstrated that intrinsic model uncertainty (i.e., uncertainty of the model as such, without effect of emission data) was amounted to ±30-40% for Europe as a whole (Fig. 1.12).

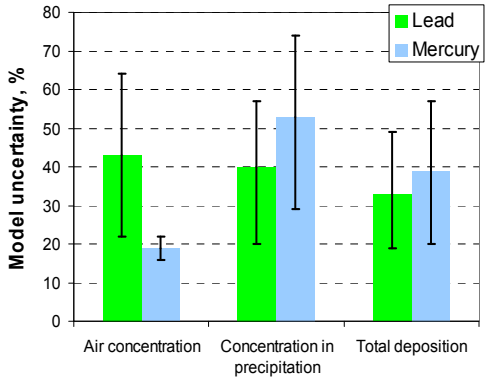

Fig. 1.12. *Averaged for the EMEP region intrinsic (without effect of emission) model uncertainty for aerosol-born metals (lead) and for mercury. Whiskers indicate range of uncertainties over space*

Quality of the model assessment is evaluated via comparison with the available background monitoring data. Values of main statistical indicators used is the comparison for lead, cadmium and mercury are summarized in Table 1.6. These indicators are Mean Relative Bias (MNB), Pearson's correlation coefficient and Normalized Root Mean Square Error (NRMSE). Besides, a share of model-measurement pairs of values differing from each other within 2-fold and 3-fold range (F2 and F3, respectively) is also presented. Scatter plots of modelled vs. observed heavy metal concentrations in air or wet deposition fluxes are presented in Fig. 1.13.

Table 1.6. *Main statistical indicators of agreement between annual modelled and measured levels of air concentrations and wet deposition fluxes in 2014*

	Lead		Cadmium		Mercury	
	C_{air}	Wet Dep	C_{air}	Wet Dep	C_{air}	Wet Dep
Mean relative bias, %	4.3	-10.0	-10.8	-20.7	3.9	31.7
Correlation coefficient	0.82	0.50	0.79	0.46	0.17	0.22
NRMSE	0.39	0.59	0.44	0.53	0.07	0.54
F2, %	89	77	76	77	100	76
F3, %	97	94	88	87	100	100

C_{air} – concentration in air

Wet Dep – wet deposition flux

NRMSE – Normalized Root Mean Square Error

F2 – fraction of values fitting to factor of 2 difference

F3 – fraction of values fitting to factor of 3 difference

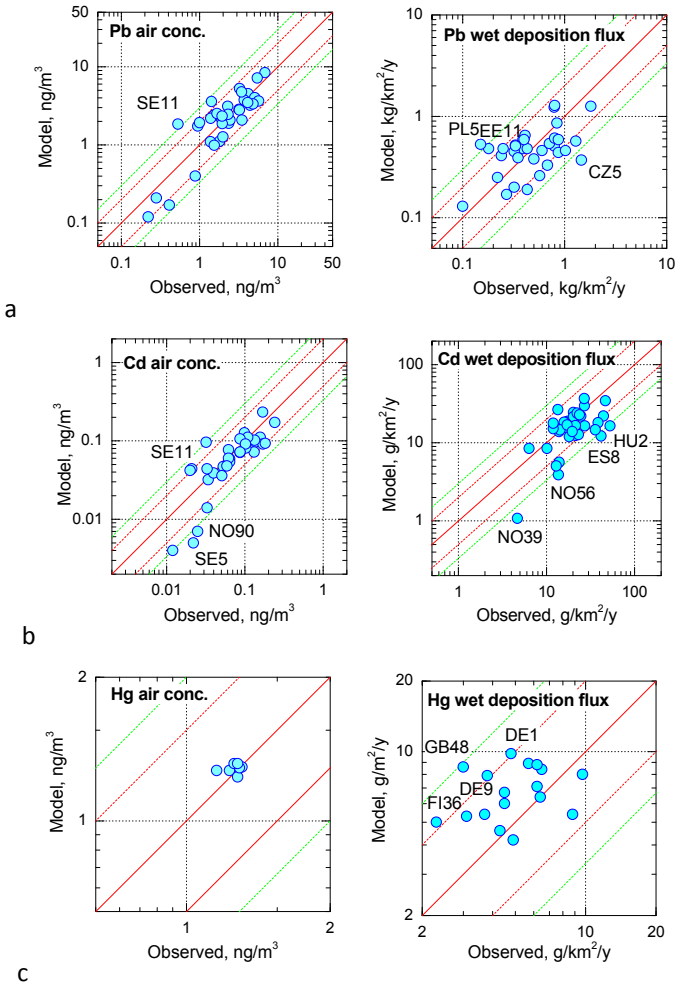

Fig. 1.13. *Modelled vs. observed concentrations in air (left) or wet deposition (right) for lead (a), cadmium (b) and mercury (c) in 2014*

As seen, lead and cadmium air concentrations were reproduced with low relative biases (within ±10%) and with significant correlation coefficients (0.82 and 0.79, respectively). For wet deposition some underestimation is indicated. For lead it is around 10%, and for cadmium – about 20%.

However, correlation for wet deposition of lead and cadmium in 2014 is relatively weak. Value of Pearson's correlation coefficient is very sensitive to outliers. Thus, the main reason of comparatively low correlation is large discrepancies between modelled and observed levels at few particular stations. Most of model-observation pairs of lead and cadmium concentration and deposition values agree within a factor of two.

Magnitude of mercury air concentrations reproduced reasonably well, since MRB is only around 4 % and all modelled and measured pairs of values agree within a factor of two. Correlation coefficient for air concentrations is not high because of very low spatial variability of modelled and observed background mercury levels. This variability is comparable with uncertainties of the model, which results to low correlation. The reason for this is similar to that for lead and cadmium, i.e. discrepancies at some stations.

Maps with modelled pollution fields and measured values at stations allow to demonstrate where the model manages to reproduce observed levels, and where discrepancies between modelled and measure levels occur. Observed air concentrations were reproduced by the model almost in all regions where measurement station were located, namely in France, Spain, Germany, the United Kingdom, Denmark, the Netherlands, the Czech Republic (Fig. 1.14a). At most of stations in these countries the agreement between annual mean modelled and observed air concentrations lay within ±50% (Fig. 1.13a, left). Higher discrepancies were noted for wet deposition fluxes. Satisfactory agreement between modelled and observed wet deposition fluxes took place for most of stations in Germany, Slovakia, Denmark (Fig. 1.14b). Underestimation of lead levels is seen for Spanish, one Norwegian, one British and the Czech stations. For stations in Poland and some stations in Germany and Sweden overestimation of observed wet deposition fluxes is noted (Fig. 1.13a, right).

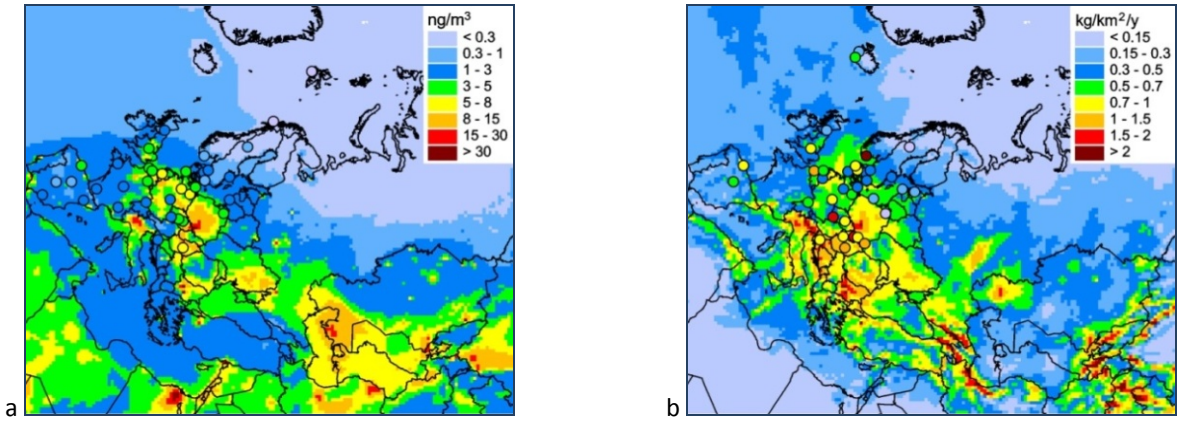

Fig. 1.14. *Spatial distribution of modelled and observed lead concentrations in air (a) and wet deposition fluxes (b) in 2014*

Comparison of modelled and observed concentrations in air and wet deposition fluxes of lead for each station is shown in Fig. 1.15. Modelled values are presented as a sum of contributions of anthropogenic and non-EMEP sources, and of secondary sources from various types of underlying surface (bare lands, urban areas, arable lands and sea surfaces). According to current model parameterizations, two main components are the major contributors of lead levels at stations: anthropogenic sources (2-69%) and re-suspension from urban territories (26-82%) (Fig. 1.15a). At

most of stations the bias between modelled and observed annual mean concentrations is within ±50%. At some stations some overestimation of the observed levels takes place (BE14, FR9, HU2, NL8). Probably, even after correction of enrichment factors the role of re-suspension at these stations is still too high. However, at some other stations (DE7, GB36, ES8, NO2) the model still underpredicts the observed air concentrations of lead. For stations in Sweden both significant underestimation (SE5) and overestimation (SE11) is noted.

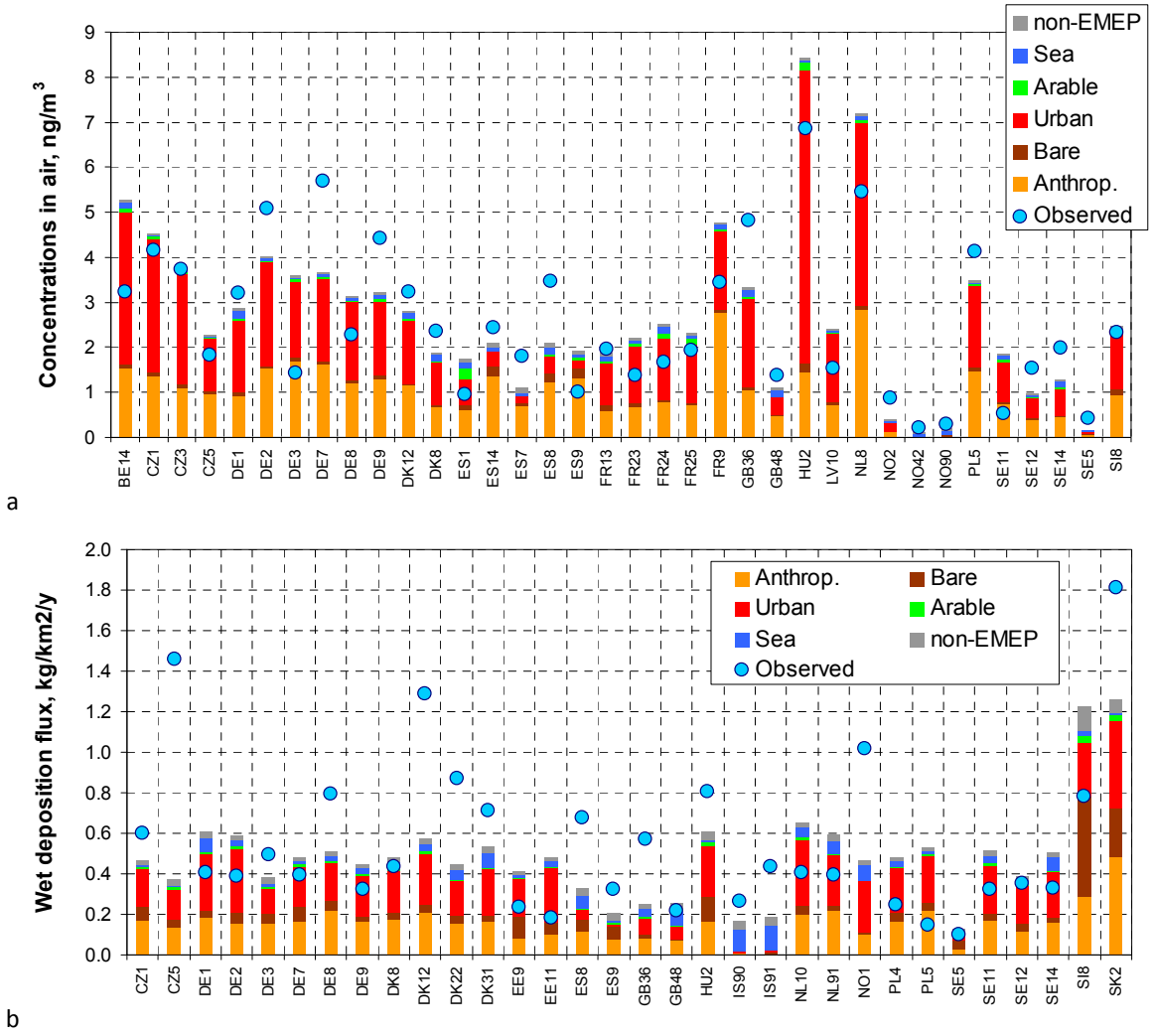

Fig. 1.15. *Modelled annual mean concentrations in air (a) and annual sum of wet deposition fluxes (b) of lead caused by various types of emission sources and observed levels at EMEP monitoring stations*

In addition to anthropogenic emissions and re-suspension from urban areas, re-suspension from bare lands is also important contributor to wet deposition fluxes. The role of this component is especially important at stations located in the southern part of the EMEP domain, where it reaches 41% of total modelled value (Fig. 1.15b). Relative difference between modelled and observed wet deposition fluxes stays within ±50% for most of stations. At some stations the model underestimates observed fluxes. These are stations located in Denmark, one station in Czech Republic, Germany, the United Kingdom and Spain. However, there are some stations where overestimation also takes place. First of all, these are stations in the Netherlands and Slovenia, where the overestimation can be explained by overestimation of contribution of wind re-suspension. Besides, in Poland and in Estonia the modelled

fluxes exceed the observed ones by a factor 1.7-3.5. Even if only anthropogenic sources are considered, the observed levels at Polish station PL5 would remain overestimated. Quality of analytical methods, used by Polish laboratory, is good. Deviations of between theoretical value and value reported by laboratory are negligible [*CCC*, 2016]. Contamination of samples also can hardly be a reason, because it usually leads to high observed levels. Therefore, possible reasons of the overestimation can be associated with uncertainties of the model parameterizations or location of emission sources. This issue can be studied in detail during the forthcoming EMEP case study of heavy metal pollution levels in Poland.

Model performance for air concentrations of cadmium is similar to that for lead. The model reproduced cadmium levels at most of stations in various parts of the EMEP region. In particular, reasonable accuracy (within ±50%) was achieved for stations in the United Kingdom, Belgium, the Czech Republic, Hungary, most of German stations (Fig. 1.16a). Observed air concentrations were underestimated by the model at most of Scandinavian stations (Fig. 1.13b, left). Wet deposition fluxes, simulated by the model, match the observed fluxes within ±50% agreement at most of monitoring stations (Fig. 1.16b). At some monitoring stations observed levels were much higher than the modelled ones. These stations are located in Spain, Norway, Hungary. Besides, the underestimation of observed fluxes is noted for one Swedish and one Slovak station (Fig. 1.13b, right). For one of German stations the model overestimates cadmium deposition levels by almost 70%. Discrepancies at these few stations resulted to relatively low spatial correlation coefficient (Table 1.6).

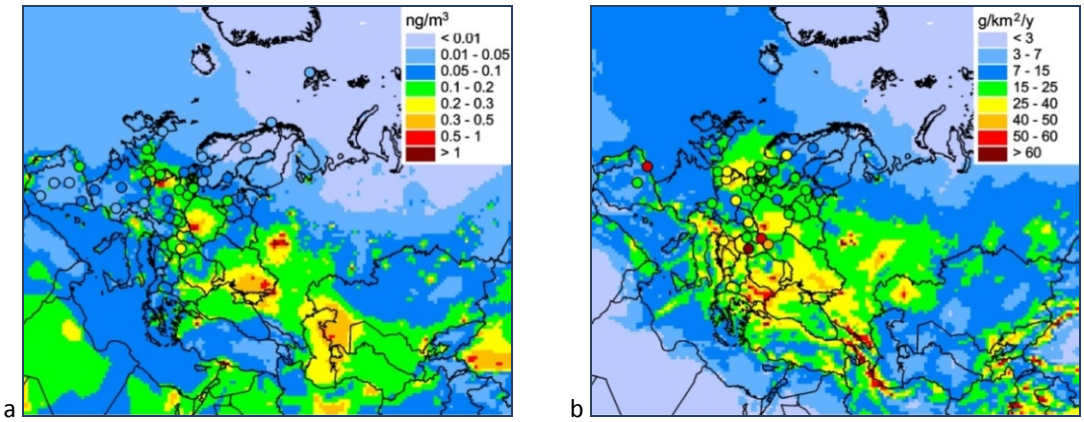

Fig. 1.16. *Spatial distribution of modelled and observed cadmium concentrations in air (a) and wet deposition fluxes (b) in 2014*

Similar to lead, significant contribution to air concentrations of cadmium is made by secondary sources. Its fraction of annual mean concentrations in air varies from 21 to 74% (Fig. 1.17). The contribution of anthropogenic sources ranges from 8 to 84% (Fig. 1.17a). For majority of stations modelled and measured values agree within ±50%. Some overestimation of observed levels is indicated for stations in Spain, Swedish site SE11 and for German site DE3. It is interesting to note that the underestimation for site DE3 occurs even if only anthropogenic sources are considered. This station is located in mountainous region. Most likely, the reason of this discrepancy is the fact that

the model spatial resolution of 50x50 km^2 is insufficient to reproduce peculiarities of atmospheric circulation in regions with complex terrain.

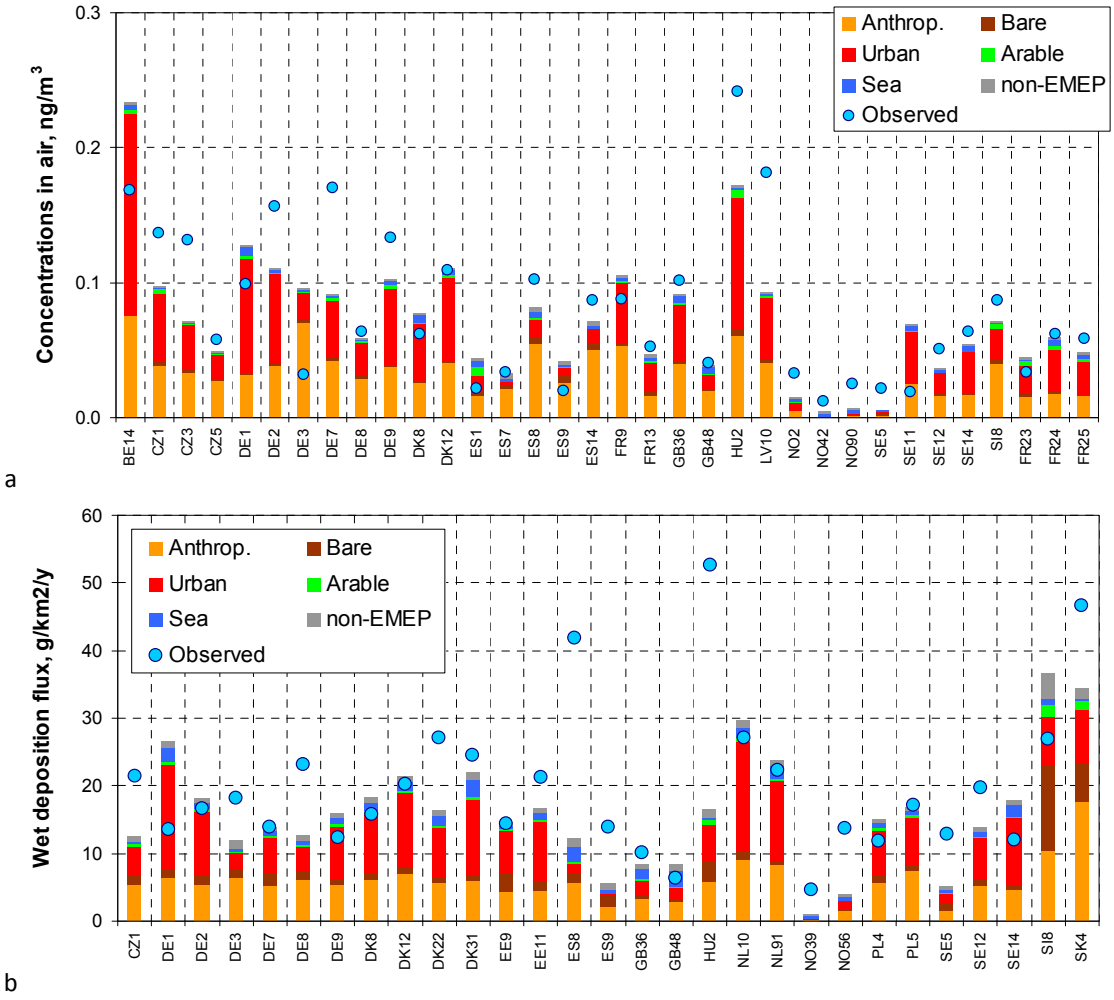

Fig. 1.17. *Modelled annual mean concentrations in air (a) and annual sum of wet deposition fluxes (b) of cadmium caused by various types of emission sources and observed levels at EMEP monitoring stations*

Although at most of stations modelled wet deposition fluxes of cadmium agree with the observed ones with accuracy ±50%, at some stations underestimation of the measured levels occurs (Fig. 1.17b). These are stations in Spain, Norway, Hungary, one station in Sweden and one - in Slovakia. Similar to deposition of lead, often the underestimation takes place in certain periods, while in other periods the agreement between modelled and observed values is satisfactory. For example, weekly sums of modelled and measured wet deposition fluxes at Hungarian station agree well in period from January to April (Fig. 1.18). But in summer the model does not catch high peaks of observed fluxes. There is a need to establish the origin of these high peaks. It could be connected with uncertainties of the model parameterization of scavenging in warm period or with uncertainty of measurements.

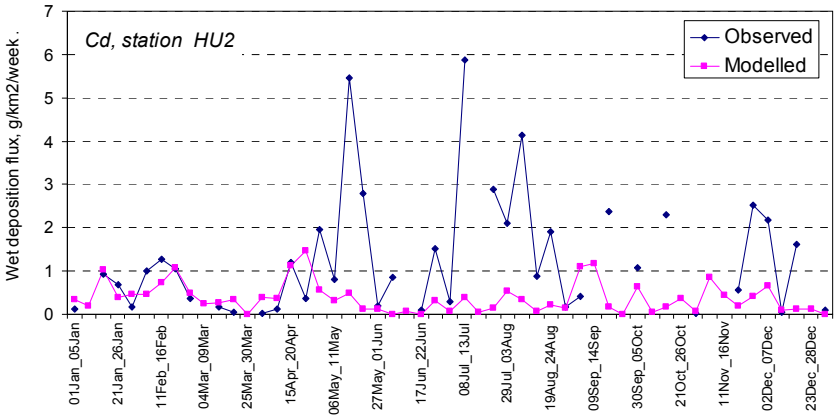

Fig. 1.18. *Time series of modelled and observed concentrations of cadmium at the EMEP station HU2 (Hungary)*

At some stations the model produces values which are considerably higher than the observed ones. One of these stations is DE1 in Germany, where modelled fluxes are two-fold higher than the observed ones. Comparison of modelled and observed time series of weekly deposition sums shows that the large overestimation occurs in some periods, for example, in January/February and in autumn (October/November) (Fig. 1.19). These peaks negatively affect temporal correlation between modelled and observed values. While the correlation between observed fluxes and anthropogenic component of modelled fluxes is around 0.6, the correlation for sum of the components is only 0.2. At the same time, observed levels in some periods are reproduced reasonably well. Therefore, the attention should be paid to analysis of periods when wind re-suspension occurs. For example, parameterization of wind re-suspension, used in the modelling, assumes that re-suspension depends on soil wetness, while the wetness strongly depends on precipitation amount and duration of rainfall. However, in [*Bergametti et al.,* 2016] it was shown that this dependence is much weaker than thought before. Therefore, there is a need to study how the findings of the paper could affect parameterization of wind re-suspension of heavy metals in the EMEP region.

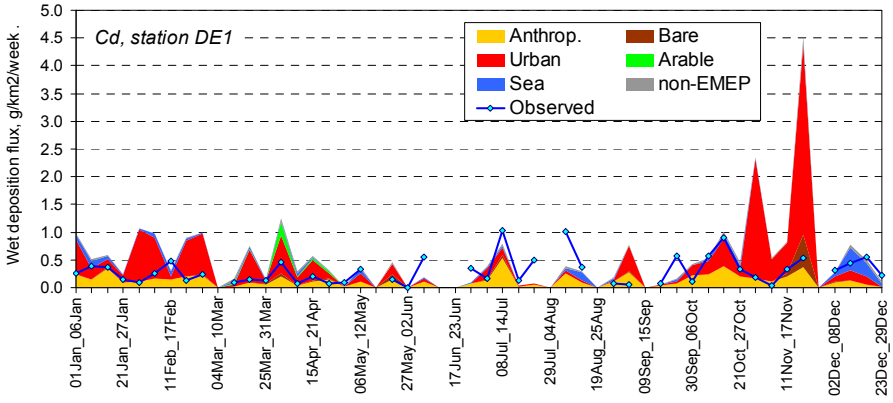

Fig. 1.19. *Time series of modelled concentrations of cadmium in air caused by various types of emission sources and observed levels at station DE1 (Germany)*

There are numerous reasons leading to the discrepancies between modelled and measured levels. To some extent the discrepancies can be explained by modelling uncertainties. Average value of the intrinsic model uncertainty is around ±40% for concentrations in air and ±30% for deposition, which is not enough to explain two-three-fold difference between modelled and observed levels at some

stations. Another possible reason is uncertainties of anthropogenic or secondary emissions. As shown above, in some countries these uncertainties of their national emission can reach as much as 500%. Secondary emission is another source of the model uncertainties. Parameterization of this process is complicated because it requires various environmental data which are often uncertain, such as soil texture and water content and concentration of heavy metals in soils. Introduction of wind re-suspension of heavy metals allows to reach reasonable bias between measured and modelled concentrations and deposition. However, at some stations the contribution of re-suspension is likely too high and leads to the overestimation of observed levels. This year re-calculation of lead enrichment factor for topsoils has been undertaken, which favoured to reduce the overestimation. Nevertheless, further activity on improvement of parameterization of wind re-suspension should be continued. Finally, measurement data also contain uncertainty. Part of this uncertainty is identified by laboratory intercomparison tests. However, information on full measurement uncertainty is needed for interpretation of discrepancies between modelled and monitored heavy metal levels.

Discrepancy between modelled and observed concentrations of mercury lay within ±8% for all stations except SE5, which levels were significantly lower than those at other monitoring stations (Fig. 1.20a). For most of stations modelled wet deposition fluxes matched the observed fluxes within ±50% range (Fig. 1.20b). However, at some stations around two-fold overestimation of the observed fluxes took place. These are two stations in Germany, one in the United Kingdom, one in Finland and in the Netherland.

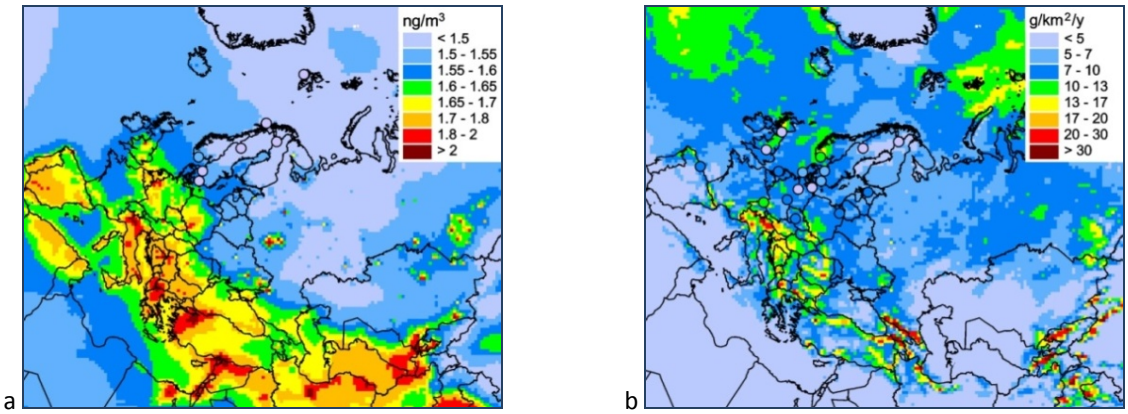

Fig. 1.20. *Spatial distribution of modelled and observed elemental mercury concentrations in air (a) and wet deposition fluxes (b) in 2014*

Uncertainties of modelling, anthropogenic emissions and monitoring data, identified for lead and cadmium, are also relevant for mercury. However, unlike lead and cadmium, another important source of uncertainty of mercury modelling is parameterization of its atmospheric chemical transformations. Te role of chemical reactants as well as products of chemical reactions are still under discussion [*Lin et al*., 2006; *Gustin et al*., 2015]. Another peculiarity of mercury is speciation of anthropogenic emissions. The emission occurs in three forms: relatively inert and long-lived elemental mercury and short-lived particulate and gaseous oxidized mercury forms. Currently information about mercury emission speciation is not officially reported and obtained only in emission expert estimates.

1.3. Multi-model study of mercury atmospheric processes

Oleg Travnikov, Ashu Dastoor, Francesco De Simone, Ian M. Hedgecock, Andrei Ryjkov, Noelle Selin, Shaojie Song

Oxidation chemistry and speciation of mercury in the atmosphere determine its ability to long-term atmospheric transport and deposition to various terrestrial and aquatic regions. Current knowledge on mercury behaviour in the atmosphere and its potential to cycling between different environmental media is still incomplete. There are significant gaps in the understanding of chemical processes affecting mercury atmospheric transport and deposition, characteristics of the air-surface exchange and processes responsible for re-emission of mercury to the atmosphere. Application of chemical transport models (CTM) complimented by extensive measurement data can facilitate a better understanding of the principal mechanisms governing Hg dispersion and cycling in the environment and lead to improvements in model parameterizations.

Multi-model study of mercury atmospheric processes has been performed as a part of Mercury Modelling Task Force organized within the framework of the EU funded GMOS (Global Mercury Observation System) project [www.gmos.eu]. A brief summary of the research results were given in EMEP Status Report 2/2016 [*Ilyin et al.*, 2016]. More detailed analysis is presented below.

1.3.1. Measurement data and model setup

The simulation results were evaluated against observations from several monitoring networks. The measurements dataset is based on the EMEP regional network for Europe [*EMEP*, 2016], the NADP/MDN [*NADP/MDN*, 2016], AMNet [*AMNet*, 2016] and NAtChem [*NAtChem*, 2016] networks for North America as well as the global GMOS mercury network [*GMOS*, 2016]. In total, the dataset include 50 selected measurement sites measuring mercury concentration in the air (Fig. 1.21). Among them, 18 sites provide measurements of mercury species (Hg^0, $Hg(II)_{gas}$, $Hg(II)_{part}$). Besides, there are 124 sites measuring mercury wet deposition and concentration in precipitation. Air concentration measurements are relatively uniformly distribution over the globe with somewhat higher density in the Northern Hemisphere. In contrast, most observations of wet deposition are located in Europe and North America limiting possibility of model evaluation in other regions.

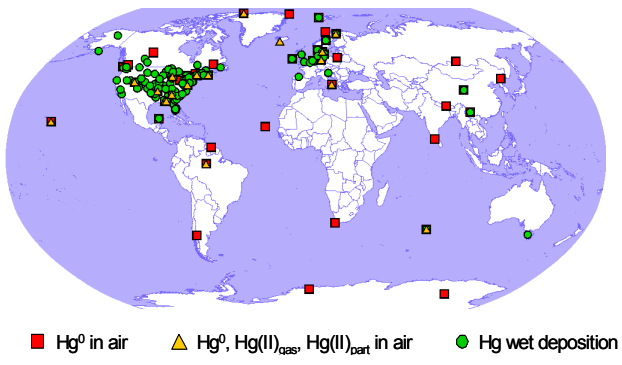

Fig. 1.21. *Location of measurement sites*

Table 1.7. *Chemical transport models participating in the study*

	GLEMOS	GEOS-Chem	GEM-MACH-Hg	ECHMERIT
Spatial resolution				
Horizontal	1° × 1°	2.5° × 2°	1° × 1°	T42 (~ 2.8° × 2.8°)
Vertical	20 levels, top 10 hPa	47 levels, top 0.01 hPa	58 levels, top 7 hPa	19 levels, top 10 hPa
Driving meteorology				
Data support type	off-line	off-line	on-line	on-line
Meteorological driver	WRF / ECMWF	GEOS-FP	GEM	ECHAM5
Anthropogenic emission				
Global emission, t/y	1875	1875	1875	1875
Average speciation (base) Hg^0: Hg(II)	81 : 19	81 : 19 [(a)]	96 : 4	81 : 19
Natural and re-emission				
Natural/secondary emission input	prescribed and dynamic [(b)]	prescribed and dynamic [(c)]	prescribed and dynamic [(d)]	prescribed and dynamic [(e)]
Global emission (base), t/y	3995	5070	3660	8600
Gaseous chemistry (base-case reactions are in bold)				
Reaction rates [(f)], cm^3 $molec^{-1}$ s^{-1}				
$Hg^0 + Br \rightarrow HgBr$	$3.7 \cdot 10^{-13}$ [(g)]	**$3.7 \cdot 10^{-13}$ [(g)]**	$3.7 \cdot 10^{-13}$ [(g)]	$3.7 \cdot 10^{-13}$ [(g)]
$HgBr \rightarrow Hg^0 + Br$	$9.4 \cdot 10^{-2}$ s^{-1} [(h)]	**$9.4 \cdot 10^{-2}$ s^{-1} [(h)]**	$1.7 \cdot 10^{-1}$ s^{-1} [(i)]	$9.4 \cdot 10^{-2}$ s^{-1} [(h)]
$HgBr + Br \rightarrow Hg^0 + Br_2$	$3.9 \cdot 10^{-11}$ [(j)]	**$3.9 \cdot 10^{-11}$ [(j)]**	—	—
$HgBr + Y \rightarrow HgBrY$, $Y = Br, OH$	$2.5 \cdot 10^{-10}$ [(k)]	**$2.5 \cdot 10^{-10}$ [(k)]**	$2.5 \cdot 10^{-10}$ [(k)]	$2.5 \cdot 10^{-10}$ [(k)]
$Hg^0 + O_3 \rightarrow Hg(II)$	**$3.0 \cdot 10^{-20}$ [(l)]**	—	$3.0 \cdot 10^{-20}$ [(l)]	**$3.0 \cdot 10^{-20}$ [(l)]**
$Hg^0 + {}^{\bullet}OH \rightarrow Hg(II)$	**(0.9-8.7) $\cdot 10^{-14}$ [(n)]**	—	**$3.0 \cdot 10^{-14}$ [(o)]**	**$8.7 \cdot 10^{-14}$ [(m)]**
Reduction agents	—	—	—	—
Aqueous chemistry (in cloud water)				
Oxidation agents	O_3, OH, HOCl/OCl-	—	—	O_3, OH
Reduction agents	$SO_3^=$	—	—	—
Reference	*Travnikov and Ilyin,* 2009; *Travnikov et al.* 2009	*Holmes et al.,* 2010; *Amos et al.,* 2012; *Song et al.,* 2015	*Durnford at al.,* 2012 *Kos et al.,* 2013; *Dastoor et al.,* 2015	*De Simone et al.,* 2014; *Jung et al.,* 2009

[(a)] Dynamic gas-particle partitioning of Hg(II) in the atmosphere according to *Amos et al*., [2012]; [(b)] Prescribed fluxes from terrestrial and aquatic surfaces as a function of temperature and solar radiation, dynamic re-emission from snow; [(c)] Prescribed fluxes from terrestrial surfaces as a function of temperature and solar radiation, dynamic fluxes from aquatic surfaces based on multi-media modelling; [(d)] Prescribed fluxes from terrestrial surfaces as a function of temperature and solar radiation, dynamic re-emission from snow and aquatic surfaces; [(e)] Prescribed fluxes from terrestrial surfaces as a function of temperature and solar radiation, dynamically calculated ocean emissions; [(f)] Temperature and pressure dependence applied to most reactions, the reaction rates are given at 298 K and 1 atm; [(g)] *Donohoue et al*. [2006]; [(h)] *Goodsite et al*. [2012]; [(i)] *Dibble et al.* [2012]; [(j)] *Balabanov et al*. [2005]; [(k)] *Goodsite et al*. [2004]; [(l)] *Hall* [1995]; [(m)] *Sommar et al.* [2001]; [(n)] *Sommar et al.* [2001] scaled down by a factor 0.1 in the cloud environment and below clouds to account for reduction of photochemical activity [*Seigneur et al*., 2001]; [(o)] *Sommar et al*. [2001] scaled down by a factor 0.34 to take into account possible dissociation/reduction reactions; [(p)] *Parrella et al.* [2012]; [(q)] *Yang et al*. [2005, 2010]; [(r)] *Emmons et al.* [2010].

The model ensemble of the study includes four chemical transport models simulating mercury on a global scale (Table 1.7). The models differ in their formulation, spatial resolution, and applied parameterizations of physical and chemical processes. The horizontal spatial resolution varies from 1 to 2.8 degrees. Two of the models (GLEMOS, GEOS-Chem) utilize off-line meteorological data

prepared by external pre-processor, whereas the two others (GEM-MACH-Hg and ECHMERIT) simulate the meteorological fields along with the pollutant transport. All the models used the same dataset of Hg anthropogenic emissions [*AMAP/UNEP*, 2013b] with somewhat different speciation of mercury forms applied in the BASE case. In contrast, parameterizations of natural and secondary emissions significantly differ among the models. The major chemical mechanisms applied in the base model configurations are also essentially different. The base-case reactions of GLEMOS and ECHMERIT include Hg oxidation by ozone and OH radical. The chemical scheme of GEM-MACH-Hg is base on the reaction with OH only. GEOS-Chem considers the bromine oxidation chemistry as the only pathway of Hg oxidation in gas phase. Two of four models also include the Hg redox chemistry in the aqueous phase in cloud water.The study was organized in a form of multiple model experiments aimed at evaluation of particular processes and mechanisms of mercury atmospheric chemistry, anthropogenic and natural/secondary emissions, deposition etc. A summary of the major model experiments is given Table 1.8. The model experiments include the base run (BASE) presenting the state-of-the-art model configurations. Two model experiments are focused on the effects of anthropogenic and natural/secondary emissions (NOANT, NONAT). And four other experiments (BRCHEm1, BRCHEM2, O3CHEM, OHCHEM) were performed to evaluate three different chemical mechanisms of Hg transformations in the atmosphere.

Table 1.8. *Specifications of model experiments*

Code	Anthropogenic emissions	Gas-phase chemistry	Comment
BASE	UNEP2010[(a)]	Model standard configuration	Base run
NOANT	No emission	Model standard configuration	Effect of anthropogenic emissions
NONAT[(b)]	—	—	Effect of natural/secondary emissions
BRCHEM1	UNEP2010, all emissions as Hg^0[(c)]	Hg^0 oxidation by Br	Br dataset from GEOS-Chem[(d)]
BRCHEM2	UNEP2010, all emissions as Hg^0	Hg^0 oxidation by Br	Br dataset from p-TOMCAT[(e)]
O3CHEM	UNEP2010, all emissions as Hg^0	Hg^0 oxidation by O_3	O_3 dataset from MOZART[(f)]
OHCHEM	UNEP2010, all emissions as Hg^0	Hg^0 oxidation by OH	OH dataset from MOZART[(f)]

[(a)] *AMAP/UNEP* [2013b]; [(b)] Virtual experiment obtained by subtraction of NOANT results from the BASE case; [(c)] All GOM and PBM emissions summed to Hg^0 to keep constant total Hg emissions; [(d)] *Parrella et al*. [2012]; [(e)] *Yang et al.* [2005, 2010]; [(f)] *Emmons et al.* [2010].

1.3.2. Gaseous elemental mercury

Figure 1.22 shows global distributions of Hg^0 concentration in the surface air simulated by four global models according to the BASE case along with ground-based observations presented by colored circles in the same color palette. The models predict similar spatial patterns of Hg concentration with pronounced gradient between the Southern Hemisphere (ca. 0.9-1.1 ng/m^3) and the Northern Hemispheres (ca. 1.1-1.6 ng/m^3) and elevated concentrations in the major industrial regions -- East and South Asia, Europe and North America (above 1.4 ng/m^3). Elevated concentrations are also predicted in tropical areas of South America, Central Africa and Southeast Asia, where considerable Hg emissions from the artisanal and small-scale gold mining are expected [*AMAP/UNEP*, 2013a]. The

models generally agree with ground-based observations shown in Fig 1.22. The measurements demonstrate evidence of the statistically significant inter-hemispheric gradient and relatively high concentrations in industrial regions [*Sprovieri et al.*, 2016]. The model-measurement divergence does not commonly exceed ±30%. In general, the models demonstrate lower spatial variation of annual Hg^0 concentration than the measurements do. This can be partly explained by relatively low spatial resolution of the model grids (1-3 hundreds of kilometres) that can hardly allow them to reproduce local meteorological conditions at a measurement.

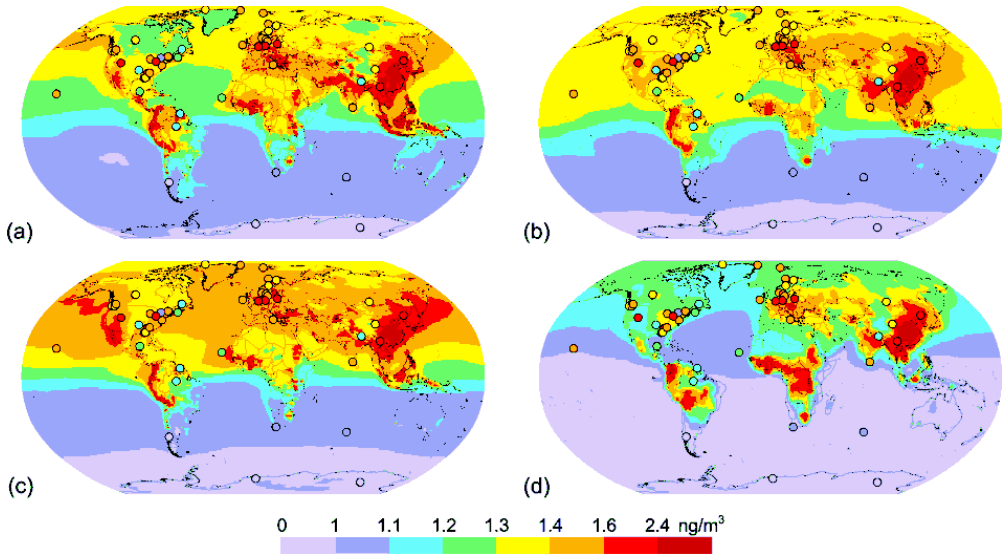

Fig. 1.22. *Spatial distribution of Hg^0 air concentration in 2013 simulated according to the BASE case by four global models: (a) - GLEMOS; (b) - GEOS-Chem; (c) – GEM-MACH-Hg; (d) – ECHMERIT. Circles show observed values in the same colour scale*

It should be noticed that the models predict similar levels and global spatial patterns of Hg^0 concentration in spite of significant deviations in applied parameterizations of physical and chemical processes. The models in their base configurations apply quite different chemical mechanisms of Hg^0 oxidation in the atmosphere. Besides, even utilizing the same anthropogenic emissions data they largely differ in their estimates of natural and secondary emissions and Hg air-surface exchange. Higher oxidative capacity of the atmospheric chemistry leads to shorter residence time of Hg^0 in the atmosphere and ultimately to larger deposition to the ground, which, in its turn, can be compensated by more intensive natural or re-emission to the atmosphere. Thus, combination of these compensative factors allows simulation of realistic Hg^0 concentration levels using different model approaches. Evaluation of particular processes governing Hg cycling in the atmosphere requires more detailed analysis of its spatial and temporal variation.

Analysis of the inter-hemispheric gradient of Hg^0 concentration is shown in Fig. 1.23. The figure present the meridional distribution of both observed and model predicted concentration in the surface air. The later is split into two fractions contributed by anthropogenic and natural/secondary sources. As seen all four models reproduce the observed increase of Hg^0 concentration between the Southern and Northern Hemispheres. The lowest concentrations (below 1 ng/m^3) are typical for the high and temperate latitudes of the Southern Hemisphere. There is a weak maximum of zonal-mean

Hg^0 concentration (1.4-1.6 ng/m^3) in the temperate latitudes of the Northern Hemisphere corresponding to location of the majority of anthropogenic emission sources. The models predict some decrease of concentration further northward, which is not evident from the observations. It can be connected with overestimation of the oxidation chemistry in the Arctic or with underestimation of Hg re-emission from snow and seawater. As seen the inter-hemispheric gradient is largely formed by contribution of direct anthropogenic emissions which is larger in the Northern Hemisphere. Contribution of natural and secondary emissions also increases northward but the gradient is commonly smaller.

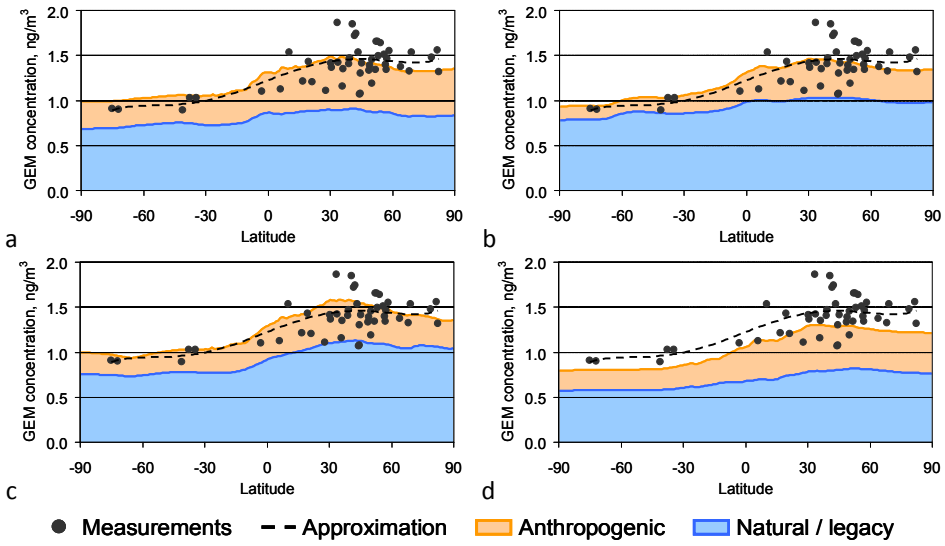

Fig. 1.23. *Global zonal-mean distribution of Hg^0 air concentration in 2013 simulated by four models: (a) – GLEMOS; (b) – GEOS-Chem; (c) – GEM-MACH-Hg; (d) – ECHMERIT. Black dots are the same observations as in Fig. 1.22 and dotted line is a polynomial approximation*

Statistics of the comparison of simulated and observed Hg^0 concentration for different model experiments (see Table 1.8) is shown in Fig. 1.24 in terms of the spatial and temporal correlation coefficients and the relative bias. In the BASE simulation all the models produce concentration distributions, which well agree with measurements (the correlation coefficient is about 0.7 and the bias is around zero). On the other hand, the models differ in their ability to reproduce temporal variation of Hg^0 in the surface air. The coefficient of temporal correlation between simulated and observed monthly mean values varies between -0.3 and 0.5. (Fig. 1.24b). *Sprovieri et al.* [2016] found consistent seasonal cycle of Hg^0 concentration observed at most measurement sites of both Northern and Southern Hemispheres with higher concentrations during winter and spring and lower concentrations in summer and fall. However, it should be noted that seasonal variation of monthly mean concentration is not significant at temperate and low latitudes where most of the sites are located and commonly does not exceed ±20%. Therefore, reproduction of the Hg^0 temporal variation is a challenging task for models taking into account absent data on seasonal variation of anthropogenic emissions used in the study [*AMAP/UNEP*, 2013b].

Switching off anthropogenic emissions (NOANT) leads to decrease of Hg^0 levels in the atmosphere (the bias is ~40%) and some decrease of spatial correlation with measurements. It is worth to say

that spatial distribution of Hg concentration in this experiment is largely determined by model-specific natural and secondary emissions and, therefore, the change of spatial correlation considerably differs among the models. Removing anthropogenic emissions from the model simulations does not affect the temporal variation of the modelling result. In contrast, results of the experiment with no natural and secondary emissions (NONAT) demonstrates significant improvement of temporal correlation with measurements for the models showed poor correlation in the BASE run. Besides, the exclusion of natural and secondary emissions leads to some decrease of spatial correlation and large negative bias (~100%). Simulations with different chemical mechanisms (BRCHEM1, BRCHEM2, O3CHEM, OHCHEM) do not lead to considerable changes of both spatial distribution and temporal variation of Hg^0 concentration in the surface air. Somewhat better spatial correlation was obtained for the oxidation reactions with Br (BRCHEM1) and OH radical (OHCHEM) and worse for the reaction with ozone (O3CHEM).

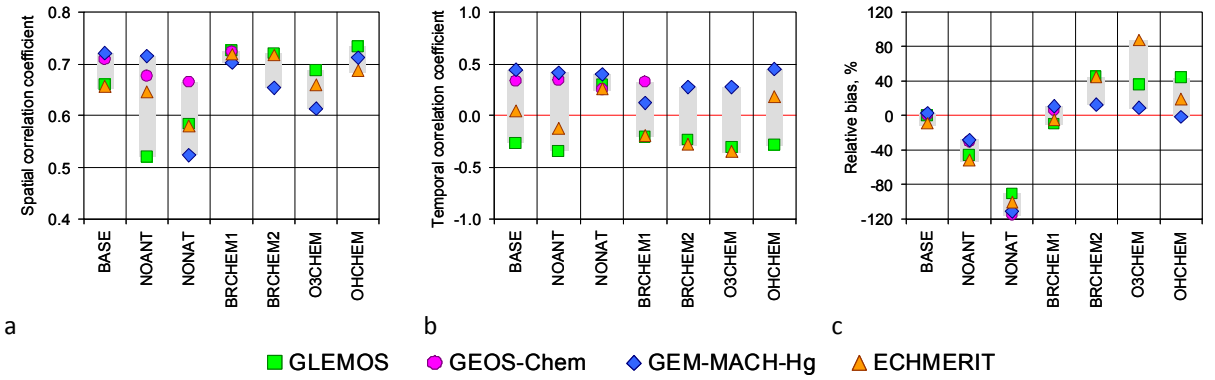

Fig. 1.24. *Spatial correlation coefficient (a), temporal correlation coefficient (b) and relative bias (c) between simulated and observed Hg^0 air concentration for different model experiments*

1.3.3. Reactive mercury

Simulated global patterns of reactive mercury Hg(II) concentration in the near surface air is shown in Fig. 1.25. Reactive mercury originates in the atmosphere both from direct anthropogenic emissions and through oxidation of Hg^0 in gas phase or aqueous phase of cloud water. Therefore, simulations of Hg(II) by contemporary models is much more challenging task taking into account incomplete current knowledge on Hg atmospheric chemistry as well as lack and uncertainty of measurement data. As seen from the figure the models predict considerably different levels of Hg(II) concentration particularly in remote regions. The simulated spatial patterns of Hg(II) concentration highly depend on applied chemical mechanisms and parameterisations of dry deposition. Indeed, the models that apply ozone and/or OH oxidation chemistry (Figs. 1.25a,c,d) predict increased Hg(II) concentrations at low latitudes (the tropics and equatorial zone) due to high concentrations of these photo-oxidants in these regions. On the other hand, application of the Br-derived chemistry (Fig. 1.25b) leads to the spatial pattern with elevated Hg(II) concentrations in the polar regions and over continents. Lower concentrations over the ocean resulted from effective removal of Hg(II) by seasalt aerosol.

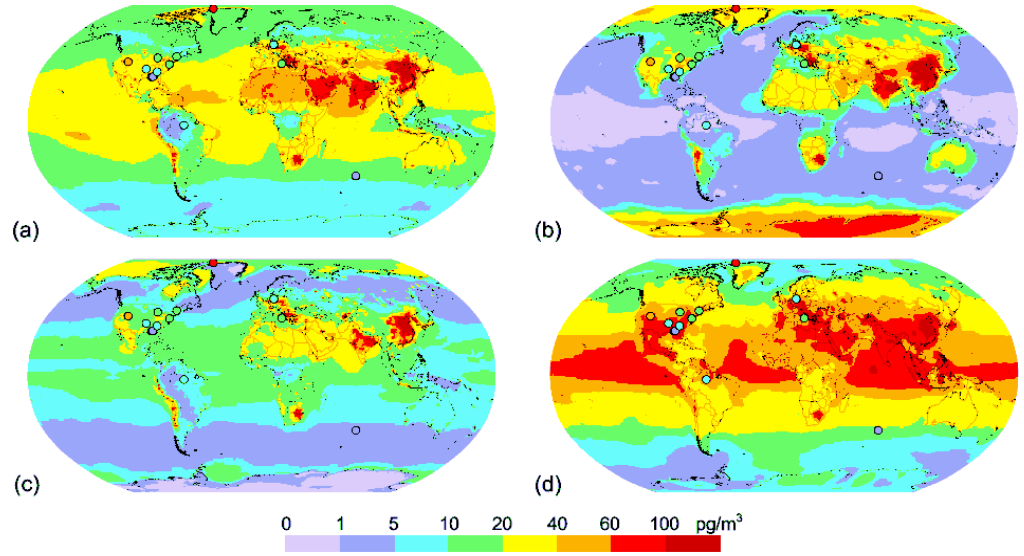

Fig. 1.25. *Spatial distribution of Hg(II) air concentration in 2013 simulated according to the BASE case by four global models: (a) - GLEMOS; (b) - GEOS-Chem; (c) – GEM-MACH-Hg; (d) – ECHMERIT. Circles show observed values in the same colour scale*

Figure 1.26 shows detailed statistics of model-to-measurement comparison of Hg(II) air concentration for different model experiments. In the BASE case the models considerably overestimate observed values. This can be explained by a number of factors including wrong speciation of anthropogenic emissions, uncertainties of oxidation chemistry and uncertainty of measurement data for Hg(II) [*Gustin et al.*, 2015]. Besides, the models differ in their ability to reproduce temporal variation of Hg(II) concentration (the correlation coefficient vary within the range -0.5–0.6). Anthropogenic and natural/secondary emissions directly or through the oxidation chemistry affect levels of Hg(II). So exclusion of these emission sources (NOANT and NONAT) leads decrease of Hg(II) concentration. However, this only slightly affects its temporal variation. Among the chemical mechanisms the best correlation between modelled and observed values were obtained for reactions with Br (BRCHEM1 and BRCHEM2).

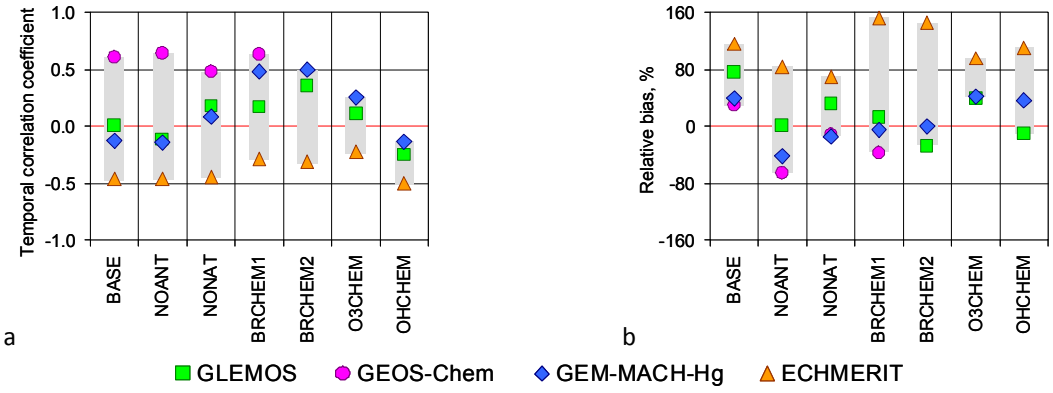

Fig. 1.26. *Temporal correlation coefficient (a) and relative bias (b) of simulated and observed monthly mean Hg(II) air concentration for different model experiments*

In contrast to elemental mercury levels, air concentration of reactive mercury Hg(II) largely depends on Hg oxidation chemistry in the atmosphere. Ratio of Hg(II) concentration to Hg^0 concentration in the air can characterize oxidation capability of Hg atmospheric chemistry. Therefore, comparison of simulated and observed Hg(II)/Hg^0 ratios at measurement sites was used for evaluation of different oxidation mechanisms. Figure 1.27 shows evaluation of the ratio of annual mean concentrations of Hg(II) and Hg^0 simulated with application of three chemical mechanisms (reactions with Br, O_3 and OH). Br oxidation chemistry was applied with two different datasets of Br concentrations: generated by GEOS-Chem (BRCHEM1) and by p-TOMCAT (BRCHEM2) models. As seen the best agreement of the simulated and measured annual Hg(II)/Hg^0 ratios is for oxidation by Br with the first concentration dataset (BRCHEM1) and by ozone (O3CHEM). In the former case three of four models provide the simulated values that agree with measurements within a factor of three but the fourth model predicts strong overestimation the Hg(II)/Hg^0 ratios (Figs. 1.27a). It can be partly explained by underestimation of Hg(II) removal from the atmosphere via wet and dry deposition. In the latter case the models predict similar levels of the Hg(II)/Hg^0 ratio with some overestimation of observed values (Figs. 1.27c). It should be also mentioned BRCHEM1 was the only mechanism that successfully reproduced observed seasonal cycle of Hg(II)/Hg^0 with maximum in spring and minimum in late summer (not shown here).

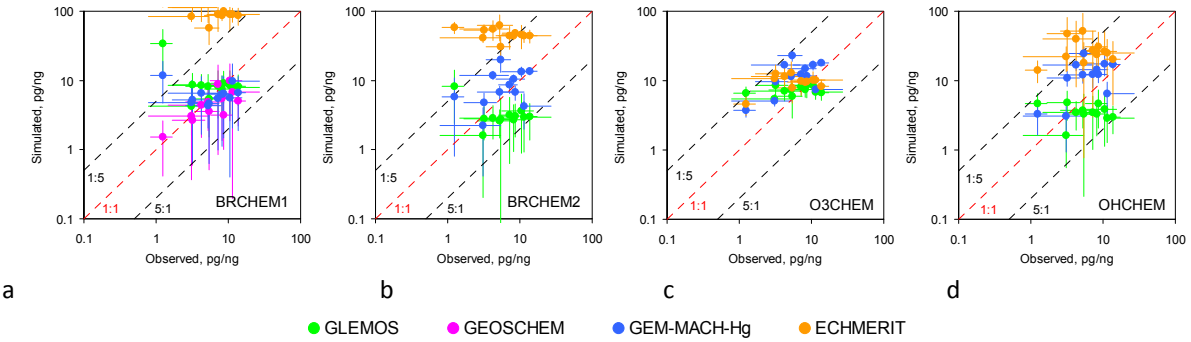

Fig. 1.27. *Scatter plots of simulated vs. observed ratios of annual mean Hg(II) concentration to Hg^0 concentration in 2013 for different model experiments: (a) – BRCHEM1; (b) – BRCHEM2; (c) – O3CHEM; (d) – OHCHEM. Whiskers show standard deviation of monthly mean simulated and observed values. Dotted red line depicts the 1:1 ratio; dashed black lines show deviation by a factor of 5*

1.3.4. Wet deposition

Wet deposition is one of the major removal mechanisms responsible for cycling of Hg between the atmosphere and other environmental compartments. It is largely determined by precipitation events, on one hand, and by availability of soluble Hg forms in the atmosphere. Simulated fields of annual Hg wet deposition have similar spatial distribution reflecting the global precipitation pattern (Fig. 1.28). High deposition fluxes are typical for industrial regions with significant emissions and areas with elevated precipitation amount (e.g. the Intertropical Convergence Zone). The lowest wet deposition fluxes are in dry areas (e.g. in Northern Africa, Greenland, and Antarctica). The models relatively well agree with long-term observations of Hg wet deposition. The mode-to-measurement deviations commonly do not exceed a factor of two. However, it should be noticed that available observations of Hg wet deposition are still mostly limited by two regions – North America and Europe. Only few measurements are available in other regions and, in particular, in the Southern Hemisphere.

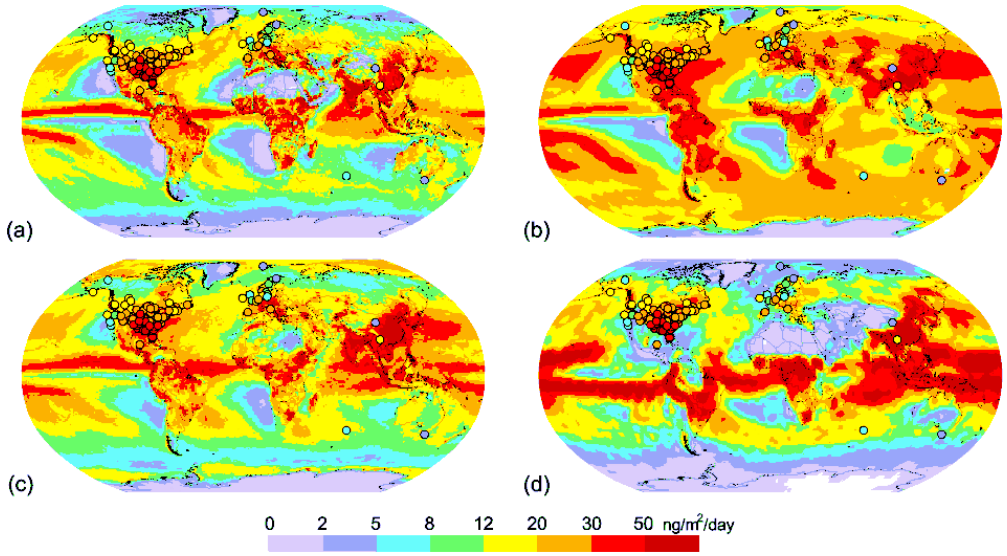

Fig. 1.28. *Spatial distribution of Hg wet deposition in 2013 simulated according to the BASE case by four global models: (a) - GLEMOS; (b) - GEOS-Chem; (c) – GEM-MACH-Hg; (d) – ECHMERIT. Circles show observed values in the same colour scale*

As follows from the statistical analysis the BASE case simulation results of the models relatively well correlate with wet deposition measurements (Fig. 1.29). Anthropogenic and natural/secondary emissions significantly contribute to wet deposition and so their elimination (NOANT, NONAT) leads to noticeable negative bias. Nevertheless, temporal variation of wet deposition is not sensitive to emission changes. In contrast, the oxidation chemistry considerably affects both general level and temporal variation of Hg wet deposition. The Br oxidation mechanism provides relatively good correlation with observations but there is a large difference between results for two different Br concentration datasets (BRCHEM1 and BRCHEM2). The highest correlation is obtained for the reaction of Hg oxidation by OH (OHCHEM). It should be noticed that one of the models demonstrates systematic poor correlation and large underestimation of measurements in most of the experiments. It is connected with uncertainties of the model simulation of precipitation. To avoid biasing of the statistics these results will not be used in the following analysis.

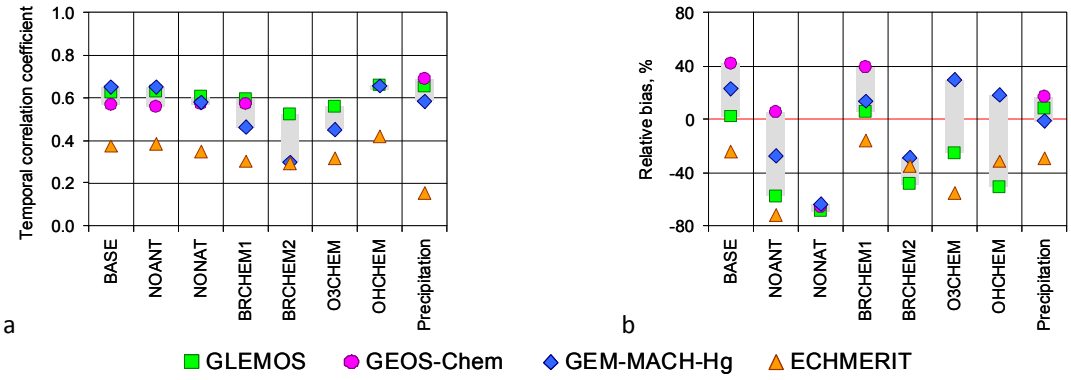

Fig. 1.29. *Temporal correlation coefficient (a) and relative bias (b) of simulated and observed annual mean Hg wet deposition for different model experiments*

Mercury wet deposition is a parameter, which is strongly determined by atmospheric oxidation chemistry. Elemental mercury is a poorly soluble substance that is almost not scavenged by precipitation. Therefore, Hg concentration in precipitation and wet deposition flux mostly depend upon two factors – direct emissions of oxidized Hg forms from anthropogenic sources and Hg oxidation in the atmosphere. Besides, the influence of the first factor rapidly subsides with a distance from emission sources. Thus, analysis of wet deposition can be also used for evaluation of chemical mechanisms of Hg oxidation in the atmosphere. Figure 1.30 shows comparison of modelled and measured seasonal variation of monthly mean wet deposition flux in North America and Europe. The observations demonstrate well pronounced seasonal cycle with the maximum in summer and the minimum during the cold season (winter and early spring). It is worth to note that measured precipitation amount does not reveal similar seasonality to explain intra-annual variation of wet deposition. As seen both model runs with Br oxidation chemistry (BRCHEM1 and BRCHEM2) predict maximum wet deposition during the spring months instead of summer (Figs. 1.30a-d). Simulations with the ozone oxidation mechanism (O3CHEM) do not provide a noticeable seasonality of deposition flux (Fig. 1.30e-f). The OH-initiated oxidation chemistry (OHCHEM) is the only mechanism that allows reproducing observed seasonal variation of wet deposition (Fig. 1.30g-h).

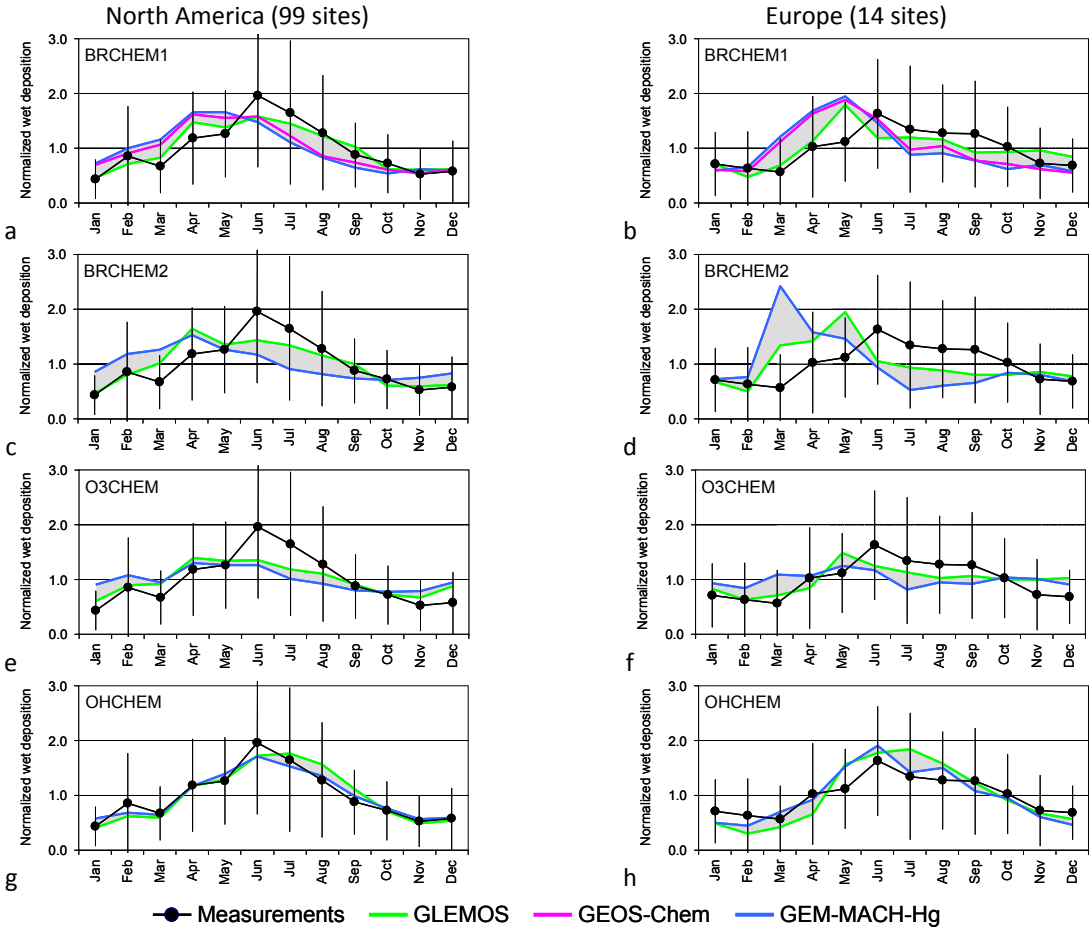

Fig. 1.30. *Normalized seasonal variation of monthly mean wet deposition flux in North America (left column) and Europe (right column). Black line with dots shows observations averaged over all sites in the regions (whiskers are standard deviation). Colored lines present model simulations averaged over the same cites for different model experiments: (a) – BRCHEM1; (b) – BRCHEM2; (c) – O3CHEM; (d) – OHCHEM*

However, it is worth mentioning that available emissions inventories do not include information on temporal variation of mercury anthropogenic emissions. Therefore, more detailed data on seasonal variation and chemical speciation emissions could improve understanding of mercury processes and, ultimately, quality of the model assessment.

1.3.5. Concluding remarks

The study of Hg atmospheric processes has been performed by means of multi-model simulations of Hg cycling in the atmosphere and detailed evaluation against measurements. The major conclusions of the analysis include the following:

- The inter-hemispheric gradient of mercury concentration is largely determined by spatial distribution of anthropogenic and natural/secondary emissions. The oxidation chemistry does not affect considerably both spatial distribution and temporal variation of Hg^0 concentration in the surface air.
- Oxidation chemistry of mercury in the atmosphere contains significant uncertainties. There is possibility of multiple oxidation mechanisms governing transformation and removal of mercury from the atmosphere.
- Seasonal variations of Hg(II) air concentration and Hg wet deposition are mostly defined by oxidation chemistry. However, the role of temporal variation of anthropogenic emission is to be further identified.
- The Br oxidation mechanism allows successfully reproducing observed seasonal cycle of the $Hg(II)/Hg^0$ ratio in the surface air, whereas the OH-initiated chemistry provides the best temporal correlation for wet deposition. Thus, particular oxidation pathways can differ in the boundary layer and the free troposphere.

2. PERSISTENT ORGANIC POLLUTANTS

2.1. Country-specific trend analysis for PCB-153

Last year the work on investigation of long-term trends of POP pollution in the EMEP region with the help of the approach worked out by MSC-E for pollutants with variable reduction rates for the period beginning from 1990 to 2010 was initiated. In particular, this analysis included evaluation of country-specific trends of PAHs (represented by "indicator chemical" B[a]P). The results of this analysis were contributed to the CLRTAP scientific assessment report [*Maas and Grennfelt*, 2016], to the TFMM assessment report [*Colette et al.,* 2016], and to the WGE assessment report [*de Wit et al*., 2015].

This year the work on the evaluation of trends of POP contamination was continued. Current work was focused at examination of country-specific trends of contamination by PCB-153 (used as indicator compound for PCB contamination) in the EMEP region on the basis of model results. To do this average annual means of contamination of the EMEP countries by PCB-153 for the period from 1990 to 2014 were estimated with the help of MSCE-POP regional model. The model used official emission data complemented by expert estimates by *Breivik et al.* [2007]. Trend analysis was performed for the period from 1990 to 2012. Years 2013 and 2014 are used for testing the possibility to expand the constructed trends for projections.

As it was already mentioned in the previous Technical Report, for evaluation of trends for PCB-153 (as well as for HCB) a modification of the approach to the trend analysis compared with that for B[a]P and heavy metals is needed. Detailed description of this modification id presented in the next section including evaluation of number of exponential compounds. Short description of these results is given in EMEP Status Report 2016 [*Gusev et al.*, 2016].

2.1.1. Modification of the methodology of trend analysis

The approach applied to the investigation of trends of pollution can be applied both at annual average level (ignoring seasonal variations of pollution) and at monthly average level. For the sake of simplicity, we begin with description of methodology modification at the level of annual averages considering seasonal variations of pollutions later in this section.

The approach applied for B[a]P and heavy metals involves representing time series of (say) concentrations of the considered pollutant in the form:

$$C(t) = a_1 \cdot \exp(-\lambda_1 \cdot t) + a_2 \cdot \exp(-\lambda_2 \cdot t) + \ldots + a_m \cdot \exp(-\lambda_m \cdot t) + \omega(t), \qquad [2.1]$$

where the sum of m exponentials is considered as *trend* and $\omega(t)$ is the so-called *residual component*. The reduction rate constants λ_i, $i = 1, \ldots, m$ were supposed to be constant within the entire period.

The latter supposition is not valid for time series of PCB-153 air concentrations. To calculate reliable trend for these series it is necessary to involve the time-dependence of reduction rate constants. In the present investigation polynomial dependence of these constants is used:

$$\lambda_i = \lambda_i(t) = \lambda_i^0 + \lambda_i^1 \cdot t + \ldots + \lambda_i^p \cdot t^p, \quad i = 1, \ldots, m. \qquad [2.2]$$

The constants a_i, $i = 1, \ldots, m$ and λ_i^j, $i = 1, \ldots, m$, $j = 1, \ldots, p$ are calculated by minimizing residual sum of squares:

$$\chi^2 = \Sigma_t \, \omega^2(t) = \Sigma_t \, (C(t) - (a_1 \cdot \exp(-\lambda_1 \cdot t) + a_2 \cdot \exp(-\lambda_2 \cdot t) + \ldots + a_m \cdot \exp(-\lambda_m \cdot t))). \qquad [2.3]$$

The necessity of consideration of time-dependent reduction rate constants is evidently seen from the comparison of trends of PCB-153 air concentrations for the period from 1990 to 2012 calculated for m = 2 without time-dependent reduction rate constants and with rate constants calculated according to [2.2] with polynomial approximation of the first power (Fig. 2.1).

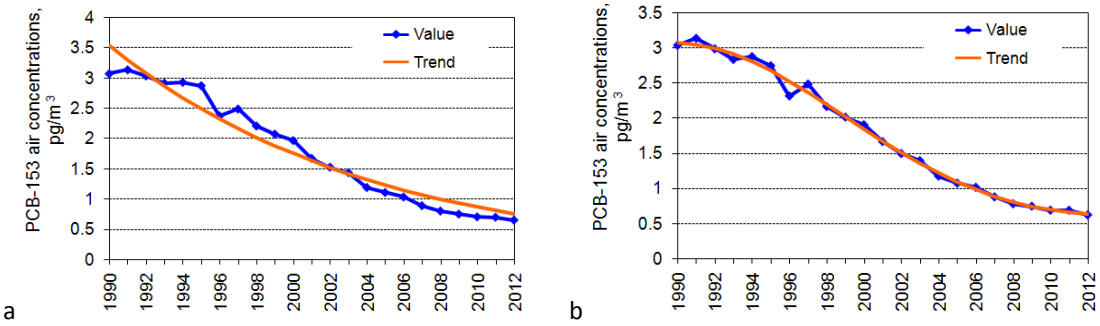

Fig. 2.1. *Trends of PCB-153 air concentrations for the period from 1990 to 2012 calculated for m = 2 without time-dependent reduction rate constants (a) and with rate constants calculated according to (2) with p = 1 (b). Taken from MSC-E Technical Report 2015 [Shatalov et al., 2015]*

The number m of the considered exponential terms and the degree p of approximation of reduction rate constants should be determined by another way. One of possible ways of determination of these parameters is the usage of F-statistics obtained from differences in sums of squares (see [*Smith,* 2002]). More precisely, to verify statistical significance of the last exponential in [2.1] the F-value is used:

$$F = (SS_1 - SS_2) \cdot (N - m \cdot (p + 2)) \,/\, (p + 2) \,/\, \chi^2. \qquad [2.4]$$

Here SS_1 and SS_2 are residual sums of squares calculated without and with last exponential, respectively, N is the number of years in time series, $N - m \cdot (p + 2)$ is overall degree of freedom, and $p + 2$ is degree of freedom due to the last exponential. It is known that F-value follows approximately an F-distribution on p + 2 and $N - m \cdot (p + 2)$ degrees of freedom. In the case if F-value calculated by [2.4] exceeds the corresponding quantile, the last exponential is assumed to be statistically significant.

Similarly, for the verification of last power in [2.2] the following F-value is used:

$$F = (SS_1 - SS_2) \cdot (N - m \cdot (p + 2)) \,/\, m \,/\, \chi^2 \qquad [2.5]$$

with similar notation.

It was found that for time series of PCB-163 air concentrations the values m = 2 and p = 1 are sufficient (in exceptional cases m should be put to 3). Let us illustrate evaluation of the number of parameters by example of the number of exponentials. The values of quantiles of the Fisher distribution at various confidence levels for m = 3 and p = 1 are displayed in Table 2.1.

Table 2.1. *Quantiles of the Fisher distribution at various confidence levels for m = 3 and p = 1*

Confidence level	Quantiles
90%	2.5222
95%	3.3439
99%	5.564

Calculated F-values for countries where these values are large enough are shown in Table 2.2.

Table 2.2. *F-values for PCB-153 air concentrations from 1990 to 2012 with m = 3 and p = 1*

Country	F-value
Turkey	7.31
Turkmenistan	7.29
Kazakhstan	6.24
Greece	5.51
Bulgaria	4.70
Tajikistan	4.31
Macedonia	3.90
Republic of Moldova	3.45
Uzbekistan	3.42
Russian Federation	3.40
Monaco	3.22
Albania	3.15
Spain	3.12
Montenegro	3.02
Azerbaijan	3.01
Poland	2.80
Ireland	2.71
…	…

For the rest countries obtained F-values do not exceed the 90% confidence level.

Let us demonstrate the influence of third exponential on the long-term trend for three EMEP countries with high values of F-statistics (Fig. 2.2).

It is seen that application of trend with three exponentials for the countries with high values of F-statistics can essentially improve the agreement between trend and initial time series in the end of the considered period.

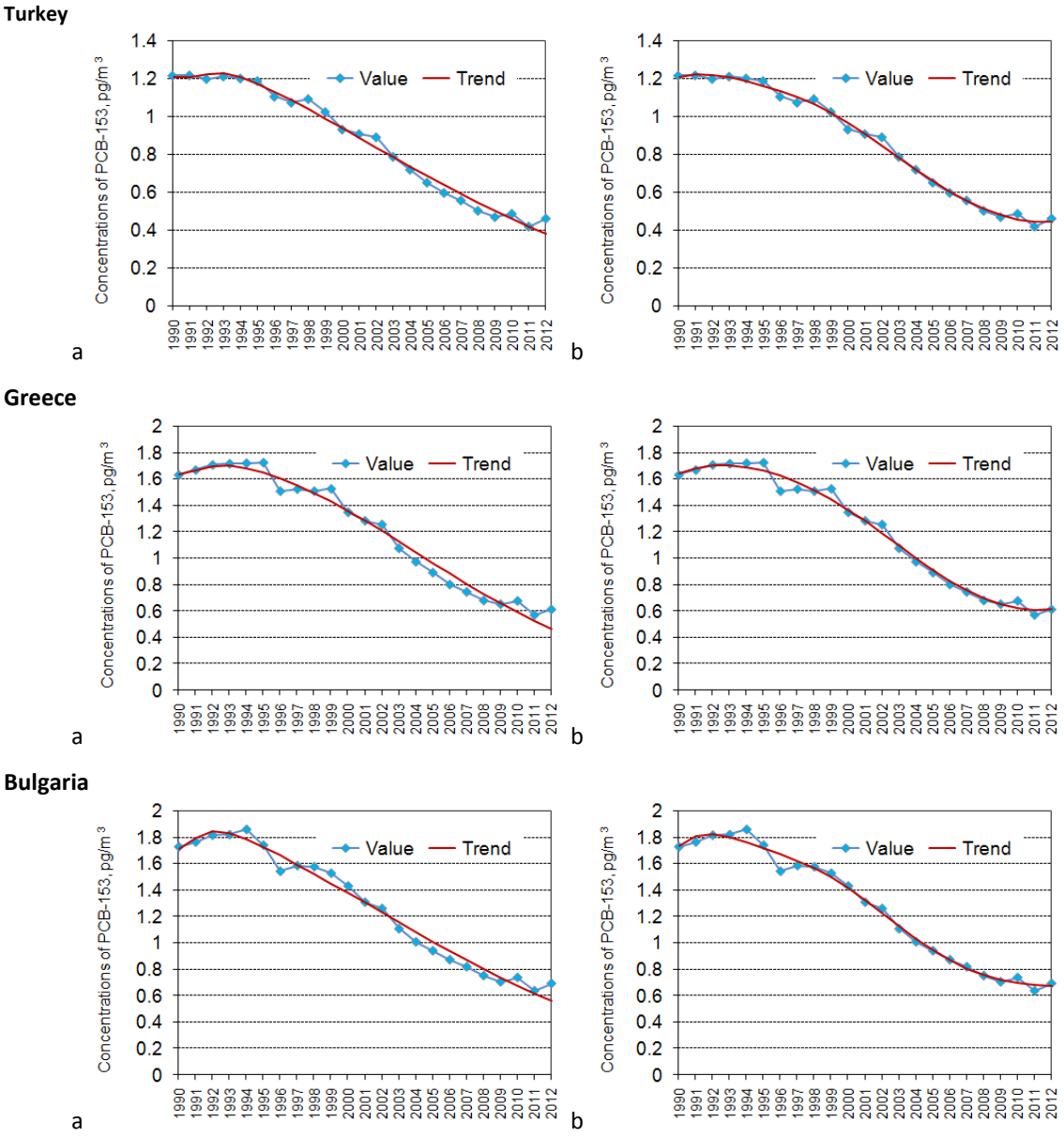

Fig. 2.2. *Calculated trends without (a) and with (b) third exponential for three EMEP countries*

Similar calculations for evaluation of statistical significance of second power in representation [2.3] show that second power is not statistically significant for all EMEP countries, and, hence, representation [2.3] should be used with $p = 1$.

Let us turn our attention to the trend construction for monthly averages of PCB-163 air concentrations (that is, taking into account seasonal variations of pollution). Here in equation [2.1] each exponential should be multiplied by the corresponding harmonic factor:

$$a_j \cdot \exp(-\lambda_j \cdot t) \rightarrow \exp(-\lambda_j \cdot t) \cdot (a_j + b_{j1} \cdot \cos(2\pi \cdot t - \varphi_{j1}) + \ldots + b_{jk} \cdot \cos(2k\pi \cdot t - \varphi_{jk})) \qquad [2.6]$$

for each $j = 1, \ldots m$. Here k is the number of harmonics involved into trend expression. It was found that $k = 1$ is sufficient for trend evaluation. The sum:

$$a_1 \cdot \exp(-\lambda_1 \cdot t) + a_2 \cdot \exp(-\lambda_2 \cdot t) + \ldots + a_m \cdot \exp(-\lambda_m \cdot t) \qquad [2.7]$$

is then referred as main component of the trend, and the sum of expressions:

$$\exp(-\lambda_j \cdot t) \cdot (b_{j1} \cdot \cos(2\pi \cdot t - \varphi_{j1}) + \ldots + b_{jk} \cdot \cos(2k\pi \cdot t - \varphi_{jk})) \qquad [2.8]$$

over all $j = 1, \ldots, m$ – as seasonal component.

For calculations, number of exponentials and power of approximation of reduction rate constants are taken to be the same as for annual averages.

Results of trend evaluation are exemplified by the trend of average PCB-153 concentrations over the joint area of the EMEP countries (Fig. 2.3) calculated with two exponential terms. The difference between trend calculations with two and three exponential terms is also shown on the diagram.

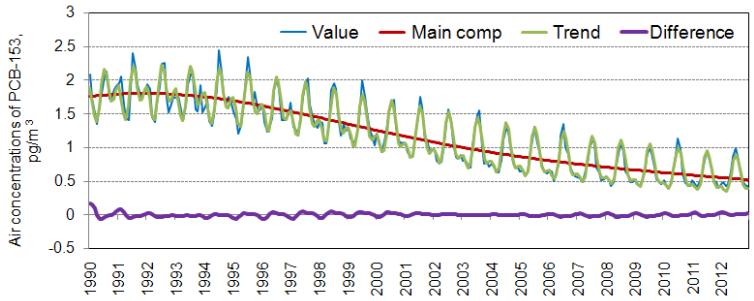

Fig. 2.3. *Trend of average PCB-153 concentrations over the joint area of the EMEP countries and difference between trend calculations with two and three exponential terms*

On the average, relative difference between trends calculated with two and three exponents is as small as 2.3%. Maximum differences (not more than 10%) are found for small values of PCB-153 air concentrations in cold periods of each year.

For evaluating number of exponentials for usage of trend calculations it is important to estimate the differences between main statistical parameters obtained with two and three exponential trends. For POPs, such parameters are total reduction of contamination within the period and seasonal variation parameter (the ratio of seasonal variation and main components). Figs. 2.4 and 2.5 show the difference between these two parameters calculated by the two compared trend parameters.

It is seen that calculations with two and three exponential terms lead to very close results in evaluation of total reduction and seasonal variation parameter.

However, the results of evaluation of reduction rates in the last year of the period calculated with two and three exponential terms differ more essentially from each other (see Fig. 2.2 and the discussion after this figure). Fig. 2.6 shows the difference between evaluation of reduction rates in the end of the period in the end of the considered period (in 2012).

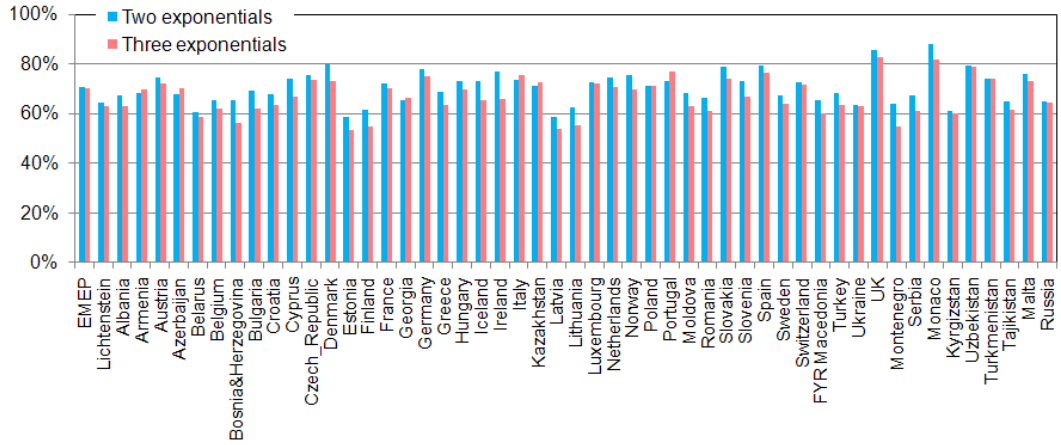

Fig. 2.4. *Comparison of total reductions of PCB-153 air concentrations for the period from 1990 to 2012 in the EMEP countries calculated with two and three exponential terms*

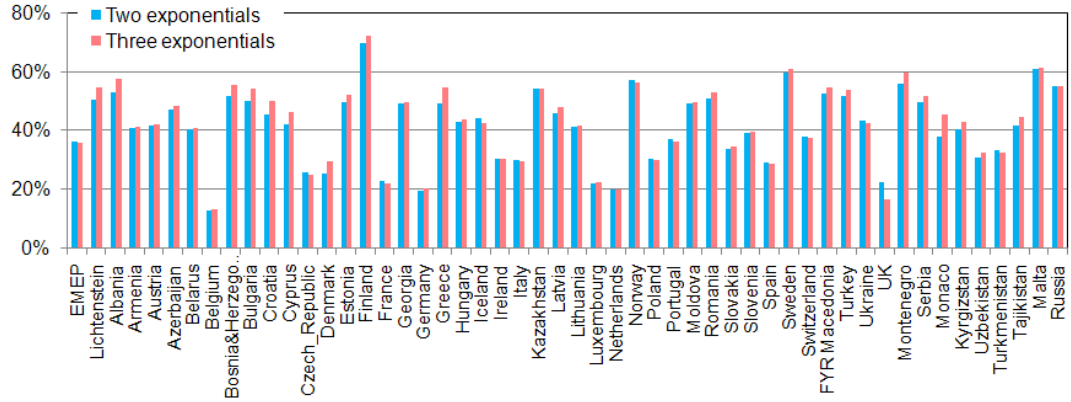

Fig. 2.5. *Comparison of seasonal variations of PCB-153 air concentrations for the period from 1990 to 2012 in the EMEP countries calculated with two and three exponential terms*

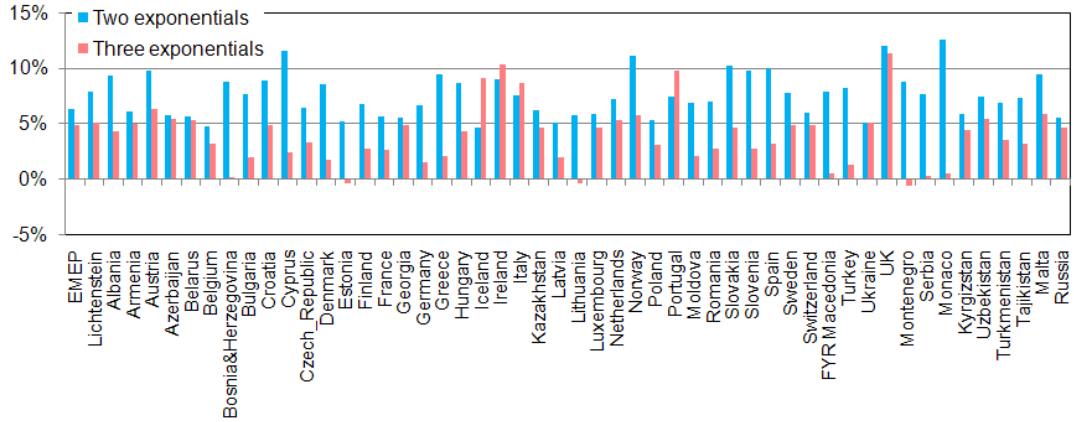

Fig. 2.6. *Comparison of reductions of PCB-153 air concentrations in the EMEP countries in 2012 calculated with two and three exponential terms*

Thus, for evaluation of total reductions of PCB-153 air concentrations for the entire period it is sufficient to use trends calculated with two exponential terms whereas for evaluation of reduction rates in the end of the period it is reasonable to use three-exponential approximation.

As a conclusion of the above analysis it can be stated that the following trend parameters are recommended for the evaluation of reduction rates within the entire period and of seasonal parameter for PCB-153 contamination.

Table 2.3. *Parameters recommended for evaluation of trends of PCB-153 contamination*

Parameter	Value
Number of exponential terms	2
Power of approximation of reduction rate constants	1
Number of harmonics	2

However, for evaluation of reduction rates in the end of the period it is recommended to use three-exponential approximations with the same rest parameters.

2.1.2. Results and discussion

Results of trend analysis of long-term variations of PCB-153 air concentrations, averaged over the area of all EMEP countries and over the EECCA countries for the period from 1990 to 2014, are shown in Fig. 2.7. Trends are extrapolated for 2013 and 2014 using the parameters obtained for the period from 1990 to 2012.

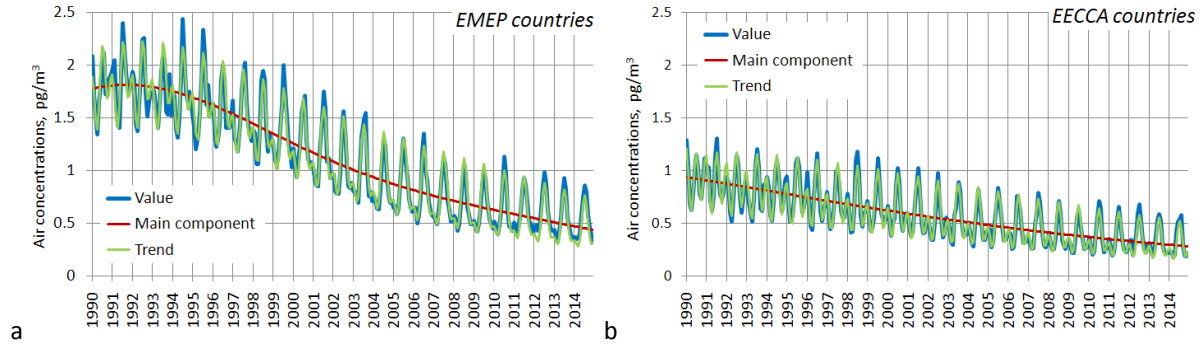

a b

Fig. 2.7. *Trends in monthly mean air concentrations of PCB-153 for the area of the EMEP countries on the whole (a) and for the EECCA countries (b), extrapolated to the period from 1990 to 2014*

The results of extrapolation show that the trend calculated for the period from 1990 to 2012 can be used for the longer period provided that the conditions of contamination in the wider period were not changed.

Analysis of trends has been carried out also for each particular EMEP country. For most countries extrapolation of the trend obtained for the period 1990 – 2012 is reasonably good for the two subsequent years (2013 and 2014). This situation is shown in Fig. 2.8 for Austria.

However, for some countries the agreement between the extrapolated trend and calculated values of PCB-153 concentrations is worse. Such situation takes place, for example, for Germany (Fig. 2.9).

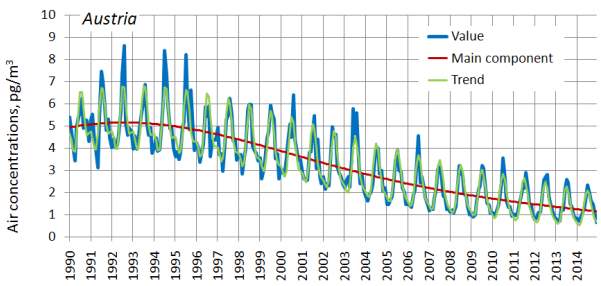

Fig.2.8. *Trends in monthly mean air concentrations of PCB-153 for the Austria, extrapolated to the period from 1990 to 2014*

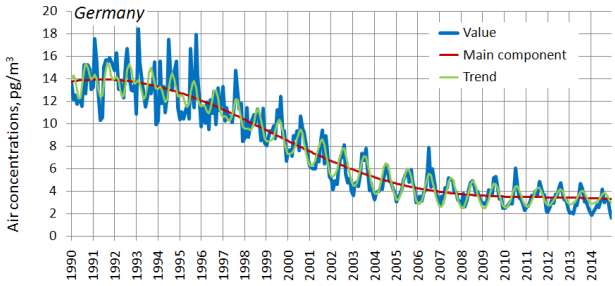

Fig. 2.9. *Trends in monthly mean air concentrations of PCB-153 for the Germany, extrapolated to the period from 1990 to 2014*

It can be noticed that for this country trend extrapolated to 2013 and 2014 shows higher values of contamination than predicted by model calculations based on the official German data. This may be conditioned, for example, by strengthening of environment-protection measures in the country, changes in the structure of industry, or by some other reason.

Statistics of reduction rates within the entire period and of seasonal parameter for PCB-153 contamination is shown in Fig. 2.10.

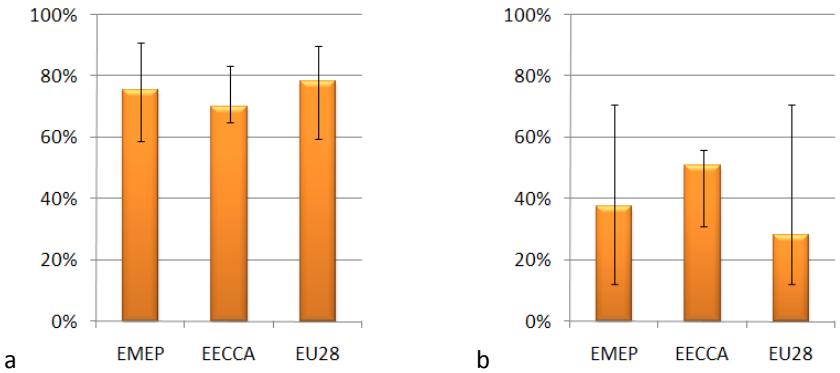

Fig.2.10. *Total reduction of PCB-153 contamination in the EMEP countries, EECCA region and EU28 countries (a) and seasonal variation parameters (b)*

The analysis indicates that levels of PCB-153 air pollution in the EMEP countries have declined on average by 75% during the two recent decades (Fig. 2.10a). Relatively higher rates of reduction (about 80%) are estimated for the EU28 countries, varying for individual countries from 60% for Estonia to almost 90% for the United Kingdom. The EECCA countries are characterized by relatively lower decrease of pollution levels (about 70%).

Air concentrations of PCB-153 are subject to pronounced seasonal variations with maximum concentrations in warmer months and minimum concentrations in the colder months during the year. Seasonal variability of air concentrations, averaged over the area of all EMEP countries, is about 40% of the main component. Results of the analysis indicate that seasonal variations of air concentrations, evaluated for the EECCA countries, are larger (about 50%) in comparison to the

estimates of variations for the EU28 countries (about 30%) (Fig. 2.10b). This difference can be explained by the influence of geographical location of the countries. In particular, higher estimates of seasonal variations are obtained for continental countries comparing to the countries located closer to coastal areas.

The values of reduction rates in the last year of the period (2014) are calculated with the help of three-exponential trends (cf. Fig. 2.2 above). Statistics of these results over EMEP, EECCA and EU28 countries is shown in Fig. 2.11a.

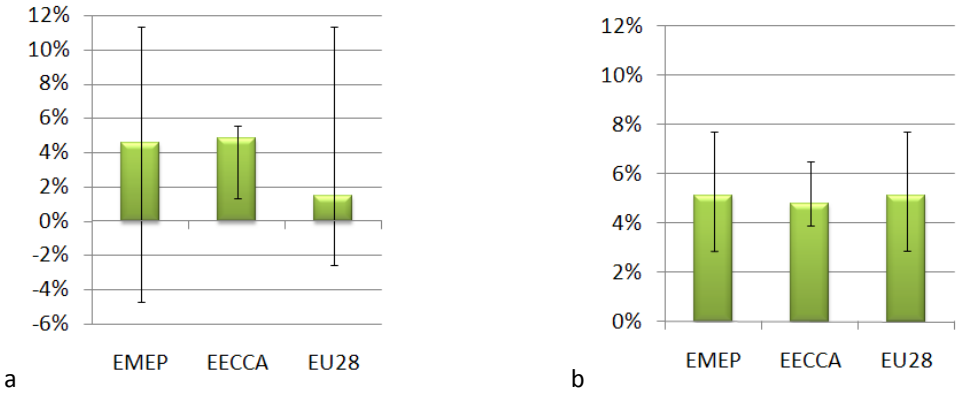

Fig. 2.11. *Reduction of PCB-153 contamination in the EMEP countries, EECCA region and EU28 countries (a) in the end of evaluation period (calculated by three-exponential trend) and (b) average annual reduction over the entire period*

The plots in Figs. 2.7 – 2.9 show that the reduction of contamination of PCB-153 is not homogeneous within the considered period. More precisely, reduction in the first part of the period is normally higher than that in the end of the period. It can be illustrated by the comparison of plots in Fig. 2.11a,b. These plots show that the reductions in the end of the period (in 2014) are lower than annual reductions averaged over the entire period. Maximum difference is calculated for EU28 where average reduction is about 6.5% whereas the reduction in 2014 is 1.5% only.

Further, trend analysis shows that reduction of the contamination over the joint area of EMEP countries in the last year of the considered period to be about 4.5% This reduction is higher in EECCA countries (about 5% and lower in EU28 countries (1.5%). However, in some countries trend analysis shows growth of PCB-153 air concentrations. The maximum growth in 2014 is found for Bosnia and Herzegovina, Serbia and Montenegro (4% – 5%). Among EU28 countries growth of contamination is calculated for Estonia and Lithuania (about 2.5%). Since last year reduction is less robust parameter obtained by trend analysis, these conclusions require further consideration.

2.1.3. Concluding remarks

The above analysis allows drawing the following conclusions.

- For evaluation of trends of PCB contamination (air concentrations) poly-exponential trend with polynomial approximation of reduction rate constants is suitable. For majority of EMEP

countries two exponential terms are sufficient (third exponential is not statistically significant. To reflect seasonal variation of pollution harmonic approximation with two subsequent frequencies can be used.

- Evaluation of reductions within the entire period and seasonal variation parameter can be performed with the use of two-exponential approach for all EMEP countries. For evaluation of reduction rates for particular year in the end of the period third exponential term should be taken into account.
- For most countries extrapolation of the trend obtained for the period 1990 – 2012 to the two subsequent years (2013 and 2014) describe PCB-153 contamination with sufficient accuracy. Non-applicability of extrapolation for particular countries may be caused by changes in emission source structures and/or environment-protection measures applied.
- The analysis indicates that levels of PCB-153 air pollution in the EMEP countries have declined on average by 75% during the two recent decades. Relatively higher rates of reduction (about 80%) are estimated for the EU28 countries, varying for individual countries from 60% for Estonia to almost 90% for the United Kingdom. The EECCA countries are characterized by relatively lower decrease of pollution levels (about 70%).
- The reductions of PCB-153 air concentrations are not homogeneous within the considered period. These reductions are high in the first part of the period and become lower in the end of the period. Particularly, average annual reduction over the whole period for the joint area of all EMEP countries is 6.5% in contrast with reduction in 2014 that is as small as 1.5%.
- Air concentrations of PCB-153 are subject to pronounced seasonal variations with maximum concentrations in warmer months and minimum concentrations in the colder months during the year. Seasonal variability of air concentrations, averaged over the area of all EMEP countries, is about 40% of the main component.

2.2. Preparation of PCDD/F congener-specific emission data for modelling

This section is devoted to the construction of emission scenarios for PCDD/Fs modelling aimed at closer agreement between model predictions and available measurements. Evaluation of PCDD/F environmental toxicity is under special attention of a lot of national and international organizations, such as CLRTAP, Stockholm Convention, US EPA, German Environmental protection agency (UBA), Swedish Environmental Protection agency (SEPA) and others. In particular, in EU POPs Regulation it is stated that[1]

"The Commission and the Member States shall establish, in close cooperation, appropriate programmes and mechanisms, consistent with the state of the art, for the regular provision of

[1] Regulation (EC) No 850/2004 (POPs Regulation), consolidated version of 04. 12. 2015, Article 9. PCDD/Fs are included to Annex III (release reduction) Annex IV (waste management), Annex V (wastes from iron and steel industry) of the Regulation.

comparable monitoring data on the presence of dioxins, furans and PCBs as identified in Annex III in the environment."

In addition, it should be mentioned that a number of countries have established maximally admissible levels of contamination by dioxins/furans in the atmosphere and other environmental compartments, especially soils.

It is known that emission inventories for PCDD/Fs are subject to essential uncertainties. These uncertainties arise due to uncertainties in both total toxicity of the mixture of 17 toxic PCDD/F congeners and due to uncertainties of congener composition of this mixture.

Uncertainties of total PCDD/F toxicity were investigated in a lot of studies. For example, in MSC-W Technical Report 1/2006 the following estimation of PCDD/F emission uncertainty was indicated based on the TNO investigations [*Pulles et al.,* 2005, 2006]: "The annual total emissions for the year 2000 in thirteen countries in Central and Eastern Europe can be estimated with 90 % confidence within a range that is about a factor of 2 to 3 lower to a factor of 3 to 5 higher than a point value obtained from a more classical approach". Further, according to the TNO estimates total emitted PCDD/F toxicity was 11.7 kg TEQ/y in 2000 and projections for 2010 and 2020 was 8.6 kg TEQ/y and 3.8 kg TEQ/y. These results give impression on emission totals and the range of their uncertainty and certainly should be taken into account in the construction of PCDD/F emission scenarios.

However, it should be noted that due to differences in their physical-chemical properties, environmental fate of different PCDD/F congeners differs from one another so that uncertainties in congener composition of the considered pollutants can also lead to the inaccuracy of evaluation of PCDD/F toxicity. This is especially important for the evaluation of PCDD/F levels in the environmental media, particularly in soil and seawater.

Unfortunately, official manuals for evaluating PCDD/F emissions (such as SC Dioxin Toolkit and EMEP/EEA air pollutant emission inventory guidebook) consider just estimates of total toxicity of PCDD/F mixture and do not pay attention to its congener composition. For the purpose of congener-specific modelling, MSC-E initiated the work on investigation of congener composition of PCDD/F emissions. It should be taken into account that congener composition of PCDD/F emissions vary essentially between various source categories.

In course of model assessment of PCDD/F pollution levels in the EMEP countries MSC-E performed analysis of available data on the emissions of dioxins and furans and their congener composition. In particular, collection of information on emissions of the seventeen 2,3,7,8-substituted PCDD/Fs in the EMEP countries and their congener profiles was carried out at the previous stages of the work [*Vulykh and Shatalov*, 2001]. This year analysis of information on congener-specific PCDD/F emissions from various source categories has been continued in order to elaborate experimental scenario of congener patterns of reported emission and to apply it for the evaluation of environmental pollution by dioxins and furans. This study includes collection of additional information on the PCDD/F emission profiles for various types of emission sources available in literature, and preliminary analysis of collected.

This section contains a detailed description of the study including the description of the method that is supposed to be applied for constructing typical congener pattern for various emission sectors, description of the information available in literature and preliminary analysis of the collected information. Short presentation of the study results is given in the EMEP Status Report [*Gusev et al.,* 2016].

2.2.1. Description of the literature data used in the analysis

According to various inventories (both CLRTAP data and TNO investigation) main aggregated emission sectors contributing to PCDD/F toxicity are A_PublicPower, C_OtherStationaryCombustion, B_Industry, J_Waste, F_RoadTransport and L_AgriOther. These sectors are the main focus of our study.

To evaluate congener composition of PCDD/F emissions, literature search on the information on congener composition in emissions from source categories making main contributions to total toxicity of PCDD/F mixture was performed. Table 2.4 presents the list of available information on congener composition for emission sectors with essential contributions in PCDD/F toxicity (according to the data presented by CEIP for 2014) and number of individual data on congener profiles in emissions from the sources from these sectors.

Table 2.4. *Information on congener profiles for main PCDD/F source categories found in literature*

Aggregated emission sector	Contribution of emissions from the sector to total PCDD/F toxicity, %	Number of literature data found
A_PublicPower	3	12
C_OtherStationaryCombustion	36	63
B_Industry	30	63
J_Waste	25	48
F_RoadTransport	3	19
L_AgriOther	2	2

In turn, aggregated emission categories are split to individual categories, and the data on congener patterns was collected for these categories separately.

The list of literature sources used for the analysis of PCDD/F congener profile is given in Annex A.

2.2.2. Proposed methodology (preliminary analysis)

At the first stage of the work, two emission sectors with essential contributions to the total toxicity of PCFF/F mixture in the EMEP region were selected for preliminary analysis of the data from Iron and steel production and Residential stationary sources sectors.

There are 20 congener profiles found for Iron and steel production sector, for references see Annex A. The comparison of these profiles is shown in Fig. 2.12.

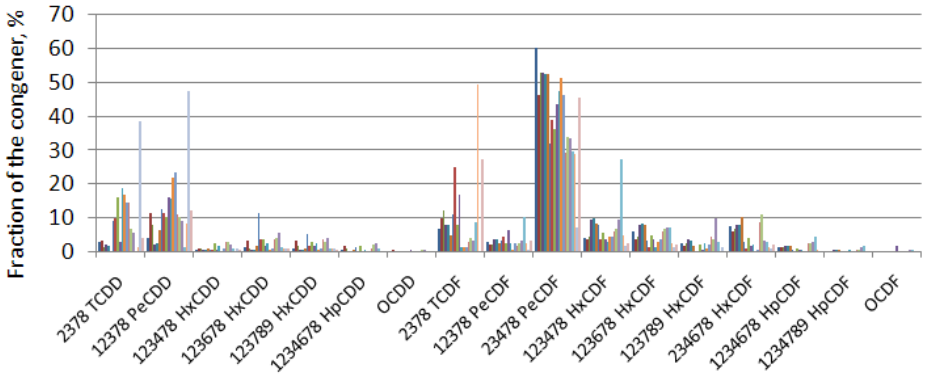

Fig. 2.12. *Congener profiles found for iron and steel production sector*

It can be seen that the individual profiles obtained from literature sources for one and the same emission sector can be essentially different. So, at the first stage of the analysis it is reasonable to select groups of profiles being close to one another (clusters). The measure of closeness between two profiles is selected as:

$$Dist\,(F_1, F_2) = \sqrt{\sum_{i=1}^{17} (F_{1,i} - F_{2,i})^2 / 17}\ , \qquad [2.9]$$

where the sum is taken over all 17 toxic congeners, and $F_{1,i}$ and $F_{2,i}$ are fractions of i-th congener in the profiles F_1 and F_2, respectively measured in per cent. In fact, Dist(F_1,F_2) is the root mean square error (RMSE) between two sets of fractions F_1 and F_2.

By *cluster* within the set of considered profiles we mean the group of profiles with distance between each two profiles included into the cluster being less than some *threshold level*. The choice of the threshold level is subject to expert estimate. In fact, if too small threshold level is chosen, each cluster will consist of one profile only. On the opposite, too big threshold level leads to existing of only one cluster containing all profiles considered. In our opinion, the threshold level of 5% is an optimal choice.

Matrix of distances between 20 considered profiles is shown below:

0	4.1	2.6	2.4	2.5	2.6	8.2	7.6	7.0	5.9	6.2	6.5	6.9	8.4	6.9	7.4	9.7	13.2	19.1	6.8
4.1	0	2.1	3.5	3.5	3.2	4.5	4.6	4.1	2.7	4.6	5.2	4.8	5.4	3.9	4.5	7.9	10.7	15.8	4.5
2.6	2.1	0	2.4	2.5	2.5	6.3	5.5	5.6	3.7	5.7	6.0	6.0	7.1	5.5	6.0	8.5	11.0	17.6	4.6
2.4	3.5	2.4	0	0.2	1.6	6.9	6.8	6.0	5.3	6.2	6.8	6.9	7.1	5.4	5.8	7.5	12.1	18.4	6.3
2.5	3.5	2.5	0.2	0	1.5	6.9	6.8	6.0	5.3	6.3	6.9	6.9	7.1	5.4	5.8	7.4	12.1	18.4	6.3
2.6	3.2	2.5	1.6	1.5	0	6.8	7.2	6.0	5.2	6.0	6.4	6.3	6.9	5.0	5.7	7.8	12.7	17.9	6.7
8.2	4.5	6.3	6.9	6.9	6.8	0	4.5	3.1	4.6	5.7	6.8	5.9	3.8	3.6	3.8	6.9	10.0	13.3	6.1
7.6	4.6	5.5	6.8	6.8	7.2	4.5	0	4.7	3.2	6.5	7.3	6.9	6.5	6.1	6.5	8.5	7.0	14.9	2.4
7.0	4.1	5.6	6.0	6.0	6.0	3.1	4.7	0	4.7	3.7	5.2	4.6	2.6	3.2	3.8	7.5	11.0	13.0	6.2
5.9	2.7	3.7	5.3	5.3	5.2	4.6	3.2	4.7	0	5.6	5.8	5.2	6.3	5.2	5.6	8.0	9.0	15.2	3.0
6.2	4.6	5.7	6.2	6.3	6.0	5.7	6.5	3.7	5.6	0	2.3	2.4	5.2	5.4	5.8	9.8	13.4	13.4	7.3
6.5	5.2	6.0	6.8	6.9	6.4	6.8	7.3	5.2	5.8	2.3	0	1.6	6.7	6.6	6.9	10.7	13.9	13.5	7.6
6.9	4.8	6.0	6.9	6.9	6.3	5.9	6.9	4.6	5.2	2.4	1.6	0	5.7	5.7	6.0	9.9	13.4	12.7	7.4
8.4	5.4	7.1	7.1	7.1	6.9	3.8	6.5	2.6	6.3	5.2	6.7	5.7	0	2.4	3.3	7.4	12.1	12.3	8.0
6.9	3.9	5.5	5.4	5.4	5.0	3.6	6.1	3.2	5.2	5.4	6.6	5.7	2.4	0	2.6	6.5	11.6	14.0	7.1
7.4	4.5	6.0	5.8	5.8	5.7	3.8	6.5	3.8	5.6	5.8	6.9	6.0	3.3	2.6	0	5.9	11.9	14.4	7.5
9.7	7.9	8.5	7.5	7.4	7.8	6.9	8.5	7.5	8.0	9.8	10.7	9.9	7.4	6.5	5.9	0	11.7	17.2	9.2
13.2	10.7	11.0	12.1	12.1	12.7	10.0	7.0	11.0	9.0	13.4	13.9	13.4	12.1	11.6	11.9	11.7	0	18.6	6.9
19.1	15.8	17.6	18.4	18.4	17.9	13.3	14.9	13.0	15.2	13.4	13.5	12.7	12.3	14.0	14.4	17.2	18.6	0	16.6
6.8	4.5	4.6	6.3	6.3	6.7	6.1	2.4	6.2	3.0	7.3	7.6	7.4	8.0	7.1	7.5	9.2	6.9	16.6	0

Rows and columns in the table correspond to the considered congener profiles. The profiles are ordered in such a way that the profiles belonging to one and the same cluster stand together. Four clusters found are marked by thick frames. One of clusters contains 6 profiles, one – four profiles, and two – three profiles. The rest four profiles are not close to any other profiles and to one another. Congener profiles for all these clusters are shown in Fig. 2.13.

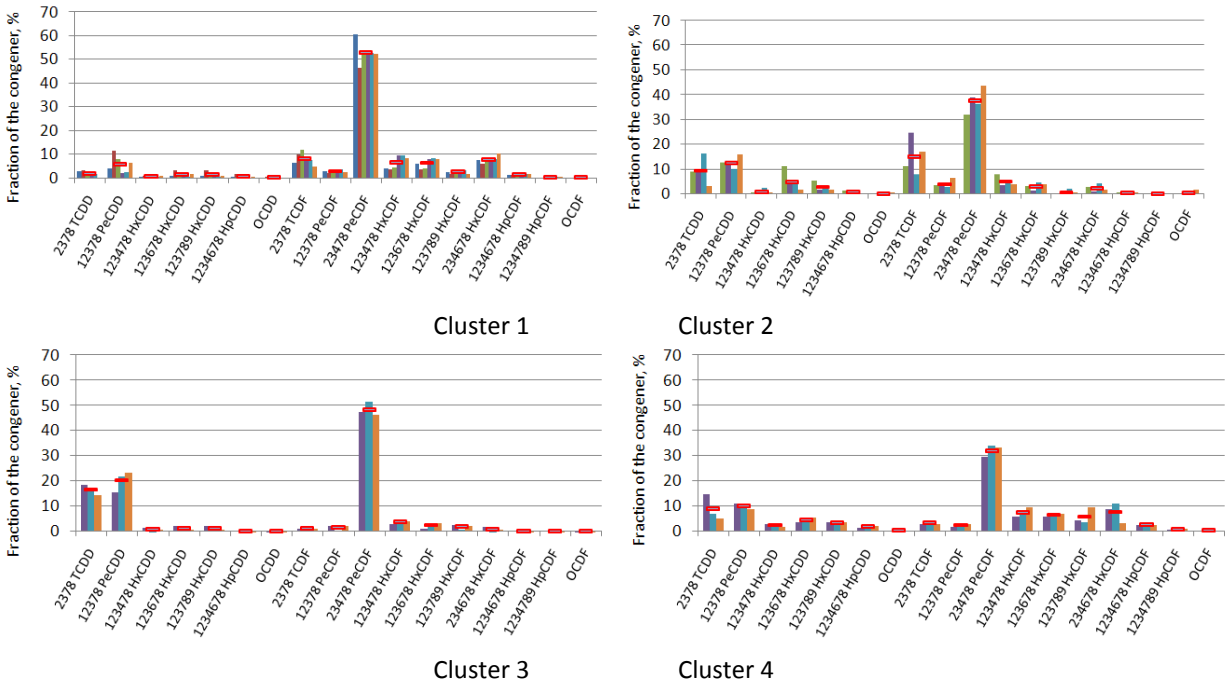

Fig. 2.13. *Congener profiles for four selected clusters. Red markers denote averages over the cluster*

It is evident that congener patterns in four considered clusters are different so that more sophisticated analysis of congener composition for this sector is needed. To compare congener composition of the clusters average congener pattern for each cluster was calculated. The comparison of average profiles included into the considered clusters is given in Fig. 2.14.

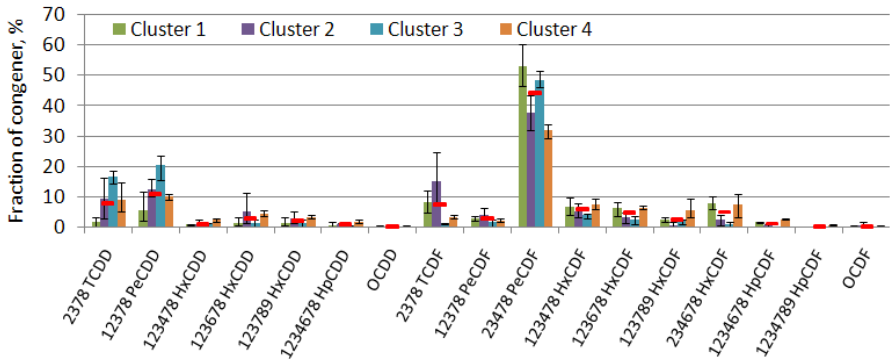

Fig. 2.14. *Comparison of the average congener profiles for the selected clusters. The whiskers show ranges of congener fractions included to the given cluster. Red markers show congener profile averaged between clusters*

To evaluate numerically the difference between average congener profiles of the selected clusters, distance matrix for these averages was calculated.

	Cluster 1	Cluster 2	Cluster 3	Cluster 4
Cluster 1	0	5.2	5.8	5.7
Cluster 2	5.2	0	5.1	3.9
Cluster 3	5.8	5.1	0	5.7
Cluster 4	5.7	3.9	5.7	0

It is seen that the distances between average cluster profiles exceed the chosen threshold level but not essentially. So, it can be supposed that averaging of congener profiles between four selected clusters can serve as a reasonable estimate of congener profile for the considered emission sector. This average was calculated with weights determined by the number of profiles containing in each cluster and marked by red in Fig. 2.14. In the case when the distance between cluster averages is large repeated cluster analysis may be needed.

Thus, the proposed approach allows selecting similar congener patterns and computing averages for the use as the pattern for the analyzed sector.

As one more example, emission sector – Residential stationary sources will be considered. As follows from the EMEP emission data, this source is one of the most important among PCDD/F emission sources. 63 individual congener patterns were found for this source in the literature. Average values of congener fractions together with their range are shown in Fig. 2.15.

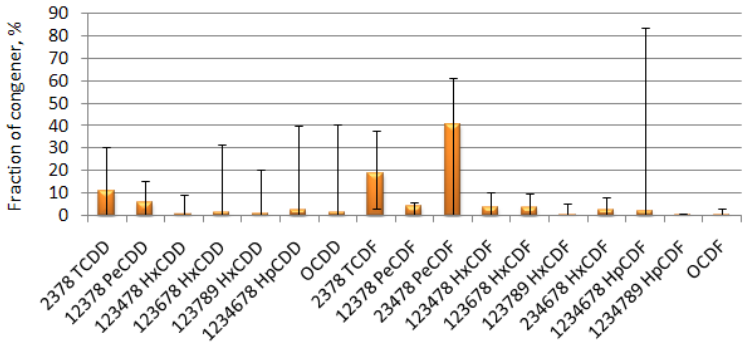

Fig. 2.15. *Averages of all congener profiles for emission Residential stationary sources sector. Whiskers show the range of congener fractions*

Large dispersion of individual values of congener fractions lead to the necessity of selecting similar congener patterns as this was done above. In selection of clusters containing similar congener patterns clusters containing only two patterns were not taken into account. So, three clusters were selected: one containing 38 congener patterns, and two containing 6 congener patterns each. Averaged profiles for these three clusters together with dispersion of congener fractions for each cluster are shown in Fig. 2.16.

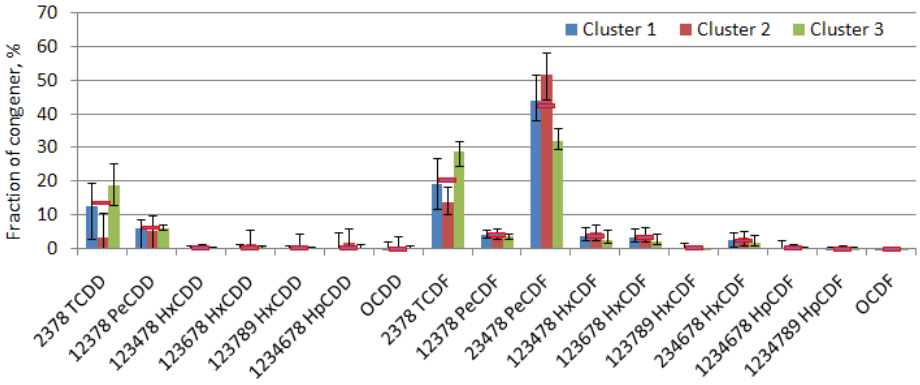

Fig. 2.16. *Comparison of the average congener profiles for the three selected clusters. The whiskers show ranges of congener fractions included to the given cluster. Red markers show congener profile averaged between two of three clusters (see the discussion below)*

From the above plot it is seen that two of average profiles are close to each other (Clusters 1 and 3) whereas the third profile (Cluster 2) has essential differences from those two. This can be confirmed by the calculated distance matrix for the three average profiles:

	Cluster 1	Cluster 2	Cluster 3
Cluster 1	0	3.3	4.0
Cluster 2	3.3	0	7.1
Cluster 3	4.0	7.1	0

Thus, it is reasonable to exclude Cluster 2 from the consideration and calculate average profile using Clusters 1 and 3 only. As above, here weighted averages with weights determined by number of elements in each cluster are used. The values of average profiles are shown by red markers in Fig. 2.16. To justify the choice made additional analysis of the omitted profiles should be done.

2.2.3. Concluding remarks

- To evaluate congener composition of PCDD/F emissions, literature search on the information on congener composition in emissions from source categories making main contributions to total toxicity of PCDD/F mixture was performed. A lot of measurement data on congener composition of PCDD/F mixture in emissions from main aggregated emission sectors contributing to PCDD/F toxicity are A_PublicPower, C_OtherStationaryCombustion, B_Industry, J_Waste, F_RoadTransport and L_AgriOther was found.
- Preliminary analysis of the data for sectors 2C1 – Iron and steel production and 1A4bi – Residential stationary sources was performed at the first stage of the work. It was found that congener profiles for one and the same emission sector taken from the literature can be essentially different. To work out typical congener composition for a particular sector hierarchical cluster analysis should be applied.

- The above analysis allowed working out the methodology of the analysis of the data on PCDD/F congener composition in emissions. The work on the literature search of additional data on congener profiles and analysis of the obtained data is planned to be continued in the forthcoming year for preparation of emission scenarios for congener-specific modelling.

2.3. Evaluation of B[a]P contamination in urban/suburban areas of the Czech Republic

Each year, in accordance with the requirements of POP Protocol, MSC-E performs evaluation of pollution of the EMEP region and transboundary fluxes of persistent organic pollutants including B[a]P as an indicator compound of PAHs. The results of this evaluation are exemplified by the map of annual means of B[a]P concentrations in 2013 calculated by MSC-E (Fig. 2.17).

The comparison of the obtained results with measurements at EMEP monitoring sites and rural background sites included in EU database AirBase shows relatively good agreement of calculation results with monitoring data. In particular, correlation coefficient between measurements and calculation results is about 0.7, and relative bias equals 45%. About 60% of calculated values are found to be within a factor of two with respect to measurements.

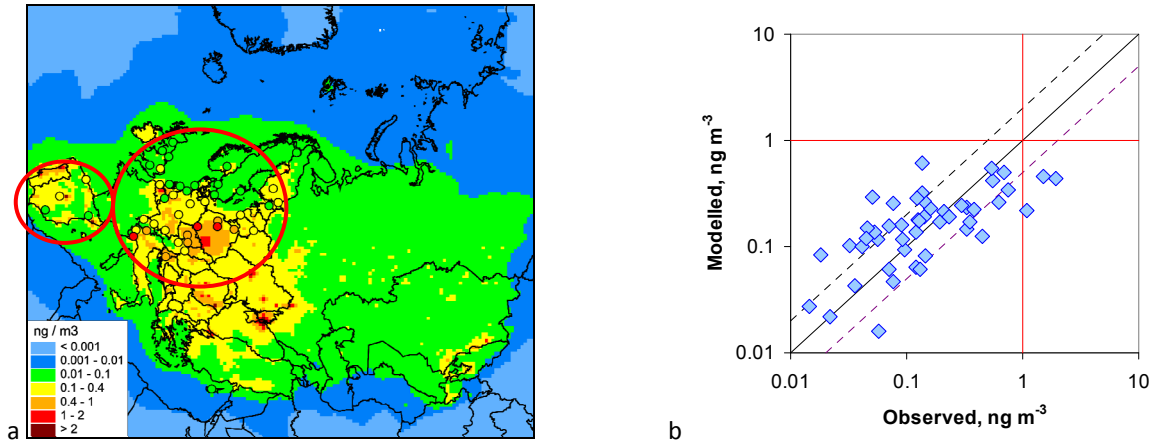

Fig. 2.17. *Modelled B[a]P annual means of air concentrations for 2013 (a) and comparison of calculation results with EMEP/AirBase measurements at rural/background monitoring sites*

The results of model estimations shows elevated levels of concentrations in Central and Eastern Europe and in some regions of Portugal and Spain (see Fig. 2.17). Based on calculation results population in EMEP countries living in regions with exceeded EU target values was estimated (Fig. 2.18). According to these results about 5% of population in the EMEP countries is living in areas with exceeded EU target value (1 ng/m^3) for B[a]P air concentrations.

At this stage contamination in cities with high population density in the Czech Republic (Prague and Ostrava regions) for 2013 is investigated. This year was selected for the analysis since a lot of measurement data for this year is presented in the EU database AirBase. Short description of these results was given in the MSC-E Status Report [*Gusev et al.*, 2016]. In addition, to make the results of the present study consistence with the results of evaluation of Cd contamination obtained earlier for the Czech Republic (see [*Ilyin et al.*, 2012]), calculations were provided for 2007 with resolution 5×5 km^2.

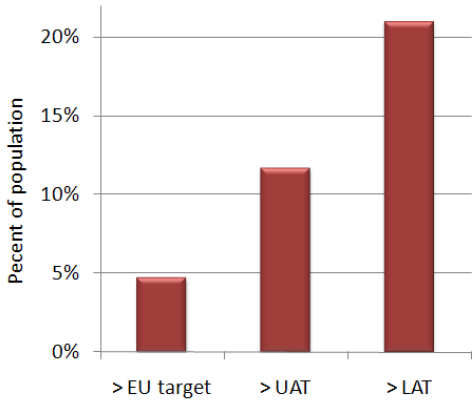

Fig. 2.18. *Percentage of population of the EMEP countries living in the areas with annual mean B[a]P air concentrations above the EU limit values: EU target value for B[a]P – 1.0 ng/m^3, UAT – 0.6 ng/m^3, LAT – 0.4 ng/m^3*

2.3.1. Input data

Calculations of background concentrations for the evaluation of contamination in urban regions in the Czech Republic were made by MSCE-POP model for 2007 and 2013 with resolutions 50×50 km^2 (standard EMEP calculations) and 5×5 km^2. For the latter resolution, calculations were performed in a sub-domain containing the Czech Republic and parts of neighbouring countries. Emissions for these calculations were generated with the use of national emission data and official data received from CEIP. As an example, emission data for 2013 is shown in Fig. 2.19. Emission data for calculations with fine spatial resolution (5×5 km^2) was prepared for four source groups (industry, residential heating, road transport and waste incineration).

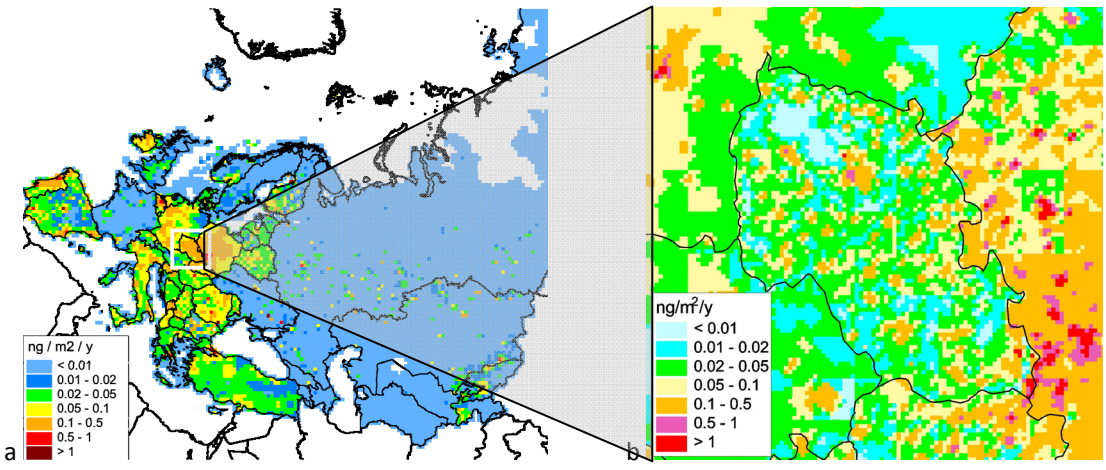

Fig. 2.19. *Emission data used for calculations of background concentrations in the Czech Republic with resolution 50×50 km^2 (a) and 5×5 km^2 (b)*

Further, measurement data from EU database AirBase for 2007 and 2013 were used.

2.3.2. Investigation of contamination in 2007

Calculation results

B[a]P air concentrations obtained by fine resolution modelling together with locations of measurement sites is shown in Fig 2.20. For comparison, measurement data obtained from AirBase database for 2007 is used. The range of measured B[a]P annual means of concentrations at sites of various types is as follows: background rural (0.3-0.5 ng/m^3), background suburban (0.7-2.2 ng/m^3), urban (1.2-5 ng/m^3).

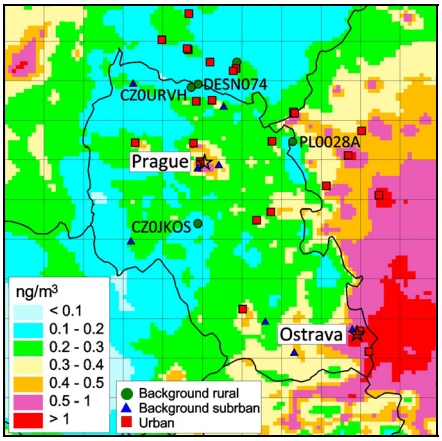

Fig. 2.20. *Air concentrations of B[a]P calculated by MSC-E model with resolution 5×5 km^2 together with available measurements*

Calculations made by the model essentially underestimate air concentrations. So, for background rural locations model shows concentrations varying from 0.12 ng/m^3 to 0.17 ng/m^3, for background suburban locations – from 0.3 ng/m^3 to 0.7 ng/m^3, and for urban locations – from 0.2 ng/m^3 to 3.5 ng/m^3. Underestimation of measured concentrations by the model is conditioned by averaging of air concentrations over the cells of modelling grid, which can lead to diminishing of concentration levels compared with measurements at particular locations especially in highly populated regions. More detailed comparison between observed and modelled concentrations will be given below.

Comparison with measurements

The comparison between observations and modelling results will be performed separately for various site locations (background suburban, urban and background rural).

<u>Background suburban and urban sites</u>

For background suburban and urban sites marked in Fig. 2.20 by triangles and squares, respectively, average observation-to-model ratio is 3.5 (for suburban background sites) and 4.5 (for urban sites). The plots of these ratios for all considered sites are displayed in Fig. 2.21. For comparison, values of observation-to-model ratios obtained by 50×50 km^2 resolution calculations are also added. It should be noticed that, in spite of underestimation of absolute values, the model correctly reproduces spatial distribution of contamination for suburban background sites and urban sites. So, correlation between observed and modelled values for background suburban locations is 0.75, and for urban locations 0.85.

It is seen that for almost all urban sites observation-to-model ratio for fine resolution calculations has been diminished compared to 50×50 km^2 resolution calculations (with exception of CZ0LLIM and CZ0SKLS), and the same is true for most of suburban background sites. So, transition to fine

resolution modelling can slightly reduce the difference between model results and observations even at such types of sites.

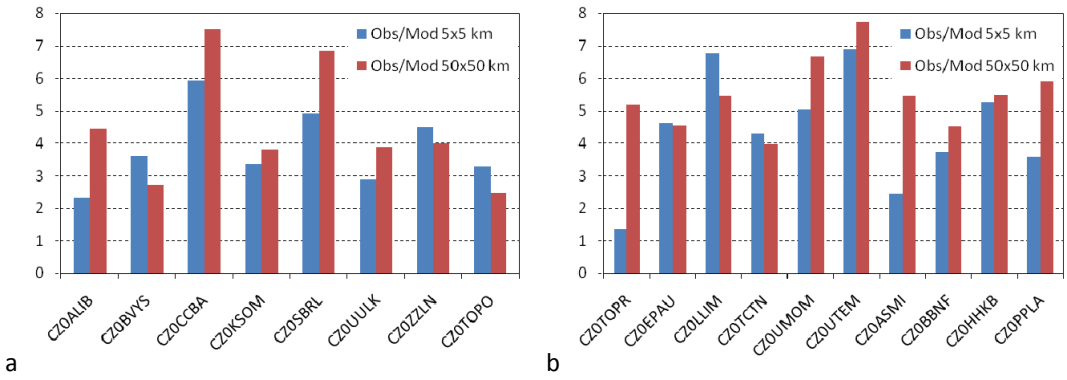

a b

Fig. 2.21. *Observation-to-model ratio for suburban background sites (a) and urban sites (b) for calculations with 5x5 km^2 and 50x50 km^2 resolutions*

Rural background sites

There are four rural background sites located in the Czech Republic or near its boundary: Czech sites CZ0JKOS (EMEP site Kosetice) and CZ0URVH, German site DESN074, and Polish site PL0028A (Fig. 2.20). The plots of observed and modelled annual averages of B[a]P air concentrations at these sites are shown in Fig. 2.22.

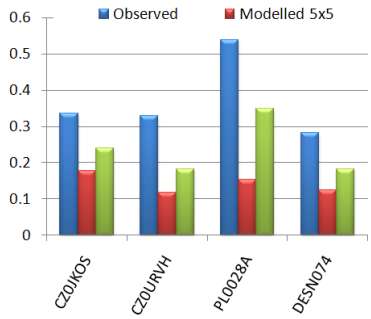

Fig.2.22. *Observed B[a]P concentrations and modelling results with 5x5 km^2 and 50x50 km^2 resolutions*

It can be noticed that the results of calculations with 5x5 km^2 resolution show worse agreement with observations than those with 50x50 km^2 resolution. To reveal the reason of this phenomenon ***relative local variability*** of pollution in a neighbourhood of the particular site could be considered. Relative variations of modelled B[a]P air concentrations near the corresponding grid cell *j*, Var_j, is evaluated using 9-gridcell moving matrix: $Var_j = C_{max} / C_{min}$ (Fig. 2.23).

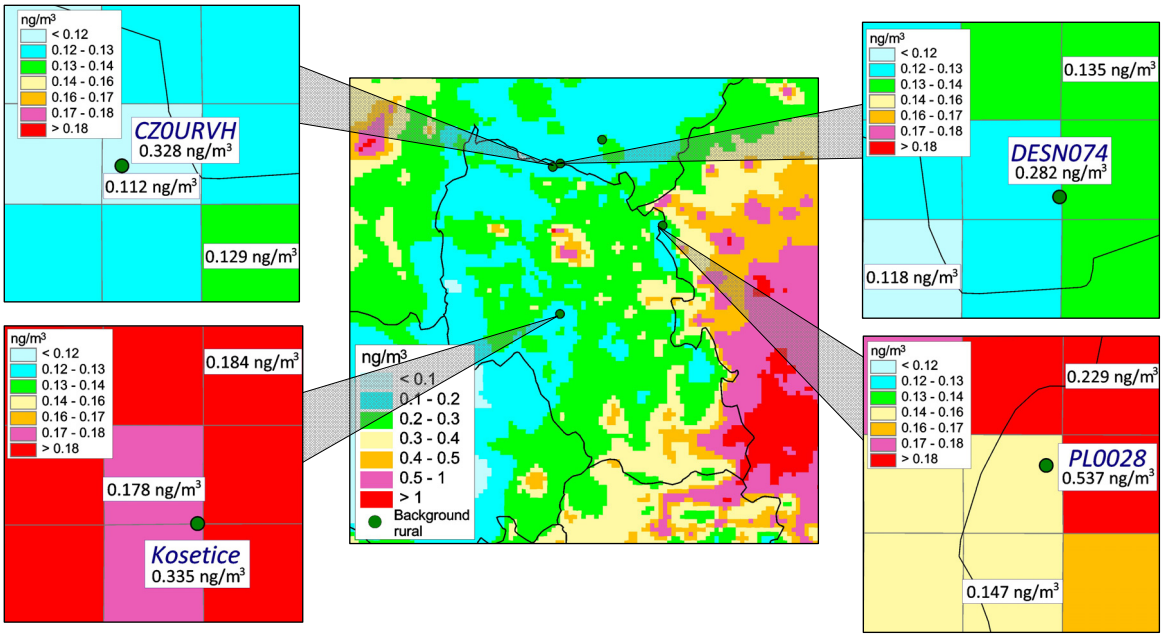

Fig. 2.23. *Local variability of B[a]P air concentrations around the sites: CZ0JKOS (Kosetice) ,CZ0URVH, PL0028A (Poland), DESN074 (Germany)*

The observed-to-model ratio together with spatial variability for the background rural sites is shown in Table 2.5.

Table 2.5. *Observed-to-model ratio for fine resolution modelling and spatial variability of concentrations for the considered four background rural sites*

Site	Observed	Obs/Mod ratio	Variability of modelling results
CZ0JKOS (Kosetice)	0.33	1.9	1.03
CZ0URVH	0.33	2.8	1.17
PL0028A	0.54	3.5	1.55
DESN074	0.28	2.3	1.15

It is seen that greater variability leads to worse agreement between observations and model results. For the explanation of this fact it should be taken into account that most of these sites are situated close to the boundaries of cells in which they are located. As a result, the values of concentrations at these sites can be influenced not only by concentrations at the corresponding sites themselves but also by concentrations in neighbouring sites. Consequently, the uncertainty is larger in cells with larger variability of concentrations. Availability of more detailed information on emission spatial distribution could refine observation-to-model agreement.

It is also interesting to find out which source groups are responsible for formation of air concentrations at rural background sites. The contributions of four above source groups to these sites are summarized in Table 2.6.

Table 2.6. *Contribution of different source categories (Industry (IND), Residential heating (RES), Road transport (ROT) to the pollution level in the background rural sites locations*

Site	Contribution of source categories		
	IND	RES	ROT
CZ0JKOS (Kosetice)	7.6%	87.4%	5.0%
CZ0URVH	6.9%	88.3%	4.8%
PL0028A	9.1%	86.4%	4.5%
DESN074	6.4%	89.2%	4.4%

The main input to the contamination of these sites is made by residential heating; the contributions of industry and road transport are almost negligible. So, it can be concluded that contamination at background sites reflects mostly emission levels from residential heating.

Additional information on the agreement between observed and modelled values of air concentrations can be derived from the comparison of their seasonal variations (Fig. 2.24).

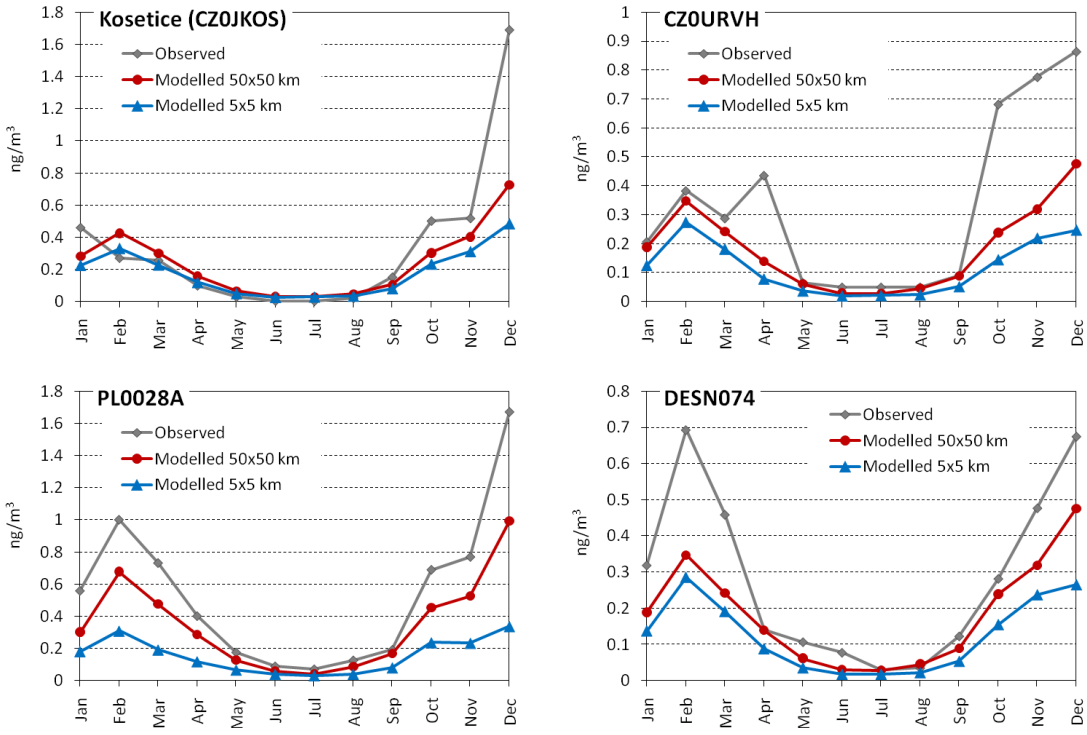

Fig. 2.24. *Comparison between observed and modelled B[a]P air concentrations at rural background sites with 5x5 km^2 and 50x50 km^2 resolutions*

Comparison between observed and modelled B[a]P air concentrations for CZ measurement sites CZ0JKOS and CZ0URVH shows significant underestimation for the end of the year. The comparison at German and Polish sites DESN074 and PL0028A shows high correlation between observed and modelled concentrations (0.95 and more). However, underestimation of concentrations in winter months takes place also. Calculations with the standard EMEP resolution show much more reasonable result. It should be noted that sites CZ0URVH and DESN074 are located within one and the same 50×50 km^2 grid cell. The plots in Fig. 2.24 show that the agreement between 50x50 km^2 calculations and observations at CZ0URVH is better in the first half of the year whereas the

agreement at DESN074 is good for the second half of the year. It leads to the assumption that modelling with fine resolution can improve the agreement provided that emissions with fine resolution are available for all neighbouring countries.

The analysis of the agreement between observation and modelling results for 2007 allows drawing the following conclusions:

- Model underestimates pollution levels especially at suburban background and urban locations. However, correlations between observations and modelling results are high for all considered types of site locations.
- Local variability of B[a]P concentrations is an important characteristic for the comparison of observed and modelled values of B[a]P concentrations. It was found that at locations with high variability of concentrations the observation/modelling agreement occurs to be worse. More detailed information on emission spatial distribution is needed for refining the agreement.
- For more reliable estimation of pollution in urban areas the information on seasonal variations of emissions for main emission sectors is needed.

Ostrava and Prague

Let us pass to the evaluation of contamination in the regions. Spatial distribution of annual means of B[a]P concentrations together with and locations of large point sources and measurements cites (CZ0TOPR, CZ0TOPO, CZ0OASMI, CZ0ALIB) is shown in Fig. 2.25. It should be stressed that the concentrations of B[a]P in winter period can exceed annual means up to the order of magnitude (see Fig. 2.24).

The locations of large point sources are taken from official emission data (for the Czech Republic) and from EPER database (for other countries). In particular, the enterprises Arcelor Mittal with essential emissions (over 300 kg per year) and LPSs of OKK Koksovny (with overall emissions about 230 kg/y) are located within the Ostrava city. LPS with emissions of 1.69 kg/y is located within the Prague city (see Fig. 2.25).

Spatial distribution and levels of B[a]P air concentrations in Ostrava are determined mainly by contribution of LPS located in the city. High variability of air concentrations in Ostrava is in a large extent conditioned by the location of these sources within the city. On the opposite, the concentration pattern in Prague city is much more homogeneous since LPS within Prague has relatively small intensity.

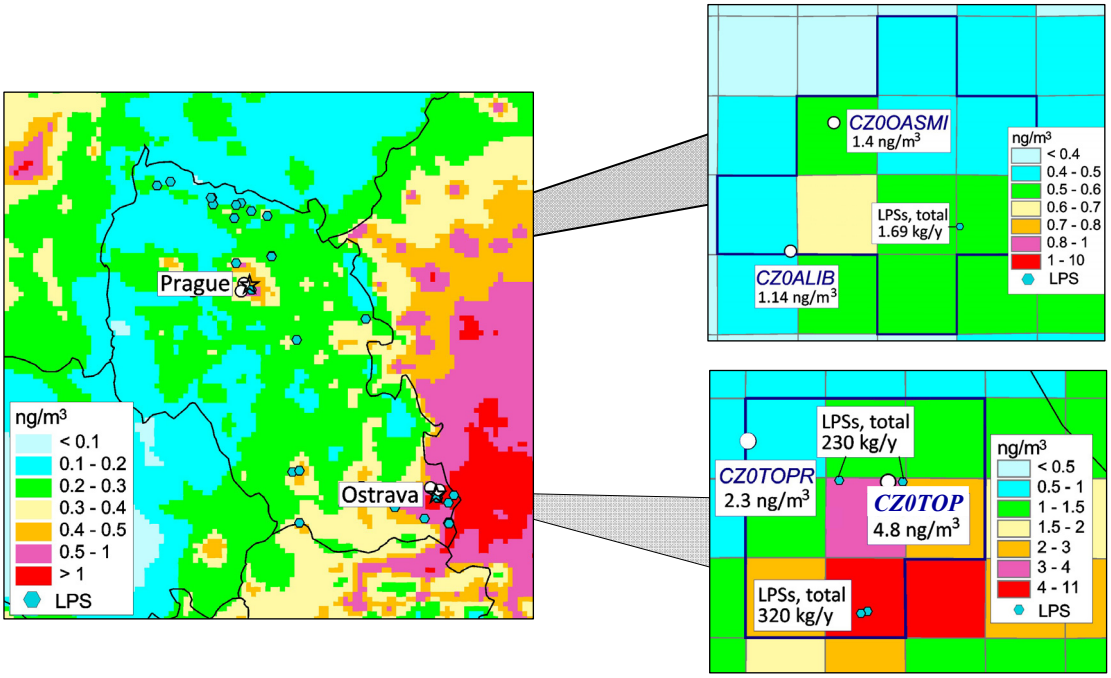

Fig. 2.25. *Spatial distribution of annual means of B[a]P air concentrations together with locations of large point sources and measurements cites (CZ0TOPR, CZ0TOPO, CZ0OASMI, CZ0ALIB).*

Spatial distribution of B[a]P annual means of air concentrations originated from Ostrava and Prague sources is shown in Fig. 2.26.

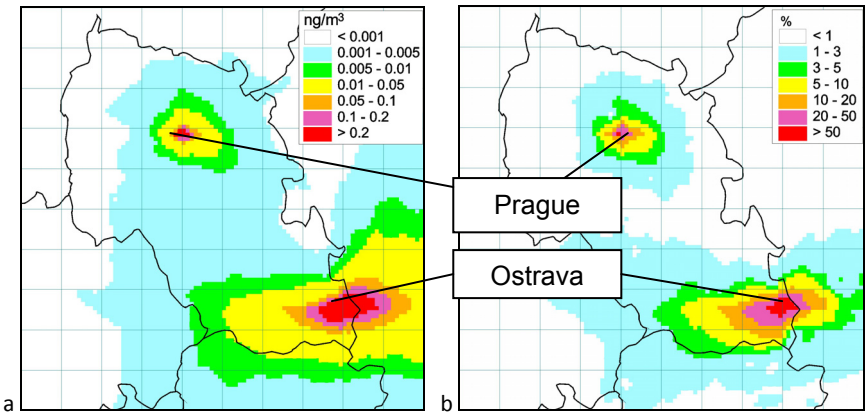

Fig. 2.26. *Spatial distribution of B[a]P annual means of air concentrations originated from Ostrava and Prague sources: absolute values (a) and relative contributions to the overall contamination (b)*

It is seen that the area covered by contamination from Ostrava sources is rather wide. Calculations show that the contribution of Ostrava sources is greater than 10% over the area of 4330 square kilometers and greater than 20% over the area of 1850 square kilometers. In particular, B[a]P emission from Ostrava can contribute to contamination in Poland (transboundary transport of pollution, see Fig. 2.26a,b). Level of contamination from emission sources located in Prague is much lower. The area over which the contribution of Prague sources is more than 20% amounts to about 220 km^2, and the contributions of 10% and more is about 700 km^2. It should be noticed that the

concentration levels in Prague is about 5 times lower than in Ostrava (at the level of annual averages).

To further illustrate the pattern of contamination in Ostrava to the B[a]P contamination, calculations of local variability were performed for sites CZ0TOPO and CZ0TOPR. The results of calculations are summarized in Table 2.7 together with contribution of main source groups to the contamination at these sites.

Table 2.7. *Observed-to-model ratio and spatial variability of concentrations for the selected sites*

Site	Obs/Mod ratio	Variability	Contribution of source groups		
			IND	RES	ROT
CZ0TOPO (Ostrava)	3.3	6.9	36.4%	60.9%	2.7%
CZ0TOPR (Ostrava)	1.4	14.7	82.9%	16.3%	0.8%

The spatial variability at these sites amounts from 7 to 15 times, which is much higher than at background rural sites (see Table 2.5 above). Maximum variability is found at site CZ0TOPR located near large point source and marked in AirBase database as Industrial Urban. Besides, the contributions of industrial sources are rather high (up to over 80%), especially at the site CZ0TOPR.

It should be mentioned that the contributions of all emission sources for pollution in cities vary both in space and time. Seasonal variations of contributions of the considered source categories to the contamination of two selected cells in Ostrava (one containing suburban site CZ0TOPO and the other containing urban site CZ0TOPR) are shown in Fig. 2.27.

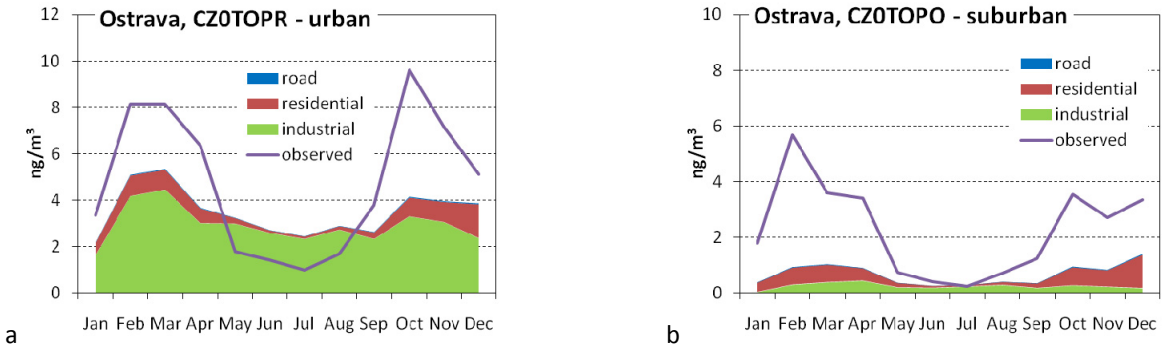

Fig. 2.27. *Seasonal variations of contamination two selected grid cells in Ostrava together with observation values (a - CZ0TOPR, b - CZ0TOPO)*

For illustration of the agreement between observed and model seasonality, values of observed and modelled concentrations for the above two locations in Ostrava are normalized by annual averages. (see Fig. 2.28). This allows focusing on seasonal variations without regard to the difference of absolute values.

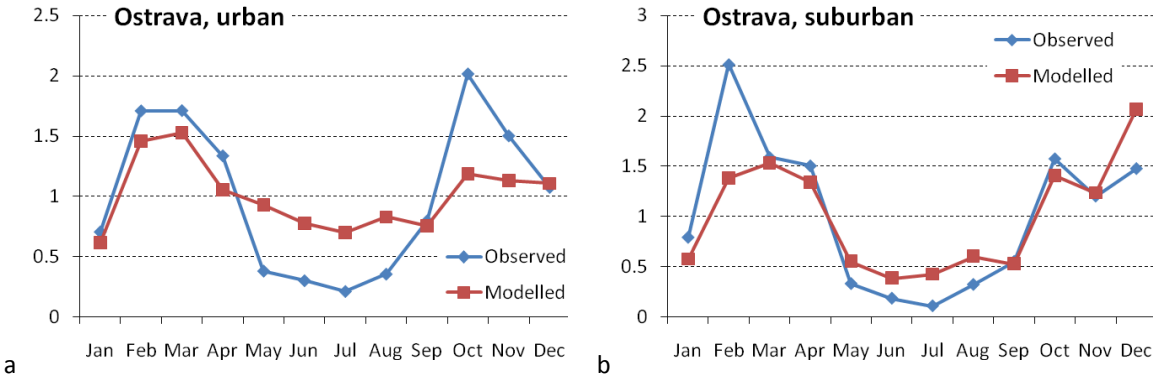

Fig. 2.28. *Comparison of observed and modelled values of air concentrations at two Ostrava sites (urban site CZ0TOPR and suburban site CZ0TOPO) normalized by annual averages*

At suburban site CZ0TOPO (Fig. 2.28b) model results and observations show better agreement of seasonality of observed and modelled B[a]P concentrations then at urban site CZ0TOPR inside Ostrava (Fig. 2.28a). This can lead to the conclusion that seasonal variations of contamination from industrial sector are underestimated by the model. Refinement of calculated seasonal variations of pollution requires country-specific information on seasonal variations of emissions from this sector.

The above analysis allows making the following conclusions:

- Contamination levels in different locations within the city can vary several times. The values of air concentrations calculated by the model strongly underestimate real values of concentrations.
- Contributions of source groups to the contamination for different grid cells can vary essentially. Thus, main contribution for urban location in Ostrava is made by industrial sources (over 80% on the average) whereas for suburban location main contributor is residential heating (over 60%).
- Contributions of source groups vary with time. In particular, contribution of industrial sources is maximum in warm months and minimum in cold ones.

2.3.3. Evaluation of contamination of urban regions

As was shown above, calculations made by EMEP modelling system with resolution 50×50 km^2 underestimate concentration levels in populated areas in Europe due to smoothing spatial distribution of concentrations thus not being able to reflect sharp gradients observed in urban areas.

For evaluation of true concentrations in urban regions, MSC-E has initiated the work on evaluation of B[a]P concentration levels in urban areas in Europe based on model calculations. At this stage contamination in cities with high population density in the Czech Republic (Prague and Ostrava regions) in 2013 is investigated using model calculation with resolution 5×5 km^2. It was found that even with fine resolution applied direct application of the model cannot reflect concentration levels in urban areas. The methodology of the evaluation of urban B[a]P concentrations regression analysis

approach using modelling results and available measurements is applied. Since maximum measurement data from AirBase is available for 2013, at the first stage the analysis was performed for this year.

The results of calculations of B[a]P concentrations in 2013 are shown in Fig. 2.29 in comparison with measurement data from AirBase at urban/suburban sites.

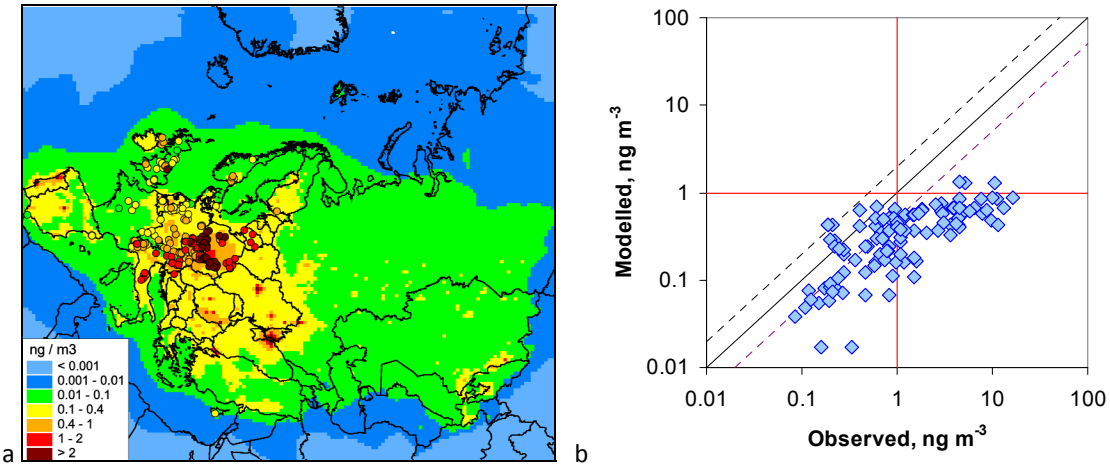

Fig. 2.29. *Modelled B[a]P annual means of air concentrations for 2013 (a) and comparison of calculation results with EMEP/AirBase measurements at suburban/urban monitoring sites (b)*

As seen from Fig. 2.29b, modelled values underestimate concentration levels in suburban and urban regions. Average values of B[a]P concentrations for EMEP countries obtained from AirBase measurements are shown in Fig. 2.30.

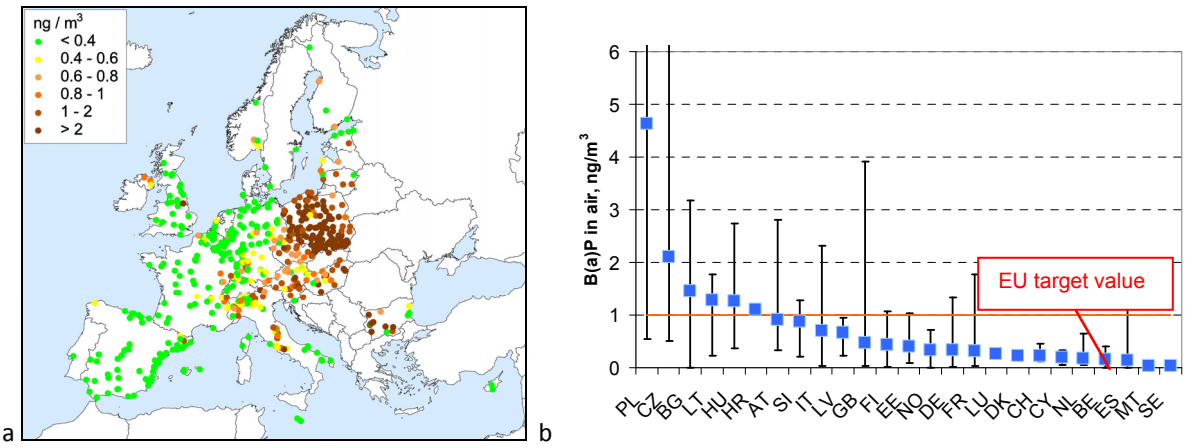

Fig. 2.30. *Measurement data on B[a]P air concentrations (annual means) in Europe in 2013 according to EEA AirBase data (a) and averages for EMEP countries (b)*

Therefore, estimates of numbers of people living in highly polluted areas presented in Fig. 2.18 should be considered as lower bounds. Of course, modelling with finer resolution can provide more reliable estimates of B[a]P concentrations in urban areas.

The fact that B[a]P concentrations exceed EU target value of 1 ng/m^3 in wide areas in Europe is confirmed by a number of studies (see, e. g., EEA SOER, 2015)

Regression analysis

Calculations with fine spatial resolution together with available measurement data allow evaluating concentration levels in urban regions. Multi-parameter regression models to determine functional relationship between regional/background and urban concentrations (urban increment) using additional parameters (altitude, emissions, wind speed, …) were used in a number of previous investigations. Among them we mention

- CityDelta project [*Cuvelier et al.*, 2007; *AtmEnv; Amann et al.,* 2007, IIASA): parameterization of functional relationship connecting urban and regional emissions with urban concentrations of $PM_{2.5}$
- [*Ortiz and Friedrich*, 2013, APR]: predictions of urban increment from measured background concentrations of PM_{10} and NO_2 concentrations in Germany
- [*Guerreiro et al.*, 2014, ETC/ATM]: estimation of gridded B[a]P air concentrations using linear regression model followed by spatial interpolation based on measurement data and additional parameters (altitude, temperature) including modelling results

Such evaluation is based on estimating so-called urban increment that is the difference between concentrations at urban locations and those in close rural locations on the basis of regression analysis. Our approach is close to that of [*Ortiz and Friedrich*, 2013] applied for NOx and PM. In this study, urban increment for several urban areas has been estimated using observational data from paired rural and urban background measurement sites. Measured urban increment was used in the regression analysis with relevant factors among which the ratio of emission density to average wind speed was considered.

Unfortunately, this approach cannot be applied directly to the investigation of B[a]P due to the deficiency of paired rural and urban background measurement sites. In the approach used by MSC-E for B[a]P regression analysis is used to evaluation of concentration levels in urban areas inside the EMEP region including their spatial distribution. Factors influencing concentrations in urban regions are constructed with the help of emission data, meteorological data and model calculations. At the first stage of investigation, evaluation of B[a]P concentrations were done for the Czech Republic taking into account high values of air contamination (see Fig. 2.31b) and availability of sufficient number of measurement data in AirBase.

In the consideration of B[a]P air contamination for 2007, it was found that variations of concentrations in a neighbourhood of the considered location and contributions of various source groups have essential influence on concentrations in urban/suburban regions. So, regression relation for evaluating B[a]P air concentrations in the corresponding grid cells may be as follows:

$$C_j = C_{est,j} + \omega_j = \alpha \cdot Var_j^* + \frac{1}{W_{av,j}}\left(\beta_{IND} \cdot e_{IND,j} + \beta_{RES} \cdot e_{RES,j} + \beta_{ROT} \cdot e_{ROT,j} + \beta_{WST} \cdot e_{WST,j}\right) + \omega_j , \qquad [2.10]$$

where: C_j is B[a]P concentration in the grid cell *j* under evaluation,

$C_{est,j}$ is the value of B[a]P concentration in grid cell *j* estimated by regression model,

$W_{av,j}$ is average wind speed in the cell j,

$e_{IND,j}$, $e_{RES,j}$, $e_{ROT,j}$ and $e_{WST,j}$ are emission densities of main emission source groups (INDustry, RESidential heating, ROad Transport and WaSTe incineration) in the cell *j*,

α, β_{IND}, β_{RES}, β_{ROT} and β_{WST} are regression coefficients, and

ω_j is the value of "random component" in the cell j that is the component influencing by factors not taken into account by the regression model.

Variations of modelled B[a]P concentrations Var_j^* in the corresponding grid cell *j* is evaluated as the product of calculated concentration $C_{j,\mathrm{mod}}$ and *relative variation* Var_j (the definition of Var_j is illustrated above in Fig. 2.25; see also the discussion therein):

$$Var_j^* = Var_j \cdot C_{j,\mathrm{mod}}. \qquad [2.11]$$

It was found that the results of regression analysis strongly depend on the country under consideration. This is conditioned by the fact that underestimation of urban/suburban concentrations by the model is different for different countries. For example, underestimation of urban concentrations is about 2.5 times for the Czech Republic and about 6.5 times for Poland. Below only measurements made at Czech sites were used for evaluation of urban concentrations in the Czech Republic.

Different factors can have different influence at the results of regression analysis. In particular, it is interesting to examine the influence of the factor Var_j^*. Further, contributions of various source groups to B[a]P emissions are different. According to CEIP data the contributions of emission source groups to the overall B[a]P emissions are as follows:

Industrial sources	16.5%
Residential heating	77.0%
Road transport	6.5%
Waste incineration	0.002%

According to these contributions it is interesting whether source group WST can be excluded from the regression analysis. To evaluate the influence of the factors Var_j^* and $e_{WST,j}$, regression scheme [2.10] was applied subsequently with one of the above parameters omitted. The results of such calculations are shown in Fig. 2.32.

Fig. 2.32. *Evaluation of statistical significance of two selected factors*

It was found that deleting the factor Var_j^* from the regression scheme essentially changes air concentrations obtained with application of the scheme, whereas omitting the factor $e_{WST,j}$ leads to inessential changes. Correlation coefficient between regression results and observations for full regression scheme and for the scheme with omitted $e_{WST,j}$ equals 0.75, and diminishes up to 0.44 with omitted Var_j^*. So, the parameter $e_{WST,j}$ can be neglected in regression (at least with current emission data) and final regression relation becomes

$$C_j = C_{est,j} + \omega_j = \alpha \cdot Var_j^* + \frac{1}{W_{av,j}}\left(\beta_{IND} \cdot e_{IND,j} + \beta_{RES} \cdot e_{RES,j} + \beta_{ROT} \cdot e_{ROT,j}\right) + \omega_j , \qquad [2.12]$$

At further stage of the work it is planned to examine possible inclusion of additional meteorological parameters influencing urban air concentrations (e.g. atmospheric stability, mixing layer height, etc.).

The application of regression model for evaluating urban concentration levels is performed into two stages. At the first stage, regression coefficients α, β_{IND}, β_{RES} and β_{ROT} are calculated minimizing square deviation of ω over all cells where background urban/suburban measurements sites are located. Then formulas for $C_{est,j}$ are used for calculation of urban B[a]P concentrations in all grid cells where urban areas exist. Finally, adjusted concentrations in all grid cells are evaluated as weighted averages of background concentrations (supposed to be equal to model estimates) and urban concentrations calculated by regression model:

$$C_j = f_{urb,j} \cdot C_{urb} + (1 - f_{urb,j}) \cdot C_{\mathrm{mod}} \qquad [2.13]$$

where $f_{urb,j}$ is the fraction of urban area in the cell j. Data on gridded distribution of urban and rural areas have been adapted from the outcome of the project GRUMP1 [http://sedac.ciesin.columbia.edu/].

For evaluation of the reliability of the obtained regression estimates available measurements were split into two sets *training set of data* containing sites marked as background urban and suburban and *test set of data* containing sites marked as industrial urban and traffic urban (see Fig. 2.33). Regression coefficients calculated with the help of sites from the training set were then applied to the sites from test set. The results are displayed in Fig. 2.34.

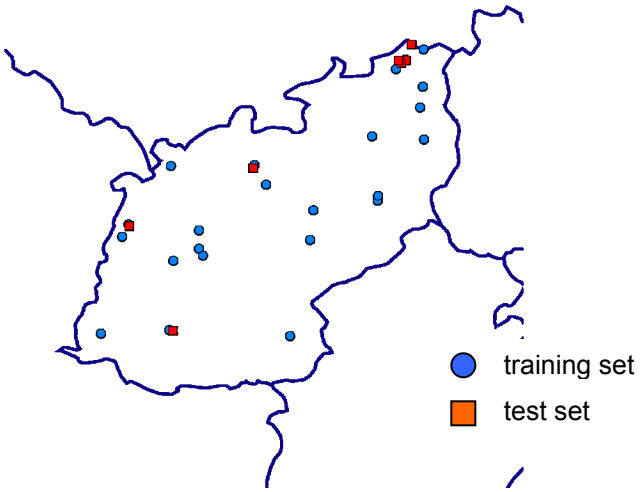

Fig. 2.33. *Location of measurement sites from EEA AirBase in the Czech Republic used for the regression analysis*

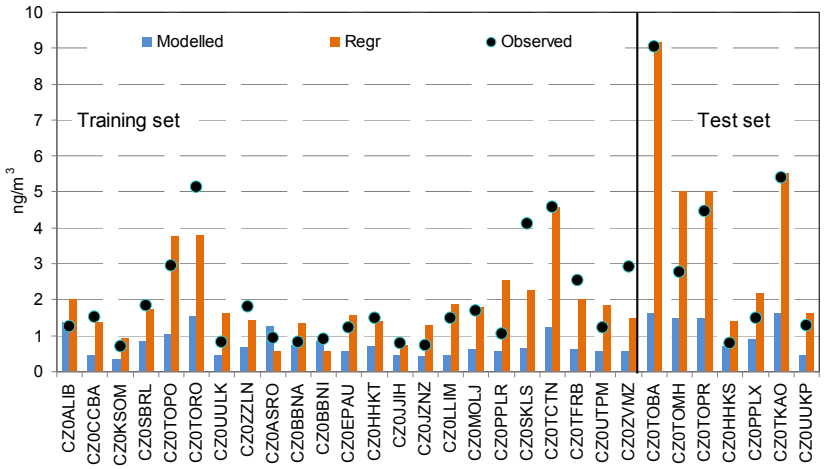

Fig. 2.34. *Observed annual mean B[a]P air concentrations at sites from training and test sets vs. results of fine resolution modelling and of regression model*

Statistical parameters describing the results of the comparison of fine resolution modelling and regression model results on annual mean B[a]P air concentrations with measurements of selected background urban and suburban sites are shown in Table 2.8.

Table 2.8. *Statistical parameters describing the results of the comparison of fine resolution modelling and regression model results on annual mean B[a]P air concentrations with measurements of selected background urban and suburban sites*

	Modelled concentrations	Regression model estimates
Relative bias	60%	0.01%
Normalized root mean square error (NRMSE)	85%	41%
Fractions of sites with agreement within a factor of 2	39%	96%
Correlation coefficient	0.52	0.79

It can be seen that application of the regression model leads to substantial decrease of bias between the modelled and observed concentrations and of normalized mean square error. Almost all values of concentrations, calculated by the regression model, are within a factor of 2 with observed concentrations. Besides, better correlation is obtained between regression model estimates and measurements in comparison with estimates of dispersion modelling.

Comparison of observation values with the results of evaluation by regression relation show the agreement within a factor of 2 for all sites. The rest statistical parameters for the comparison of are as follows:

- Relative bias – 18%
- Normalized root mean square error 27%
- Correlation coefficient 0.97

So, this comparison shows that regression relation [2.12] with the parameters obtained from the training set is reliable also for other urban/suburban locations and, hence, seems to be applicable for evaluation of B[a]P concentration levels in the grid cells in the Czech Republic where no measurements are available.

Evaluation of spatial distribution of B[a]P air concentrations in urban areas of the Czech Republic

Multiple regression analysis, performed for selected background urban and suburban monitoring sites, permits to obtain functional relationship between observed urban concentrations and additional parameters (see the equation [2.12]). This relationship can be used then to estimate B[a]P air concentrations for urban areas of the Czech Republic where measurements are absent. In Fig. 2.35a spatial distribution of air concentrations in urban areas, calculated using regression equation [2.12] and values of coefficients α, β_{IND}, β_{RES} and β_{ROT}, derived from the regression analysis, is presented. Resulted distribution of B[a]P air concentrations is subsequently merged with the output of fine resolution model simulation using the gridded information on the fractions of urban and rural areas (see formula [2.13] above). Combined spatial distribution of B[a]P annual mean air concentrations in the Czech Republic for 2013 is shown in Fig. 2.35b.

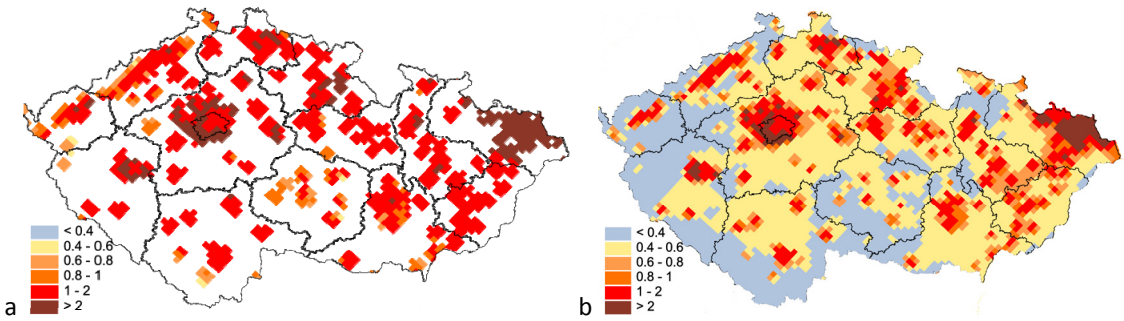

Fig. 2.35. *Spatial distribution of B[a]P air concentrations in urban areas, calculated using multiple regression analysis (a) and combined spatial distribution of B[a]P annual mean air concentrations in the Czech Republic for 2013 (b)*

To refine estimates of B[a]P air concentrations for urban areas further improvement of regression model is required, namely, inclusion of additional meteorological parameters influencing urban air concentrations (e.g. atmospheric stability, mixing layer height, etc.). At further stage of the work developing approach is planned to be applied for other EMEP countries, provided that the data on emissions and measurements are available, in close co-operation with national experts on monitoring of pollution levels and evaluation of emissions as well as with experts from TFEIP, CEIP, CCC, and EEA.

2.3.4. Concluding remarks

- Observation data show that there are essential exceedancies of B[a]P air concentrations over the EU target value of 1 ng/m^3 in mostly populated regions in the EMEP domain. So, the investigation of B[a]P contamination in cities is now a task of high relevance.

- The model reasonably represents B[a]P contamination levels at background rural locations (observed-to-model ratio equals 1.6 on the average for 50×50 km^2 resolution). For background suburban locations observed-to-model ratio is found to be about 2 – 3, and for urban locations – about 5 – 6. However, observed and modelled spatial distribution for sites of the two last types agrees with each other (with correlation about 0.5 – 0.7).

- Modelling with fine spatial resolution can refine the agreement between observations and model results. For the refinement availability of emission data with fine resolution is of crucial importance.

- A regression model for evaluation B[a]P air concentrations in urban areas is under development. At present factors included into the model are: the results of fine resolution modelling, data on emissions from main emission sectors and meteorological conditions (wind speed). It was found that the model should be used separately in various countries, taking into account the uncertainties in current emission data.

- At the first stage of the investigation spatial distribution of B[a]P concentrations in the urban areas of the Czech Republic is evaluated. At further stages of the work developing approach is planned to be applied for other EMEP countries, provided that the data on emissions and measurements are available, in close co-operation with national experts as well as with experts from TFEIP, CEIP, CCC, and EEA.

- To refine estimates of B[a]P air concentrations for urban areas further improvement of regression model is required, namely, inclusion of additional meteorological parameters influencing urban air concentrations (e.g. atmospheric stability, mixing layer height, etc.).

REFERENCES

Al-Fatlawi and Al-Alwani [2012]. Heavy metal pollution of roadside dust samples with different traffic volumes at Hilla city. *The Iraqi Journal For Mechanical And Material Engineering*, Vol.12, No.4, 2012, 660-672.

Amann M., J. Cofala, A. Gzella, C. Heyes, Z. Klimont, W. Schöpp [2007] Estimating concentrations of fine particulate matter in urban background air of European cities. IIASA Interim Report IR-07-001. Available at: http://pure.iiasa.ac.at/8454/1/IR-07-001.pdf.

AMAP/UNEP [2013a] Technical Background Report for the Global Mercury Assessment 2013a. Arctic Monitoring and Assessment Programme, Oslo, Norway / UNEP Chemicals Branch, Geneva, Switzerland. vi + 263 pp.,.

AMAP/UNEP [2013b] Geospatially distributed mercury emissions dataset 2010v1, access: 1 August 2016.

Amato F., Schaap M., Denier van der Gon H.A.C., Pandolfi M., Alastuey A., Keuken M., Querol X. [2013] Short-term variability of mineral dust, metals and carbon emission from road dust resuspension. *Atmospheric Environment*, vol. 74, pp. 134 - 140.

AMNet [2016] Atmospheric Mercury Network. http://nadp.sws.uiuc.edu/amn/. Accessed on June 28, 2016.

Amos H. M., Jacob D. J., Holmes C. D., Fisher J. A., Wang Q., Yantosca R. M., Corbitt E. S., Galarneau E., Rutter A. P., Gustin M. S., Steffen A., Schauer J. J., Graydon J. A., St Louis V. L., Talbot R. W., Edgerton E. S., Zhang Y., and Sunderland E. M. [2012] Gas-particle partitioning of atmospheric Hg(II) and its effect on global mercury deposition, *Atmos. Chem. Phys*., 12, 591-603, doi:10.5194/acp-12-591-2012.

Balabanov N., Shepler, Peterson K. [2005] Accurate global potential energy surface and reaction dynamics for the ground state of $HgBr_2$. *J. Phys. Chem*. A, 109, 8765-8773.

Bergametti G., Rajot J.L., Pierre C., Bouet C. and Marticorena B. [2016]. How long does precipitation inhibit wind erosion in the Sahel? *Geophysical Research Letters*, Volume 43, Issue 12, 28 June 2016, Pages 6643–6649.

Bessagnet B., Menut L., Aymoz G., Chepfer H., and Vautard R. [2008]. Modeling dust emissions and transport within Europe: The Ukraine March 2007 event. *Journal Of Geophysical Research*, VOL. 113, D15202, 13 PP., 2008 doi:10.1029/2007JD009541.

Birmili W., Schepanski K., Ansmann A., Spindler G., Tegen I., Wehner B., Nowak A., Reimer E., Mattis I., Müller K., Brüggemann E., Gnauk T., Herrmann H., Wiedensohler A., Althausen D., Schladitz A., Tuch T., and Löschau G. [2008]. A case of extreme particulate matter concentrations over Central Europe caused by dust emitted over the southern Ukraine. *Atmos. Chem. Phys*., 8, 997–1016.

Breivik K., Sweetman A., Pacyna J.M., Jones K.C. [2007] Towards a global historical emission inventory for selected PCB congeners - A mass balance approach-3. An update. *Science of the Total Environment*, vol. 377, pp. 296-307.

CCC, 2016. EMEP laboratory intercomparison. Results from EMEP 33. http://www.nilu.no/projects/ccc/intercomparison/index.html. Visited 16.08.2016

CEIP [2016]. Centre on Emission Inventories and Projections. Informative Inventory Reports. http://www.ceip.at/ms/ceip_home1/ceip_home/status_reporting/2016_submissions/. Accessed on June 28, 2016.

Christoforidis A. and Stamatis N. [2009]. Heavy metal contamination in street dust and roadside soil along the major national road in Kavala's region, Greece. *Geoderma*, vol. 151, pp. 257–263.

Colette A. et al. [2016] Air pollution trends in the EMEP region between 1990 and 2012. EMEP: CCC-Report 1/2016, Kjeller, Norway.

Cuvelier C., P. Thunis, R. Stern, N. Moussiopoulos, P. Builtjes, L. Rouil, M. Bedogni, L. Tarrason, M. Amann, C. Heyes [2005] City-Delta Phase 2. Final Report. February 2005. Available at: http://ec.europa.eu/environment/archives/cafe/activities/pdf/city_delta.pdf

Dastoor A., Ryzhkov A., Durnford D., Lehnherr I., Steffen A. and Morrison H. [2015] Atmospheric mercury in the Canadian Arctic. Part II: Insight from modeling, *Sci. Total Environ*., 509-510, 16-27, http://dx.doi.org/10.1016/j.scitotenv.2014.10.112, 2015.

De Miguel E., Llamas J. F., Chacon E., Berg T., Larssen S., Røyset O. and Vadset M. [1997] Origin and patterns of distribution of trace elements in street dust. Unleaded petrol and urban lead. *Atmospheric Environment,* vol. 31, pp. 2733–2740.

De Simone F., Gencarelli C. N., Hedgecock I. M. and Pirrone N. [2014] Global atmospheric cycle of mercury: a model study on the impact of oxidation mechanisms, *Environ. Sci. Pollut*. R., 21, 4110-4123.

de Wit H.A., Hettelingh J-P., Harmens H. [2016]. Trends in ecosystem and health responses to long-range transported atmospheric pollutants. Norwegian Institute for Water Research, Report No. 6946-2015, ICP Waters report 125/2015. 92 p.

Dibble T. S., Zelie M. J., and Mao H. [2012] Thermodynamics of reactions of ClHg and BrHg radicals with atmospherically abundant free radicals, *Atmos. Chem. Phys*., 12, 10271-10279.

Donohoue D. L., Bauer D., Cossairt B., and Hynes A. J. [2006] Temperature and Pressure Dependent Rate Coefficients for the Reaction of Hg with Br and the Reaction of Br with Br: A Pulsed Laser Photolysis-Pulsed Laser Induced Fluorescence Study, *J. Phys. Chem*. A, 110, 6623-6632, doi: 10.1021/jp054688j.

Durnford D., Dastoor A., Ryzhkov A., Poissant L., Pilote M. and Figueras-Nieto D. [2012] How relevant is the deposition of mercury onto snowpacks? -- Part 2: A modeling study, *Atmos. Chem. Phys*., 12, 9251-9274, 10.5194/acp-12-9251-2012.

EMEP [2016] EMEP monitoring network. http://ebas.nilu.no/Default.aspx. Accessed on June 28, 2016.

Emmons L. K., Walters S., Hess P. G., Lamarque J. F., Pfister G. G., Fillmore D., Granier C., Guenther A., Kinnison, D., Laepple T., Orlando J., Tie X., Tyndall G., Wiedinmyer C., Baughcum S.L., and Kloster S. [2010] Description and evaluation of the Model for Ozone and Related chemical Tracers, version 4 (MOZART-4), *Geosci. Model Dev*., 3, 43-67, 10.5194/gmd-3-43-2010.

Ghadimi F., Ghomi M., Ranjbar M. and Hajati A. [2013]. Statistical Analysis of Heavy Metal Contamination in Urban Dusts of Arak, Iran. *Iranica Journal of Energy & Environment* 4 (4): 406-418.

GMOS [2016] GMOS global monitoring network for mercury. http://www.gmos.eu/sdi/. Accessed on June 28, 2016.

Goodsite M. E., Plane J. M. C. and Skov H. [2012] Correction to A Theoretical Study of the Oxidation of Hg^0 to $HgBr_2$ in the Troposphere, *Environ. Sci. Technol*., 46, 5262.

Goodsite M.E., Plane J.M.C. and Skov H. [2004] A Theoretical Study of the Oxidation of Hg0 to HgBr2 in the Troposphere. *Environ. Sci. Technol.*, 38, 1772-1776.

Guerreiro C., J. Horálek, F. de Leeuw, and F. Couvidat [2015] Mapping ambient concentrations of benzo(a)pyrene in Europe. Population exposure and health effects for 2012. ETC/ACM Technical Paper 2014/6. April 2015. Available at: http://acm.eionet.europa.eu/reports/docs/ETCACM_TP_2014_6_BaP_HIA.pdf

Gusev A., Ilyin I., Mantseva L., Rozovskaya O., Shatalov V. and Travnikov O. [2006]. Progress in further development in MSCE-HM and MSCE-POP models (implementation of the model review recommendations). EMEP/MSC-E Technical report 4/2006. 114 p.

Gustin M. S., Amos H. M., Huang J., Miller M. B., and Heidecorn K. [2015] Measuring and modeling mercury in the atmosphere: a critical review. *Atmos. Chem. Phys*., 15, 5697–5713.

Hall B. [1995] The gas phase oxidation of mercury by ozone. *Water Air Soil Poll*., 80, 301-315.

Holmes C.D., Jacob D.J., Corbitt E.S., Mao J., Yang X., Talbot R. and Slemr F. [2010] Global atmospheric model for mercury including oxidation by bromine atoms, *Atmos. Chem. Phys*., 10, 12037-12057.

Ilyin I., O. Travnikov, M. Varygina, M. Vana, P. Machalek, H.Hnilikova [2012] Assessment of Heavy Metal Pollution Levels in the Czech Republic (EMEP case study). Joint MSC-E/CHMI Report. EMEP/MSC-E Technical note 1/2012.

Ilyin I., O.Rozovskaya, O.Travnikov, M.Varygina, W.Aas, K.A. Pfaffhuber [2016] Assessment of heavy metals transboundary pollution, progress in model development and mercury research. EMEP Status Report 2/2016.

Ilyin I., Varygina M., van der Swaluw E., Jimmink B., Leekstra B. [2014]. Joint MSC-E/RIVM Report 1/2014. Assessment of Lead Pollution Levels in the Netherlands (EMEP case study). 40 p.

Jung G., Hedgecock I. M., and Pirrone N. [2009] ECHMERIT V1.0 ? a new global fully coupled mercury-chemistry and transport model, *Geosci. Model Dev*., 2, 175-195, 10.5194/gmd-2-175-2009.

Khoder M. I., Al Ghamdi M. A., and Shiboob M. H. [2012] Heavy Metal Distribution in Street Dust of Urban and Industrial Areas in Jeddah, Saudi Arabia, JKAU: Met., *Env. & Arid Land Agric. Sci*., Vol. 23, No. 2, pp: 55-75.

Kos G., Ryzhkov A., Dastoor A., Narayan J., Steffen A., Ariya P. A. and Zhang L. 2013] Evaluation of discrepancy between measured and modelled oxidized mercury species, *Atmos. Chem. Phys*., 13, 4839-4863.

Li Z., Feng X., Li G., Bi X., Zhu J., Qin H., Dai Z., Liu J., Li Q., Sun G. [2013]. Distributions, sources and pollution status of 17 trace metal/metalloids in the street dust of a heavily industrialized city of central China. *Environmental Pollution*, 182, pp 408–416.

Lin C.-J., Pongprueksa P., Lindberg S.E., Pehkonen S.O., Byun D. and Jang C. [2006]. Scientific uncertainties in atmospheric mercury models I: Model science evaluation. Atmospheric Environment 40 (2006) 2911–2928.

Loredo J., Ordonez A., Charlesworth S., and De Miguel E. [2004] Influence of industry on the geochemical urban environment of Mieres (Spain) and associated health risk. *Environmental Geochemistry and Health*, vol. 25(3), pp.307–323.

Maas R. and Grennfelt P. (eds) [2016] Towards Cleaner Air. Scientific Assessment Report 2016. EMEP Steering Body and Working Group on Effects of the Convention on Long-Range Transboundary Air Pollution, Oslo. xx+50pp.

Manno E., Varrica D., and Dongarra G. [2006] Metal distribution in road dust samples collected in an urban area close to a petrochemical plant at Gela, Sicily. *Atmospheric Environment* 40, 5929–5941.

NADP/MDN [2016] National Atmospheric Deposition Program (NRSP-3). Mercury Deposition Network (MDN). NADP Program Office, Illinois State Water Survey, 2204 Griffith Dr., Champaign, IL 61820. http://nadp.sws.uiuc.edu/MDN/. Accessed on June 28, 2016.

NAtChem [2016] National Atmospheric Chemistry (NAtChem) Database. http://www.ec.gc.ca/natchem. Accessed on June 28, 2016.

Ordonez A., Loredo J., De Miguel E., and Charlesworth S. M. [2003]. Distribution of heavy metals in the street dusts and soils of an industrial city in northern Spain. *Archives of Environmental Contamination and Toxicology*, vol. 44, pp.160–170.

Ortiz S. T. and R. Freidrich [2013] A modelling approach for estimating background pollutant concentrations in urban areas. *Atmospheric Pollution Research* 4 (2013). pp 147-156.

Parrella J. P., Jacob D. J., Liang Q., Zhang Y., Mickley L. J., Miller B., Evans M. J., Yang X., Pyle J. A., Theys N., and Van Roozendael M. [2012] Tropospheric bromine chemistry: implications for present and pre-industrial ozone and mercury, *Atmospheric Chemistry and Physics*, 12, 6723-6740.

Pulles T., H. Kok and U. Quass [2006] Application of the emission inventory model TEAM: Uncertainties in dioxin emission estimates for central Europe. *Atmospheric environment* 40: 2321-2332.

Pulles T., Kok H., Quass U., Jue´ry C., Matejovicova J. [2005] Dioxin emissions in candidate countries. TNO Report R&I-A R 2005/054. Available at: http://ec.europa.eu/environment/archives/dioxin/pdf/rapport_2005.pdf

Rashed M.N. [2008]. Total and Extractable Heavy Metals in Indoor, Outdoor and Street Dust from Aswan City, *Egypt. Clean* 2008, 36 (10 – 11), 850 – 857.

Razanica A., Huremovic J., Zero S., Gojak-Salimovic S. and Memic M. [2014]. Heavy Metals in Street Dust in Sarajevo Area, Bosnia and Herzegovina. *Current World Environment* Vol. 9(1), 43-47.

Seigneur C., Karamchandani P., Lohman K., Vijayaraghavan K., and Shia R.-L. [2001] Multiscale modeling of the atmospheric fate and transport of mercury, *J. Geophys. Res*, 106, 27795-27809.

Sezgin N, Ozcan H.K., Demir G., Nemlioglu S. and Bayat C. [2003]. Determination of heavy metal concentrations in street dusts in Istanbul E-5 highway. *Environment International* 29 (2003) 979– 985.

Shatalov V., Ilyin I., Gusev A., Rozovskaya O., Sokovykh V., Travnikov O., Wiberg K. and Cousins I. [2012]. Heavy Metals and Persistent Organic Pollutants: New Developments. EMEP/MSC-E Technical Report 4/2012.

Shatalov V., Ilyin I., Gusev A., Rozovskaya O., Travnikov O. [2015] Heavy Metals and Persistent Organic Pollutants: development of multi-scale modeling and trend analysis methodology. EMEP/MSC-E Technical report 1/2015.

Smith G.K. [2002] Non-linear regression, in *Encyclopedia of Environmetrics*, Vol. 3, pp. 1405 – 1411.

Sommar J., Grdfeldt, K., Stromberg, D., and Feng, X. [2001] A kinetic study of the gas-phase reaction between the hydroxyl radical and atomic mercury. *Atmos. Environ*., 35, 3049-3054.

Song S., Selin N.E., Soerensen A.L., Angot H., Artz R., Brooks S., Brunke E.-G., Conley G., Dommergue A., Ebinghaus R., Holsen T.M., Jaffe D.A., Kang D., Kelley P., Luke W.T., Magand O., Marumoto K., Pfaffhuber K. A., Ren X., Sheu G.-R., Slemr F., Warneke T., Weigelt A., Weiss-Penzias P., Wip D. C., and Zhang Q.: T[2015] Top-down constraints on atmospheric mercury emissions and implications for global biogeochemical cycling, *Atmos. Chem. Phys*., 15, 7103-7125.

Sprovieri F., Pirrone N., Bencardino M., DAmore F., Carbone F., Cinnirella S., Mannarino V., Landis M., Ebinghaus R., Weigelt A., Brunke E.-G., Labuschagne C., Martin L., Munthe J., Wangberg I., Artaxo P., Morais F., Cairns W., Barbante C., Dieguez M.C., Garcia P.E., Dommergue A., Angot H., Magand O., Skov H., Horvat M., Kotnik J., Read K.A., Neves L.M., Gawlik B.M., Sena F., Mashyanov N., Obolkin V. A., Wip D., Feng X., Zhang H., Fu X., Ramachandran R., Cossa D., Knoery J., Marusczak N., Nerentorp M. and Norstrom C. 2016. Atmospheric Mercury Concentrations observed at ground-based monitoring sites globally distributed in the framework of the GMOS network, *Atmos. Chem. Phys. Discuss*., doi:10.5194/acp-2016-466.

Travnikov O. and I. Ilyin [2005] Regional Model MSCE-HM of Heavy Metal Transboundary Air Pollution in Europe. EMEP/MSC-E Technical Report 6/2005.

Travnikov O. and Ilyin I. [2009] The EMEP/MSC-E Mercury Modeling System, in Mercury Fate and Transport in the Global Atmosphere: Emissions, Measurements, and Models, edited by N. Pirrone and R. P. Mason, *Springer*, pp. 571-587.

Travnikov O., Jonson J. E., Andersen A. S., Gauss M., Gusev A., Rozovskaya O., Simpson D., Sokovyh V., Valiyaveetil, S., and Wind, P. [2009] Development of the EMEP global modelling framework: Progress report. EMEP/MSC-E Technical Report 7/2009, Meteorological Synthesizing Centre - East of EMEP, Moscow, 44 pp., available: http://www.msceast.org/index.php/publications/reports.

Vulykh N. and V.Shatalov [2001] Investigation of Dioxin/Furan Composition in Emissions and in Environmental Media. Selection of Congeners for Modelling. MSC-E Technical Note 6/2001.

Yang X., Cox R., Warwick N., Pyle J., Carver G., O'Connor F., Savage N. [2005] Tropospheric bromine chemistry and its impacts on ozone: A model study, *J. Geophys. Res*., 110, D23311.

Yang X., Pyle J. A., Cox R. A., Theys N., and Van Roozendael M. [2010] Snow-sourced bromine and its implications for polar tropospheric ozone, *Atmos. Chem. Phys*., 10, 7763-7773, doi:10.5194/acp-10-7763-2010.

Annex A

Literature sources on PCDD/Fs congener composition

No	Reference	Emission sector(s)
1	*An Inventory of Sources and Environmental Releases of Dioxin-like Compounds in the United States for Years* 1987, 1995, and 2000; EPA/600/P-03/002F, 667 p.	A_PublicPower (1A1a); B_Industry; Industry combustion (1A1c)4 B_Industry (2A1); B_Industry (2C1); B_Industry (2C3); B_Industry (2C5); B_Industry (2C7a); C_OtherStationary Comb (1A4bi, Residential: Stationary); J_Waste (5C1a, Municipal waste incineration); J_Waste (5C1bi, Industrial waste incineration); J_Waste (5C1bii, Hazardous waste incineration); J_Waste (5C1biv, Sewage sludge incineration)4 J_Waste (5C1biv, Sewage sludge incineration)
2	*Nielsen M., Nielsen O.-K., Thomsen M.*, 2010, Emissionskortlægning for decentral kraftv arme 2007– Energinet.dk miljøprojekt nr. 07/1882. Delrapport 5. Emissionsfaktorer og emissionsopgørelse for decentral kraftvarme, 2006. Danmarks Miljøunderøgelser, Aarhus Universitet, 105 p. Faglig rapport fra DMU nr. 781 http://www.dmu.dk/Pub/FR781.pdf	A_PublicPower (1A1a); F_RoadTransport (1A3bii);
3	*Cleverly D., Schaum J., Schweer G., Becker J., Winters D.*, 1997, The congener profiles of anthropogenic sources of chlorinated dibenzo-p-dioxins and chlorinated dibenzofurans in the United States, 17th International Symposium on Chlorinated Dioxins and Related Compounds, Organohalogen Compound, vol.32, pp. 430-43	B_Industry; Industry combustion (1A1c); B_Industry (2A1); B_Industry (2C3); B_Industry (2C5); B_Industry (2H1); F_RoadTransport (1A3bii); F_RoadTransport (1A3biii); J_Waste (5C1a, Municipal waste incineration); J_Waste (5C1bii, Hazardous waste incineration); J_Waste (5C1biii, Clinical (medical) waste incineration)4 J_Waste (5C1biv, Sewage sludge incineration)4 J_Waste (5C1biv, Sewage sludge incineration)
4	*Oehme M. and Mueller M.D.*, 1995, Levels and congener patterns of polychlorinated dbenzo-p-dioxins and dibenzofurans in solid residues from wood-fired boilers/ Influence of combustion conditions and fuel type., Chemosphere, vol.30, No.8, pp. 1527-1539	A_PublicPower (1A1a)
5	*Thoma H*., 1988, PCDD/F - Concentrations in chimney soot from house heating systems, Chemosphere, vol.17, No.7, pp. 1369-1379	A_PublicPower (1A1a); C_OtherStationary Comb (1A4bi, Residential: Stationary)

No	Reference	Emission sector(s)
6	Development of toxics emission factors from source test data collected under the Air Toxic Hot Spots Program, 1999, Part II, Final Report, Volume I, prepared for R. Propper, California Air Resources Board, p.201	A_PublicPower (1A1a); B_Industry (2A1) B_Industry (2C3); J_Waste (5C1bii, Hazardous waste incineration); J_Waste (5C1biii, Clinical (medical) waste incineration)
7	Emissions Estimation Protocol for Petroleum Refineries, 2015, version 3, submitted to Office of Air Quality Planning and Standards U.S. Environmental Protection Agency, submitted by: RTI International, 253 p.	B_Industry (A1b)
8	*Kao J.-H., Chen K.-S., Chang-Chien G.-P., Chou I-C.*, 2006, Emission of Polychlorinated Dibenzo-p-dioxins and Dibenzofurans from Various Stationary Sources, Aerosol and Air Quality Research, vol.6, No.2, pp. 170-179	B_Industry (2A1); J_Waste (5C1a, Municipal waste incineration); J_Waste (5C1bi, Industrial waste incineration); J_Waste (5C1biii, Clinical (medical) waste incineration)
9	*Thuong N.V., Nam V. D., Hue N.T.M., Son L.K., Thuy N.V., Tung H.D., Tuan N.A., Huy D.Q., Minh N.H.,* 2014, The Emission of Polychlorinated Dibenzo-p-dioxins and Polychlorinated Dibenzofurans from Steel and Cement -Kiln Plants in Vietnam, Aerosol and Air Quality Research, vol.14, pp. 1189-1198	B_Industry (2A1); B_Industry (2C1)
10	*Lin L.-F., Lee W.-J., Chang-Chien G.-P*., 2006, Emissions of Polychlorinated Dibenzo-p-dioxins and Dibenzofurans from Various Industrial Sourches, Air&Waste Manage.Assoc., vol.56, pp. 1707-1715	B_Industry (2A1); B_Industry (2C6); B_Industry (2C7a);
11	*Ames M., Zemba S., Green L., Botelho M.J., Gossman D., Linkpv I.,Palma-Oliveira J.,* 2012, Polychlorinated dibenzo-p-dioxin and furan (PCDD/F) congener profiles in cement kiln emissions and impacts, Science of the Total Environment, vol.419, pp. 37-43	B_Industry (2A1
12	*Anderson D.R. and R.Fisher,* 2003, Dioxin in the Steel Industry, pp. 163 - 188, The Coke Oven Managers' Association, Read before the Midland Section joint meeting with the Royal Society of Chemistry on 10 th April 2003 at Corus Construction and Industrial, Scunthorpe: https://www.researchgate.net/publication/265098916	B_Industry (2C1)
13	*Öberg T.,* 2007, Low-temperature formation and degradation of chlorinated benzenes, PCDD and PCDF in dust from steel production, Science of the Total Environment, vol.382, pp. 153-158	B_Industry (2C1); B_Industry (2C2)
14	*Harnly M., Stephens R., McLaughlin C., et al.,* 1995, Polychlorinated Dibenzo-p-dioxin and Dibenzofuran Contamination at Metal Recovery Facilities, Open Burn Sites, and a Railroad Car Incineration Facility, Environ.Sci.Technol., vol.29, No.3, pp.677-684	B_Industry (2C1)
15	*Rotatori M., Guerriero M., Bianchini M., Gugliucci P.F., Guarnieri A., Lutri A., Mosca S., Rossetti G., Vardè M.*, 2006, PCDD/F profiles of an iron ore sintering plant, Organohalogen compounds, vol.68, pp.2248-2251	B_Industry (2C1)
16	*Guerriero E., Guarnieri A., Moska S., Rossetti G., Rotatori M.,* 2009, PCDD/Fs removal efficiency by electrostatic precipitator and wetfine scrubber in an iron ore sintering plant, Journal of Hazardous Materials, vol.172, pp.1498-1504	B_Industry (2C1)
17	*Liberti L.,* 2014, Dioxin and PCB contamination around a heavy	B_Industry (2C1)

No	Reference	Emission sector(s)
	industrial area: A case history, International journal of Innovation and Scientific Research, vol.9, No.2, pp. 175-189	
18	*Sofilic T., Jendricko J., Kovacevic Z., Cosic M.,* 2012, Mesurement of polychlorinated ibenzo-p-dioxin and dibenzofuran emission from EAF Steel making proces, Archives of Metallurgy and Materials, vol.57, No.3, pp.811-821	B_Industry (2C1
19	*Li H.-W., Wu Y.-L., Lee W.-J., Chang-Chien G.-P.,* 2007, Fate of Polychlorinated Dibenzo-p-dioxins and Dibenzofurans in a Fly Ash Treatment Plant, Journal of the Air & Waste Management Association, vol.57, No.9, pp. 1024-1031	B_Industry (2C1
20	*Lee W.-S., Chang-Chetn G.-P., Chen S.-J. et al.*, 2004, Removal of Polychlorinated Dibenzo-p-dioxins and Dibenzofurans in Flue Gases by Ventury Scrubber and Bag Filter, Aerosol and Air Quality Research, vol.4, No.1, pp. 27-37	B_Industry (2C3)
21	*Thanner G. and W. Moche,* 2002, Emission von Dioxinen, PCBs und PAHs aus Kleinfeuerungen, Monographien, Band 153, Umweltbundesamt, (Federal Environmental Agency-Austria), Wien, 90 S.	C_OtherStationary Comb (1A4bi, Residential: Stationary)
22	*Lee R.G.M., Coleman P., Jones J.L., Jones K.C., R.Lohmann*, 2005, Emission Factors and Importance of PCDD/Fs, PCBs, PCNs, PAHs and PM10 from Domestic Burning of Coal and Wood in the UK, Environ.Sci.Technol., vol.39, No.6, pp. 1436-1447	C_OtherStationary Comb (1A4bi, Residential: Stationary)
23	*Moltó J, Gálvez A, Fuentes M J, Fullana A, Font R*: Emission of PCDD/Fs from combustion of pine needles and pine cones in a residential stove: https://rua.ua.es/dspace/bitstream/10045/2310/1/congreso_5.pdf	C_OtherStationary Comb (1A4bi, Residential: Stationary)
24	*Bacher R., Swerev M., Ballschmitter K.,* 1992, Profile and Pattern of Monochloro-through Octachlorodibenzodioxins and -dibenzofurans in Chimney Deposits from Wood Burning, Environ. Sci.Technol., vol.26, No.8, pp.1649-1655	C_OtherStationary Comb (1A4bi, Residential: Stationary)
25	*Miyabara Y., Hashimoto S., Sagai M., Morita M.,* 1999, PCDDs and PCDFs in vehicle exhaust particles in Japan, Chemosphere vol.39, No.1, pp. 143-150	F_RoadTransport (1A3bii); F_RoadTransport (1A3biii)
26	Health Assessment Document for Diesel Engine Exhaus, 2002, EPA/600/8-90/057F, 669 p.	F_RoadTransport (1A3biii)
27	*Ryan J.V. and Gullett B.K.,* 2000, On-Road Emission Sampling of a Heavy-Duty Diesel Vehicle for Polychlorinated Dibenzo-p-dioxins and Polychlorinated Dibenzofurans, Environ.Sci.Technol., vol. 34, No.21, pp. 4483-4489	F_RoadTransport (1A3biii)
28	*Chuang S.-C., Chen S.-J., Huang K.-L., Chang-Chien G.-P., Wang L.-C., Huang Y.-C.,* 2010, Emission of polychlorinated Dibenzo-p-dioxin and Polychlorinated Dibenzofuran from Motorcycles, Aerosol and Air Quality Research, vol.10, pp. 533-539	F_RoadTransport (1A3biv)
29	*Cooper D.,* 2004, HCB, PCD, PCDD and PCDF emissions from ships, IVL Rapport/report B1620, IVL Svenska Miljöinstitutet AB (IVL Swedish Environmental Research Institute Ltd.), 31 p.	G_Shipping (1A3dii)
30	*Spinnel E., Fick J., Andersson P.L., Haglund P.,* 2008, Streamlined Combustion Gas Measurements for Imoroved National Dioxin Inventories, Environ.Sci.Technol., vol.42, No.24, pp. 9555-9261	J_Waste (5C1a, Municipal waste incineration)
31	*Ni Y., Zhang H., Fan S., et al.*, 2009, Emissions of PCDD/Fs from municipal solid waste incinerators in China, Chemosphere, vo.75, pp. 1153-1158	J_Waste (5C1a, Municipal waste incineration
32	*Lee W.-S., Chang-Chien G.-P., Wang L.-C., Lee W.-J., Tsai P.-J., Chen C.-K.,* 2003, Emissions of Polychlorinated Dibenzo-p-dioxins	J_Waste (5C1a, Municipal waste incineration4

No	Reference	Emission sector(s)
	and Dibenzofurans from the Incinerations of Both Medical and Municipal Solid Waste, Aerosol and Air Quality Research, vol.3, pp.01-06	J_Waste (5C1biii, Clinical (medical) waste incineration)
33	*Abad E., Martinez K., Caixach J., Rivera J.*, 2006, Polychlorinated dibenzo-p-dioxins, dibenzofurans and 'dioxin-like' PCBs in flue gas emissions from municipel waste management plants, Chemosphere, vol. 63, pp.570-580	J_Waste (5C1a, Municipal waste incineration)
34	*Kim, B.H., Kim, J.H.,* 2004. Removal of PCDDs/Fs from a Solid Waste Incinerator Using a Dual Bag Filter System with Recycled Activated Carbon. Proceedings of the 3rd International Conference on Combustion, Incineration/ Pyrolysis and Emission Control, p.313-318	J_Waste (5C1a, Municipal waste incineration)
35	*Theisen J., Funcke W., Balfanz E., Koenig J.,* 1989, Determination of PCDDs and PCDDs in fire accidents and laboratory combustion test involving PVC-containing materials, Chemosphere, vol.19, No.1-6, pp.423-428	J_Waste (5C1bi, Industrial waste incineration)
36	*Aracil I., Font R., Conesa J.A.,* 2005, Semivolatile and volatile compounds from the pyrolysys and combustion of polyvinyl chloride, Journal of Analytical and Applied Pyrolysis, vol.7, No.1-2, pp. 465-478	J_Waste (5C1bi, Industrial waste incineration)
37	*Molto J., Font R., Galvez A., Coneca J.A.,* 2009, Pyrolysis and combustion of electronic wastes, Journal of Analytical and Applied Pyrolysis, vol.84, No.1 pp.68-78	J_Waste (5C1bi, Industrial waste incineration)
38	*Aracil I.,* 2008, Formacion de contaminantes y estudio cinetico en la pirolisis y combustion de plasticos (PE, PVC y PCP), Memoria qua, para optar al grado de Doctor en Ingenieria Quimica, https://rua.ua.es/dspace/bitstream/10045/9608/1/ tesis_doctoral_ignacio_aracil.pdf	J_Waste (5C1bi, Industrial waste incineration)
39	*Lin L.-F., Lee W.-J., Chang-Chien G.-P.,* 2006, Emissions of Polychlorinated Dibenzo-p-dioxins and Dibenzofurans from Various Industrial Sources, Air&Waste Manage.Assoc., vol.56, pp. 1707-1715	J_Waste (5C1bi, Industrial waste incineration)4 J_Waste (5C1biv, Sewage sludge incineration)
40	*Hagberg J., Bert van Bavel, Loethgren C.-J., Lindstroem G.*, 2005, Occurrence and levels of PCDD/Fs and PBDD/Fs in fly ash fron two different incinerators at a hazardous waste treatment plant, Organohalogen compounds, vol.67, pp. 2200-2203	J_Waste (5C1bii, Hazardous waste incineration)
41	POPs in residues from waste incineration in Pakistan,2006, Arnika - Toxic and Waste Programme Sustainable Development Policy Institute (SDPI), International POPs Elimination project -IPEP, Czech Republic, Pakistan, 44 p.	J_Waste (5C1biii, Clinical (medical) waste incineration)
42	*Lindner G., Jenkins A., McCormack J., Adrian R.C.,* 1990, Dioxins and furans in emissions from medical waste incinerators, Chemosphere, vol. 20, No. 10–12, pp. 1793-1800	J_Waste (5C1biii, Clinical (medical) waste incineration)
43	*Lee W.-S., Chang-Chetn G.-P., Chen S.-J. et al.,* 2004, Removal of Polychlorinated Dibenzo-p-dioxins and Dibenzofurans in Flue Gases by Ventury Scrubber and Bag Filter, Aerosol and Air Quality Research, vol.4, No.1, pp. 27-37	J_Waste (5C1biii, Clinical (medical) waste incineration)
44	*Gomez-Rico Ninez de Arenas M.F,* 2008, Estudio de Contaminantes Organicos en el Aprovechamiento del Lodos de Depuradora de Aquas Residuales Urbanas, Memoria para optar al grado de Doctor en Ingenieria Quimica https://rua.ua.es/dspace/bitstream/10045/7719/1/ tesis_doctoral_francisca_gomez.pdf	J_Waste (5C1biv, Sewage sludge incineration)
45	*Gullett B., Wyrzykowska B., Grandesso E., et al.,* 2010, PCDD/F, PBDD/F, and PBDE Emissions from Open Burning of a Residental	J_Waste (5C2, Open burning of waste)

No	Reference	Emission sector(s)
	Waste Dump, Environ.Sci.Technol., vol.44, No.1, pp. 394-399	
46	*Lemieux P. M., Lutes C.C., Abbot J.A., Aldous K.M.,* 2000, Emissions of Polychlorinated Dibenzo-p-dioxins and Polychlorinated Divenzofurans from the Open Burning of Household Waste in Barrels, Environ.Sci.Technol., vol.34, No.3, pp. 377-384	J_Waste (5C2, Open burning of waste)
47	*Zhang T., Fiedler H., Yu G., Solorzano-Ochoa G., Carroll W.F., Gulett B.K., Marklund S., Touati A.,* 2011, Emissions of unintentional persistent organic pollutants from open burning of municipal solid waste from developing countries, Chemosphere, vol.84, pp. 994-1001	J_Waste (5C2, Open burning of waste)